

Groundwater and Hydrothermal Ore Deposits

Martin Appold and Grant Garven

Groundwater and Hydrothermal Ore Deposits

The Groundwater Project

Martin Appold

*Professor
University of Missouri
Columbia, Missouri, United States*

Grant Garven

*Professor Emeritus
Tufts University
Medford, Massachusetts, United States*

*Groundwater and
Hydrothermal Ore Deposits*

*The Groundwater Project
Guelph, Ontario, Canada*

All rights reserved. This publication is protected by copyright. No part of this book may be reproduced in any form or by any means without permission in writing from the authors (to request permission contact: permissions@gw-project.org). Commercial distribution and reproduction are strictly prohibited.

Groundwater-Project (GW-Project) works are copyrighted and can be downloaded for free from gw-project.org. Anyone may use and share gw-project.org links to download GW-Project's work. It is neither permissible to make GW-Project documents available on other websites nor to send copies of the documents directly to others. Kindly honor this source of free knowledge that is benefiting you and all those who want to learn about groundwater.

Copyright © 2023 Martin Appold and Grant Garven (The Authors)

Published by the Groundwater Project, Guelph, Ontario, Canada, 2023.

Appold, Martin

Groundwater and hydrothermal ore deposits / Martin Appold and Grant Garven - Guelph, Ontario, Canada, 2023.

86 pages

ISBN: 978-1-77470-042-6

DOI: <https://doi.org/10.21083/978-1-77470-042-6>.

Please consider signing up for the GW-Project mailing list to stay informed about new book releases, events, and ways to participate in the GW-Project. When you sign up for our email list, it helps us build a global groundwater community. [Sign up](#).

APA (7th ed.) citation:

Appold, M., & Garven, G. (2023). *Groundwater and hydrothermal ore deposits*. The Groundwater Project. [10.21083/978-1-77470-042-6](https://doi.org/10.21083/978-1-77470-042-6).



Domain Editors: Eileen Poeter and John Cherry

Board: John Cherry, Paul Hsieh, Richard Jackson, Ineke Kalwij, Everton de Oliveira, and Eileen Poeter

Steering Committee: John Cherry, Allan Freeze, Paul Hsieh, Ineke Kalwij, Douglas Mackay, Stephen Moran, Everton de Oliveira, Beth Parker, Eileen Poeter, Ying Fan, Warren Wood, and Yan Zheng.

Cover Image: Massive fluorite and barite mineralization in the Blanchard mine of the Hansonburg, New Mexico Mississippi Valley-type district, Martin Appold, December 12, 2017.

Table of Contents

TABLE OF CONTENTS.....	IV
THE GROUNDWATER PROJECT FOREWORD	VI
FOREWORD	VII
PREFACE	VIII
ACKNOWLEDGMENTS.....	IX
1 INTRODUCTION: THE NATURE OF ORE DEPOSITS	1
2 EXAMPLES OF ORE DEPOSITS FORMED BY GROUNDWATER.....	6
2.1 SEDIMENT-HOSTED ORE DEPOSITS.....	7
2.1.1 Mississippi Valley-Type Deposits.....	7
2.1.2 Evaluating Conditions for MVT Deposit Formation.....	18
2.1.3 Unconformity-Type Uranium Deposits.....	18
2.1.4 Sediment-Hosted Stratiform Copper Deposits.....	23
2.2 MAGMATIC HYDROTHERMAL ORE DEPOSITS: THE PORPHYRY COPPER EXAMPLE.....	29
2.2.1 Evaluating Conditions for Hydrothermal Ore Deposit Formation.....	39
3 WRAP UP.....	40
4 EXERCISES.....	41
PART I - CONSTRAINTS AND IMPLICATIONS OF GROUNDWATER TEMPERATURE ON THE FORMATION OF MISSISSIPPI VALLEY-TYPE ZN-Pb DEPOSITS	41
INTRODUCTION.....	41
EXERCISE 1.....	43
EXERCISE 2.....	44
EXERCISE 3.....	45
EXERCISE 4.....	47
EXERCISE 5.....	48
EXERCISE 6.....	48
EXERCISE 7.....	49
EXERCISE 8.....	50
PART II – SOLUTE TRANSPORT IN A MAGMATIC HYDROTHERMAL ENVIRONMENT.....	51
INTRODUCTION.....	51
EXERCISE 9.....	52
PART III – SUBSURFACE FLUID DYNAMICS AND HEAT TRANSFER.....	54
INTRODUCTION.....	54
EXERCISE 10.....	55
EXERCISE 11.....	56
5 REFERENCES	57
6 EXERCISE SOLUTIONS	67
PART I - CONSTRAINTS AND IMPLICATIONS OF GROUNDWATER TEMPERATURE ON THE FORMATION OF MISSISSIPPI VALLEY-TYPE ZN-Pb DEPOSITS	67
SOLUTION EXERCISE 1.....	67
SOLUTION EXERCISE 2.....	67
SOLUTION EXERCISE 3.....	68
SOLUTION EXERCISE 4.....	70
SOLUTION EXERCISE 5.....	72

SOLUTION EXERCISE 6.....	75
SOLUTION EXERCISE 7.....	76
SOLUTION EXERCISE 8.....	77
PART II - SOLUTE TRANSPORT IN A MAGMATIC HYDROTHERMAL ENVIRONMENT	79
SOLUTION EXERCISE 9.....	79
PART III - SUBSURFACE FLUID DYNAMICS	81
SOLUTION EXERCISE 10.....	81
SOLUTION EXERCISE 11.....	82
7 NOTATIONS	84
8 ABOUT THE AUTHORS	85

The Groundwater Project Foreword

At the United Nations (UN) Water Summit held on December 2022, delegates agreed that statements from all major groundwater-related events will be unified in 2023 into one comprehensive groundwater message. This message will be released at the UN 2023 Water Conference, a landmark event that will bring attention at the highest international level to the importance of groundwater for the future of humanity and ecosystems. This message will bring clarity to groundwater issues to advance understanding globally of the challenges faced and actions needed to resolve the world's groundwater problems. Groundwater education is key.

The 2023 World Water Day theme *Accelerating Change* is in sync with the goal of the Groundwater Project (GW-Project). The GW-Project is a registered Canadian charity founded in 2018 and committed to the advancement of groundwater education as a means to accelerate action related to our essential groundwater resources. To this end, we create and disseminate knowledge through a unique approach: the democratization of groundwater knowledge. We act on this principle through our website gw-project.org/, a global platform, based on the principle that

“Knowledge should be free, and the best knowledge should be free knowledge.” Anonymous

The mission of the GW-Project is to promote groundwater learning across the globe. This is accomplished by providing accessible, engaging, and high-quality educational materials—free-of-charge online and in many languages—to all who want to learn about groundwater. In short, the GW-Project provides essential knowledge and tools needed to develop groundwater sustainably for the future of humanity and ecosystems. This is a new type of global educational endeavor is made possible through the contributions of a dedicated international group of volunteer professionals from diverse disciplines. Academics, consultants, and retirees contribute by writing and/or reviewing the books aimed at diverse levels of readers from children to high school, undergraduate, and graduate students, or professionals in the groundwater field. More than 1,000 dedicated volunteers from 127 countries and six continents are involved—and participation is growing.

Hundreds of books will be published online over the coming years, first in English and then in other languages. An important tenet of GW-Project books is a strong emphasis on visualization; with clear illustrations to stimulate spatial and critical thinking. In future, the publications will also include videos and other dynamic learning tools. Revised editions of the books are published from time to time. Users are invited to propose revisions.

We thank you for being part of the GW-Project Community. We hope to hear from you about your experience with the project materials, and welcome ideas and volunteers!

The GW-Project Steering Committee

January 2023

Foreword

One of the essential building blocks of our society is the mining of geological entities, known as ore deposits, that provide most of the chemical elements that our industrial society depends on. These include lead, zinc, copper, nickel, uranium, silver, gold, cobalt, fluorine, and others. Nearly all of the most important ore deposits formed tens to hundreds of millions of years ago from groundwater flowing through sedimentary rocks. The groundwater was brine which is far saltier than sea water. Physical and geochemical processes operated on the dissolved constituents (solutes) in the flowing groundwater to precipitate minerals that formed the ore deposits. These deposits result from a combination of local processes and larger-scale processes in the earth's crust that are governed by changes in temperature and pressure.

Historically ore deposits were discovered by chance, while in modern times the search for deposits is based on scientific thinking. For more than a hundred years, principles of geology and geochemistry have guided conceptual thinking about how ore deposits formed while geophysics and drilling underpinned field exploration. Each type of ore deposit represents a puzzle that, after sorting through alternative hypotheses, requires fitting the various physical and chemical processes together into a consistent and plausible story about what happened over geologic time.

Hydrogeology was the most recent (i.e., 1980's) quantitative component incorporated into the scientific framework for determining how ore deposits form. The two authors of this book: Dr. Martin Appold, a Professor of Geological Sciences at the University of Missouri; and Dr. Grant Garven, a Professor Emeritus of Hydrogeology, Tufts University, have published much of the seminal literature about the role of groundwater in formation of ore deposits.

John Cherry, The Groundwater Project Leader
Guelph, Ontario, Canada, January 2023

Preface

Until the late 1970's, the study of hydrothermal ore deposits focused completely on the use of classical geological field work, exploratory drilling, major, minor, and trace element analysis, petrographic microscopy, fluid inclusion microthermometry, and isotope and equilibrium geochemistry to interpret the processes and paragenesis of ore mineralization. The textbook by Barnes (1979) describes in detail many of the analytical geochemical and thermodynamic principles of metal transport and precipitation in ore deposits. Freeze and Cherry (1979) recognized the value of physical principles of groundwater hydrology to understanding ore genesis and anticipated some of the research discussed in this book.

Many conceptual fluid flow models have been proposed for the formation of sediment-hosted and magmatic hydrothermal ore deposits. Although a huge literature has been generated on the petrology and geochemistry of hydrothermal ore deposits, far fewer studies have evaluated the flow and transport mechanics of hydrothermal ore formation in a rigorous quantitative sense. Some of the studies that have done so have had considerable impact. For example, pioneering studies by Cathles (1977) and Norton and Knight (1977) used two-dimensional finite difference models to characterize fluid flow and heat transport around a cooling pluton at shallow crustal depths (5~15 km) to provide insights into the formation of porphyry copper deposits. In a similar vein, Garven and Freeze (1984a, 1984b) used two-dimensional finite element models to characterize fluid flow and heat transport at shallower depths (~1 to 5 km) in sedimentary basins over horizontal distances of 100's of km to gain insights into the formation of carbonate-hosted Zn-Pb deposits. Subsequent research by many authors has greatly expanded on this work to include the effects of three-dimensional flow, rock deformation, multiphase fluids, flow in faults, reactive solute transport, and the effects of changing porosity and permeability due to mineral precipitation and dissolution.

This book presents several case studies that illustrate how theoretical principles of groundwater hydrology applied mainly through numerical models have been used to advance our understanding of the formation of hydrothermal ore deposits in sedimentary basins and around cooling plutons. The book focuses specifically on Mississippi Valley-type zinc-lead, unconformity-type uranium, stratiform copper, and porphyry copper deposits, as these deposits have received particular attention from researchers in applying groundwater flow and transport models to ore genesis questions. The book includes several exercises (with solutions) that offer readers the opportunity to sharpen their skill with practical calculations regarding the physical and chemical hydrology of hydrothermal ore formation.

Acknowledgments

We deeply appreciate the valuable contributions to this book by the following reviewers:

- ❖ Philipp Weis, Senior Researcher, Division of Inorganic and Isotope Geochemistry, Helmholtz Centre Potsdam, Germany;
- ❖ Jack Sharp, Professor Emeritus, Department of Geological Sciences, University of Texas at Austin, United States;
- ❖ Warren Wood, Visiting Professor of Hydrogeology, Earth and Environmental Sciences, Michigan State University, East Lansing, Michigan, USA;
- ❖ Shemin Ge, Professor, Geological Sciences, University of Colorado, Boulder, Colorado, USA.
- ❖ Matthew Leybourne, Professor, Geology, Queens University, Kingston, Ontario, Canada;
- ❖ Connie Bryson, Editor, The Groundwater Project, Guelph, Canada; and
- ❖ Matthys Dippenaar Associate Professor, Engineering Geology and Hydrogeology, University of Pretoria, Pretoria, South America

We appreciate the contributions of Steven Ingebritsen (U.S. Geological Survey, Menlo Park, California, USA) for his impetus and insights in helping us write this manuscript, as well as Dan Hayba (U.S. Geological Survey, Reston, Virginia, USA) and Herb Wang (University of Wisconsin, Madison, Wisconsin, USA), for their helpful reviews of the original draft of this manuscript. We are grateful for Amanda Sills and the Formatting Team of the Groundwater Project for their oversight and copyediting of this book. We thank Eileen Poeter (Colorado School of Mines, Golden, Colorado, USA) for reviewing, editing, and producing this book.

Martin Appold would like to thank numerous mentors who have stimulated his interest and shaped his understanding of mineral deposits and hydrogeology including Steve Kesler (University of Michigan, Ann Arbor, Michigan, USA), Grant Garven (Tufts University, Medford, Massachusetts, USA), Dimitri Sverjensky (Johns Hopkins University, Baltimore, Maryland, USA), Jill Pasteris (Washington University, Saint Louis, Missouri, USA), and Jeff Nunn (Louisiana State University, Baton Rouge, Louisiana, USA).

Grant Garven is very grateful to his academic mentors and collaborators over the past 50 years, all of whom inspired and fostered his research in hydrogeology and the economic geology of sedimentary basins: Laurence Vigrass (University of Regina, Saskatchewan, Canada), Bill Coombe (Saskatchewan DMR), Stanley Davis and Denis Norton (University of Arizona, Tucson, Arizona, USA), Jozsef Tóth (University of Alberta, Edmonton, Canada), Allan Freeze (University of British Columbia, Vancouver, Canada), Greg Anderson (University of Toronto, Toronto, Ontario, Canada), Dimitri Sverjensky (Johns Hopkins University, Baltimore, Maryland, USA), Ross Large (University of

Tasmania, Tasmania, Australia), James Boles (University of California, Santa Barbara, California, USA), and last but not least Anne Gardulski (Tufts University, Medford, Massachusetts, USA).

1 Introduction: The Nature of Ore Deposits

“...water is the fundamental fluid genetically relating (most) mineral deposits. It is the vehicle for the transportation of materials in solution and it takes part in the reactions that result in the original dissolution of the metals and their ultimate precipitation as ore. If the movement of subsurface water were to cease, chemical and physical equilibrium between the water and the rocks would eventually occur and there would be no further opportunities for the generation of mineral deposits...(R)ecent developments in physical and chemical hydrogeology...are highly pertinent.”

Freeze and Cherry, 1979, page 521

Many of the world's important ore deposits form from groundwater. Such ore-forming groundwater is diverse in geologic origin, chemical composition, and temperature. For example, ore-forming groundwater may originate from atmospheric precipitation (i.e., meteoric water), seawater, magmatic exhalations, or metamorphic mineral dehydration reactions. Ore-forming groundwater ranges from being dilute enough to be considered 'fresh' to brines twenty times more saline than seawater. Ore-forming groundwater can be significantly hotter than surface water—by up to several hundred degrees Celsius—and then it is called a hydrothermal fluid.

Groundwater abounds in the Earth's crust but only rarely forms large ore deposits. The probability of groundwater forming a large ore deposit at a particular location increases as the magnitude and duration of solute flux at that location increase. Solute flux refers to the mass of a solute dissolved in groundwater that crosses a unit area for a unit of time (e.g., grams per square meter per second). Solute flux may increase as the concentration of solute in the groundwater increases (i.e., the mass of solute per unit volume of groundwater), as the velocity of groundwater flow increases, or as groundwater is focused through a narrower cross-sectional area of flow.

Numerous factors may increase solute concentration, and thus increase solute flux, thereby increasing the probability of ore deposit formation. Among the most important is temperature because the solubility of most solutes increases with increasing temperature, thus it is easier for groundwater to dissolve subsurface material and transport it to a location where a mineral deposit can form. Typically, groundwater is heated as it descends to greater depths below the Earth's surface or when it flows near, or is exsolved from, magma.

In addition to temperature, the solubility of most ore-forming solutes is strongly dependent on groundwater composition, particularly salinity, pH, redox potential, and the concentration of common ligand-forming elements like sulfur. A diverse array of groundwater mixing and chemical reactions with rocks may alter groundwater composition, for example, dilution of brine with meteoric water or neutralization of acidic

groundwater by reaction with limestone. In addition, pressure may affect solubility. This is particularly the case for the solubility of gaseous solutes.

High solute flux is not sufficient to form an ore deposit. A mechanism must exist to cause precipitation of solute from groundwater, otherwise the groundwater will pass a site that has potential for ore deposition without precipitating any ore. Mechanisms for precipitating ore include changes in the groundwater properties mentioned above that would decrease the solubility of ore-forming constituents. In addition, boiling can cause precipitation of solutes because it can change groundwater composition by causing some solutes to exsolve from the groundwater as gas.

Solute flux—the delivery of solute by groundwater to a potential site of ore formation—is a function of groundwater velocity, which varies in part due to variations in the permeability of geologic media caused by variations in grain size, grain packing, cementation, and mechanical deformation through compaction or secondary fracturing. Permeability can be affected by ore formation itself, such as when the precipitation or dissolution of minerals occludes or enlarges pores, or when highly pressurized groundwater fractures rock.

Groundwater velocity is also affected by various driving mechanisms that cause pressure gradients to differ from the hydrostatic pressure gradient. Important examples of groundwater driving mechanisms for ore deposit formation include topographic uplift, compaction of sediment, seismic deformation of rock, heating of groundwater by magma, expulsion of water from magma, and the production of water from the chemical breakdown of hydrous minerals during metamorphism (Figure 1). Heating of groundwater by magma may produce pressure gradients due to fluid expansion and density changes, which can cause groundwater convection, an important process for the vertical transport of water, solute, and heat. In addition, density gradients inducing groundwater convection may be caused by salinity gradients.

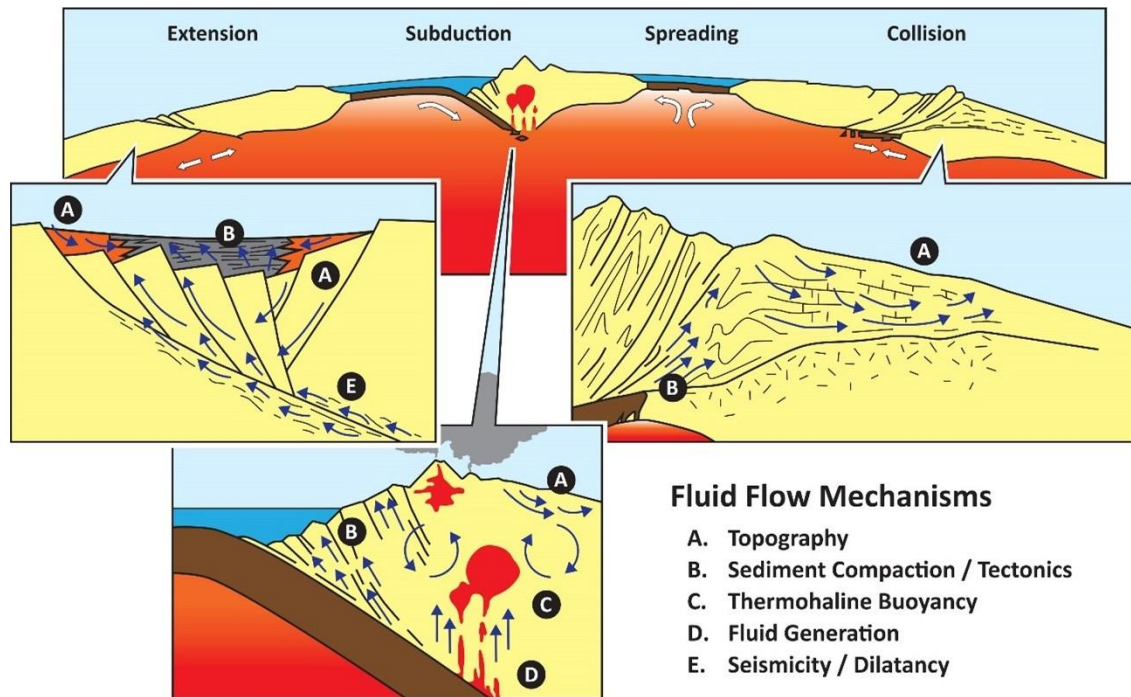


Figure 1 - Schematic diagram depicting driving mechanisms for deep groundwater flow in different tectonic regimes within the Earth's continental crust. These driving mechanisms compete with each other and evolve over time. Commonly, one driving mechanism will eventually come to dominate over the others and thus contribute the most to the formation of hydrothermal ore deposits (modified from Person et al., 1996).

- A. Topography: Gradients in the elevation of the land surface create corresponding gradients in hydraulic head, causing groundwater to flow from higher land surface elevations to lower land surface elevations.
- B. Sediment compaction: Sediment can be compacted vertically as it is buried more and more deeply, or it may be compacted horizontally by tectonic stresses. If groundwater in the shrinking pores cannot escape from the pores fast enough to maintain hydrostatic pressure as the sediment compacts, then pressure of groundwater in the pores increases, leading to pressure gradients that can drive groundwater flow.
- C. Thermohaline buoyancy: If groundwater density decreases with increasing depth such that denser groundwater overlies less dense groundwater (e.g., through dissolution of evaporites at shallow depths or heating from a magma at greater depths), then the deeper less dense water will rise due to buoyancy and the shallower denser water will sink, leading to convection.
- D. Fluid generation: The addition of water to the pores of geologic media through dehydration reactions (e.g., muscovite + quartz = K-feldspar + sillimanite + H₂O) can cause the pressure of the groundwater in the pores to increase, leading to pressure gradients.
- E. Seismicity/Dilatancy: As stress builds on a fault leading up to an earthquake, pores in the rocks on opposite sides of the fault may dilate, lowering the pressure of groundwater in the pores and causing groundwater from the surroundings to flow into the dilated pores. Once enough stress has accumulated on the fault to overcome the force of friction between the two rock blocks, then the rock blocks will slip past one another on the fault, compressing the dilated pores and causing them to expel some of their groundwater.

Focusing of fluid through a narrow area appears to be a common component of ore deposit formation. For example, Heinrich and others (2000) found fluid-rock ratios are commonly more than three orders of magnitude lower in the source regions of ore deposits than in the ore deposits themselves, indicating that the solutes were dissolved by groundwater from a large source volume and deposited down gradient in a much smaller volume that constitutes the ore deposit (Cox, 2005). Fluid focusing is intrinsic to the topography-driven groundwater flow systems that form many Mississippi Valley-type (MVT) deposits, in which recharge areas are generally larger than the discharge areas

where ore deposits were typically formed (Figure 2). Deep aquifers in foreland-type sedimentary basins tend to focus the migration of ancient brines known to have formed MVT-type ore deposits (Garven, 1995).

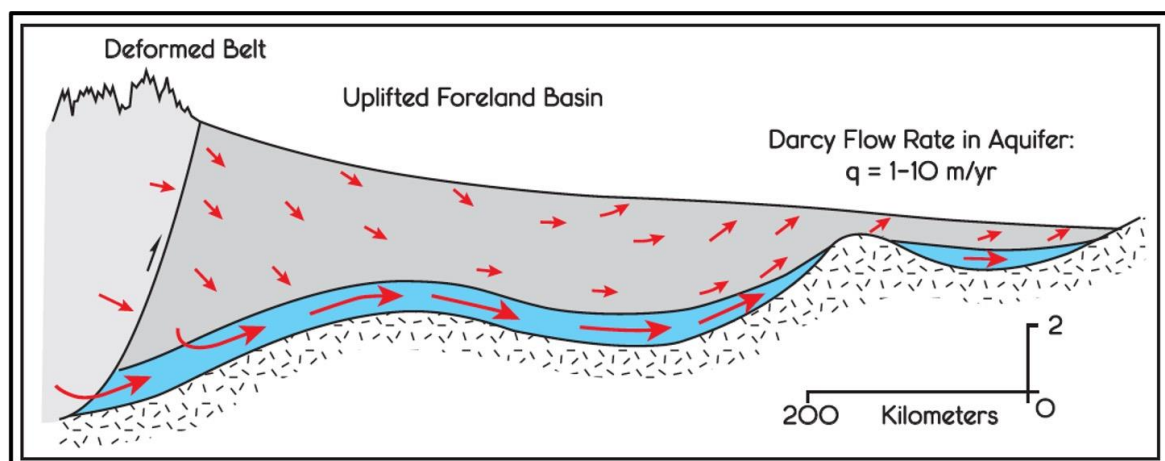


Figure 2 - Topography-driven flow in a foreland-type sedimentary basin showing the focusing of groundwater in a deeply buried aquifer (blue). The groundwater in such deeply buried aquifers tends to be highly saline (i.e., a brine) and ancient. The water table is assumed to be a subdued replica of the land-surface topography. The red arrows indicate the general direction and magnitude of groundwater flow, i.e., the longer the arrows, the faster the flow.

Fluid focusing is exhibited in some volcanic terranes where groundwater absorbs heat (at least hundreds of megawatts) from areas of over hundreds of square kilometers and discharges it in a relatively small area of thermal springs or seafloor hydrothermal vents (Manga, 1998; Ingebritsen and Mariner, 2010). This fluid focusing is accompanied by large increases in groundwater flow rates commonly on the order of 10^{-2} m^3/s but in some places as high as $10 \text{ m}^3/\text{s}$ (e.g., Benoit and Butler, 1983; Hochstein and Browne, 2000; Simmons and Brown, 2006). These groundwater flow systems are efficient at forming gold and silver deposits. For example, at a volumetric flow rate of $0.1 \text{ m}^3/\text{s}$ and an aqueous gold concentration of only 1 ppb (parts per billion), even the largest gold deposits containing around 1,000 tons of gold could be deposited in a few hundred thousand years. This is within the lifespan of 10^5 to 10^6 years considered typical for magmatic-hydrothermal systems (Hochstein and Browne, 2000).

Thus, the formation of hydrothermal ore deposits—i.e., ore deposits formed from hot groundwater—is a complex function of thermal processes (heat transport), hydraulic processes (groundwater flow, solute transport), mechanical deformation, and chemical reaction. These processes are highly interdependent (i.e., coupled), as illustrated in Figure 3. For example, heat is transported by groundwater as it flows and by conduction through the surrounding geologic media and together these two processes affect the temperature of the groundwater. The temperature of the groundwater affects how much solute can be dissolved in the groundwater and the solute concentration directly affects the rate and magnitude of geochemical reactions, including those that precipitate or dissolve minerals.

Mineral dissolution or precipitation changes the porosity and permeability of the geologic media through which groundwater is flowing, which in turn affects the rate of groundwater flow. Mechanical deformation is not explicitly shown in Figure 3, but it affects porosity and permeability because it can dilate or shrink pores.

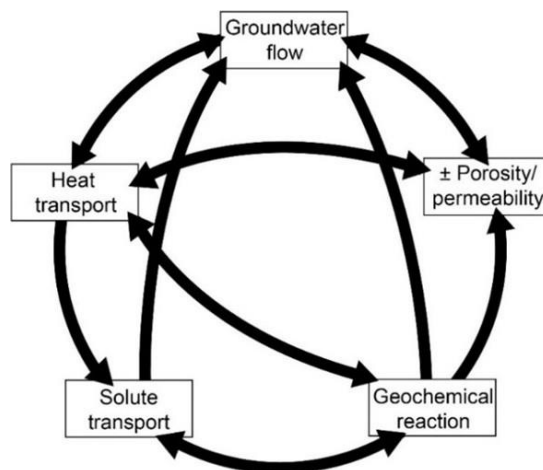


Figure 3 - Schematic diagram showing possible couplings among hydrothermal processes. Deformation processes are implicitly represented by changes in porosity and permeability. In addition to the coupling of deformation to fluid flow and heat transport, deformation may also be caused by external forces such as sedimentation or tectonism (Appold and Nabelek, 2009).

A further example of coupling is that the concentrations of solute in groundwater are altered by geochemical reactions, which are controlled by the groundwater flow paths, and the solute concentrations affect groundwater flow paths by changing the density and viscosity of the groundwater. An additional example of coupling is that changes in temperature caused by heat transport may cause a porous medium to expand, contract, or fracture, changing the porosity and permeability of the porous medium.

Exercises are included at the end of this book. The exercises provide an opportunity for readers to explore the conditions needed for ore formation in some of these environments.

2 Examples of Ore Deposits Formed by Groundwater

The spectrum of hydrothermal ore deposits formed by groundwater in the Earth's crust is wide. This overview presents four major classes of ore deposits formed in sedimentary and magmatic environments that illustrate the role of groundwater in ore deposit formation: (1) Mississippi Valley-type, (2) unconformity-type uranium, (3) sediment-hosted stratiform copper, and (4) porphyry copper deposits. Representative photographs of each deposit type are shown in Figure 4.

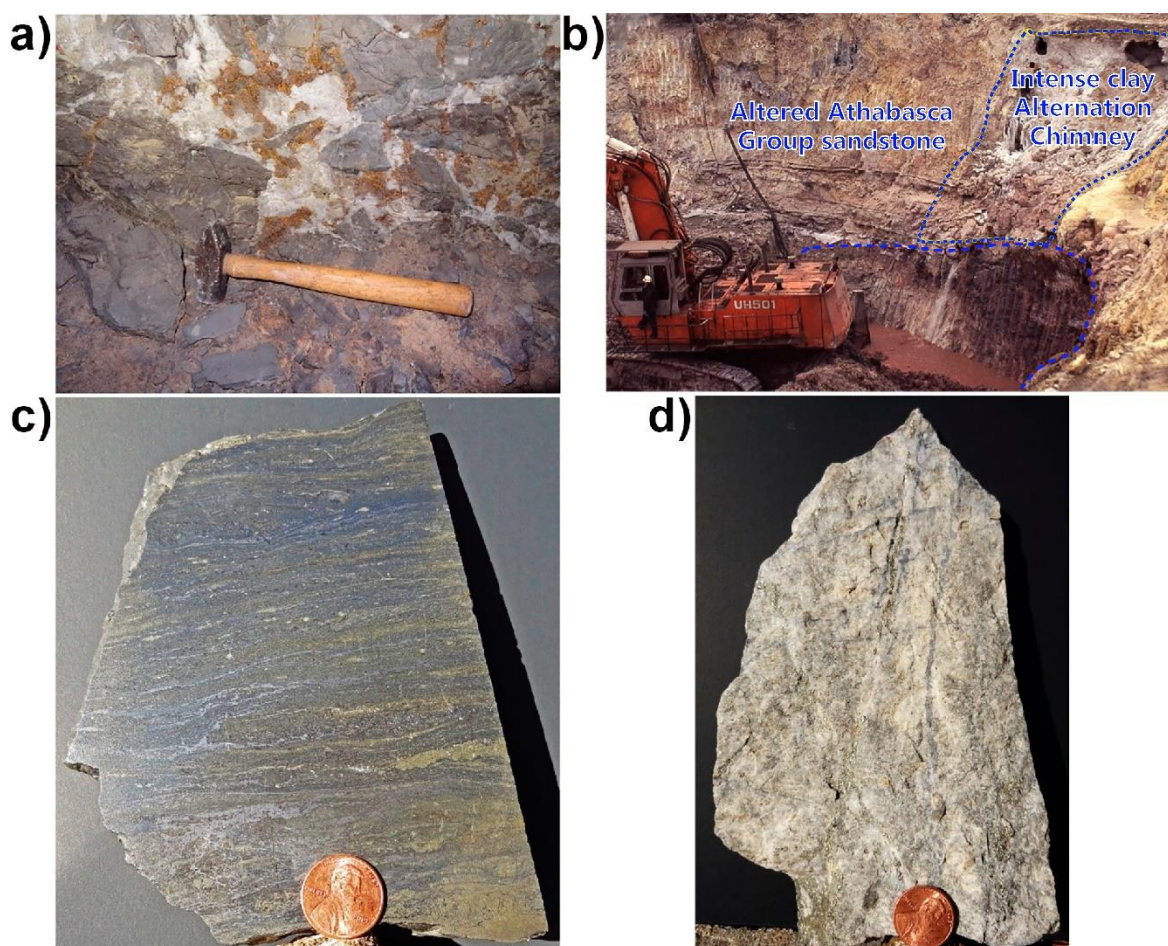


Figure 4 - Representative photographs of hydrothermal ore deposits. a) Sphalerite and sparry dolomite cementing breccia in the Elmwood mine of the Central Tennessee MVT district, USA. b) Unconformity-type uranium ore and associated alteration exposed in the open pit of the Rabbit Lake mine, northeast Saskatchewan, Canada (photograph by David Thomas, personal communication, 2022). c) Polished slab showing stratiform shale-hosted chalcopyrite-pyrite-galena mineralization from the Rammelsberg mine in the Kupferschiefer, Germany. d) Quartz monzonite transected by quartz and pyrite veins from the Butte, Montana porphyry copper deposit, USA. The diameter of the coin in c) and d) is 1.9 cm.

These examples demonstrate the fundamental role that groundwater plays in the formation of some important types of hydrothermal ore deposits in both sedimentary and igneous rocks. They illustrate how principles of physical hydrogeology, i.e., fluid flow, heat transport, and solute transport, can be used to gain insights into the processes that led to the deposits' origin.

The examples show that ore deposits can form from groundwater that has been set in motion by a variety of hydrogeologic mechanisms. The groundwater flow systems that form ore deposits can be regionally extensive, yet ore deposits form within a small fraction of the groundwater flow system. One factor that limits the occurrence of ore deposits within groundwater flow systems is that the geochemical reactants needed to induce the precipitation of ore constituents from groundwater are limited. Yet, as the examples show, physical factors are also important. For example, groundwater flow systems must be sufficiently long-lived for ore constituents to accumulate in large amounts and high concentrations.

To induce ore deposition, sometimes separate groundwater flow paths must converge such that groundwater of different compositions to mix. Both the magnitude and the gradient of groundwater temperature are strongly dependent on groundwater flow rate. Both the temperature magnitude and its gradient affect the degree of leaching of solutes from source rocks, the concentrations of the solutes during transport, and the mass of ore minerals precipitated. Changes in temperature and pressure of groundwater, mainly driven by changes in depth along its flow path, may cause some liquid groundwater to be converted to steam, which can induce precipitation of some ore minerals.

2.1 Sediment-Hosted Ore Deposits

Many of the world's most important ore deposits of lead, zinc, copper, uranium, barium, and fluorine occur in sedimentary rocks and are precipitated from groundwater. These deposits may also contain significant, albeit much lesser quantities of silver, cobalt, nickel, gold, and platinum group elements. In this section we discuss three deposit types that have been the subject of significant hydrogeologic study.

2.1.1 Mississippi Valley-Type Deposits

Mississippi Valley-type (MVT) deposits are products of highly saline groundwater (brines) with total dissolved solids contents typically between about 15 and 25 weight percent (equivalent to 150,000 to 250,000 ppm—parts per million—4 to 7 times greater than the salinity of seawater). Most of these brines originated as seawater that underwent evaporative concentration at the Earth's surface before descending into the subsurface. In some cases, the brines originated as meteoric water that acquired their salinity through dissolution of evaporites (Hanor, 1994; Kharaka and Hanor, 2004). These brines likely

became entrained within a regional groundwater flow system recharged by fresh meteoric water.

MVT deposits contain variable proportions of the ore minerals, sphalerite, galena, barite, and fluorite, and the non-economic gangue minerals, dolomite, calcite, and quartz. MVT deposits typically occur in carbonate rocks, rarely in sandstones, and were formed after their host rock formed. MVT deposits occur worldwide, but the type localities—which have been among the most studied—occur in the Mississippi River watershed of the central USA.

A further defining characteristic of MVT deposits, determined mainly from studies of fluids preserved in the rocks (fluid inclusions), is that they formed at anomalously high temperatures for their inferred formation depths of 1 to 2 km and typically in non-magmatic settings (i.e., about 80 to 150° C). Typical conductive geothermal gradients in the Earth's crust are about 25 to 35° C/km. MVT deposits formed at 1 to 2 km depth and given an average Earth surface temperature of 20° C, the temperatures would be 45 to 90° C. This temperature discrepancy has been particularly important in shaping understanding of the hydrology of MVT deposit formation. Garven and Freeze (1984a,b) recognized that advective heat transport, i.e., heat transported by flowing groundwater, could account for the observed high temperatures of MVT deposit formation, provided the groundwater was flowing fast enough. Using numerical modeling, they showed that uplift of a sedimentary basin could have discharged deep, hot brines to shallower depths in the crust fast enough to maintain the temperatures needed to form MVT deposits on the basin's edge. Figure 5 shows a topography-driven flow system and the associated temperature profile for a foreland basin under both hydrostatic and hydrodynamic conditions as numerically modeled by Garven and Freeze (1984a, 1984b). The hydrostatic condition was modeled by assigning a very-low hydraulic conductivity/permeability.

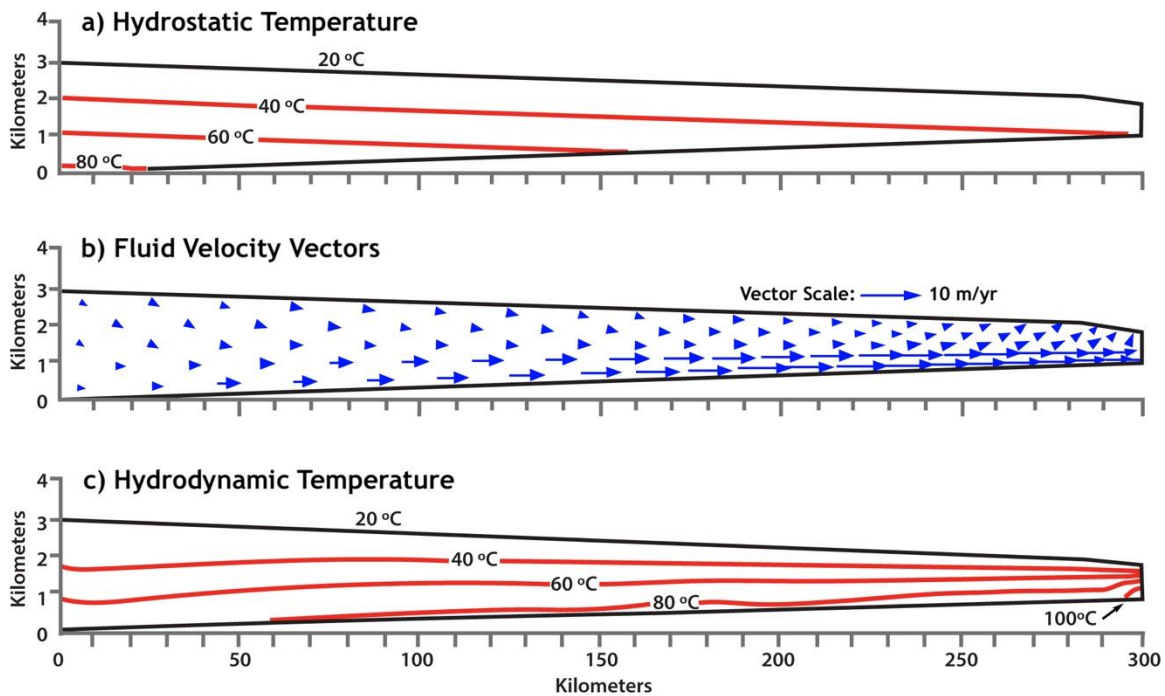


Figure 5 - Results of numerical models of fluid flow and heat transport in a generic foreland basin. In these models, temperature was set at a constant 20° C along the top boundary representing the land surface/water table, and a constant heat flux (70 mW/m²) was prescribed to the bottom boundary (redrawn from Garven and Freeze, 1984a,1984b).

The groundwater temperature profile (Figure 5a) results from heat transport occurring by thermal conduction only. If groundwater velocity is very low ($v < 0.1$ m/yr), e.g., because of assumed low permeability throughout the basin, then heat transport occurs primarily by conduction and the temperature increases roughly linearly with increasing depth from the land surface. In this case, temperature at 1 km depth at the edge of the basin (i.e., near the lower right corner of the profile), where MVT deposits commonly occur, is too low for MVT deposit formation. However, if groundwater velocity is high (Figure 5b and Figure 5c), then deep, hot groundwater is discharged toward the land surface at the basin edge, sufficiently elevating temperature there for MVT deposit formation. A zone of downward flowing water (a recharge zone) occurs on the left side of the profile and a zone of upward flowing water (a discharge zone) occurs on the right side of the profile. The groundwater temperature profile associated with the groundwater velocity profile is shown in Figure 5c. The temperatures associated with upwelling groundwater on the right margin of the profile are highly elevated relative to the temperatures shown in Figure 5a.

The numerical results shown in Figure 5 are for a steady-state model, in which the fluid flow and temperature fields have reached an equilibrium state in which they do not vary over time. The temperature elevation at the basin margin can be increased even more by transient pulses of increased groundwater flow rates and heat transport caused by rapid tectonic uplift (Garven, 1989; Garven et al., 1993; Garven and Raffensperger, 1997; Appold and Garven, 1999), and by focusing of groundwater through high

permeability zones (Garven et al., 1999). However, groundwater temperature at the basin margin does not increase indefinitely with increasing groundwater flow rate. Once the groundwater flow rate exceeds a critical threshold, then the temperature at the basin margin begins to decrease with further increases in groundwater flow rate. This occurs because further increases in groundwater velocity above this critical threshold cause the rapidly flowing groundwater to travel so quickly through the deeper, hotter parts of the basin that the groundwater becomes does not have time to extract as much heat from its surroundings.

The driving force for topography-driven flow is the gradient of the water table elevation created by uplift, as the topology of the water table tends to mimic the land surface topography (Hubbert, 1940; Tóth, 1963). In fact, in the model shown in Figure 5, the water table is coincident with the land surface. Therefore, groundwater that flows in response to water table gradients that mimics land surface topography is commonly referred to as topography-driven flow. Case studies of the Pine Point MVT deposit in the Northwest Territories, Canada (Garven, 1985) and MVT deposits in central USA (Bethke and Marshak, 1990; Garven et al., 1993; Appold and Garven, 1999; Appold and Nunn, 2005) show that topography-driven flow associated with uplift of the Western Canada sedimentary basin and Arkoma basin, respectively, could account for the high formation temperatures in these deposits. A similar deep groundwater flow mechanism is also proposed for the largest known MVT ore district in the world, the Southeast Missouri district, as depicted by Garven and others (1993) as shown in Figure 6.

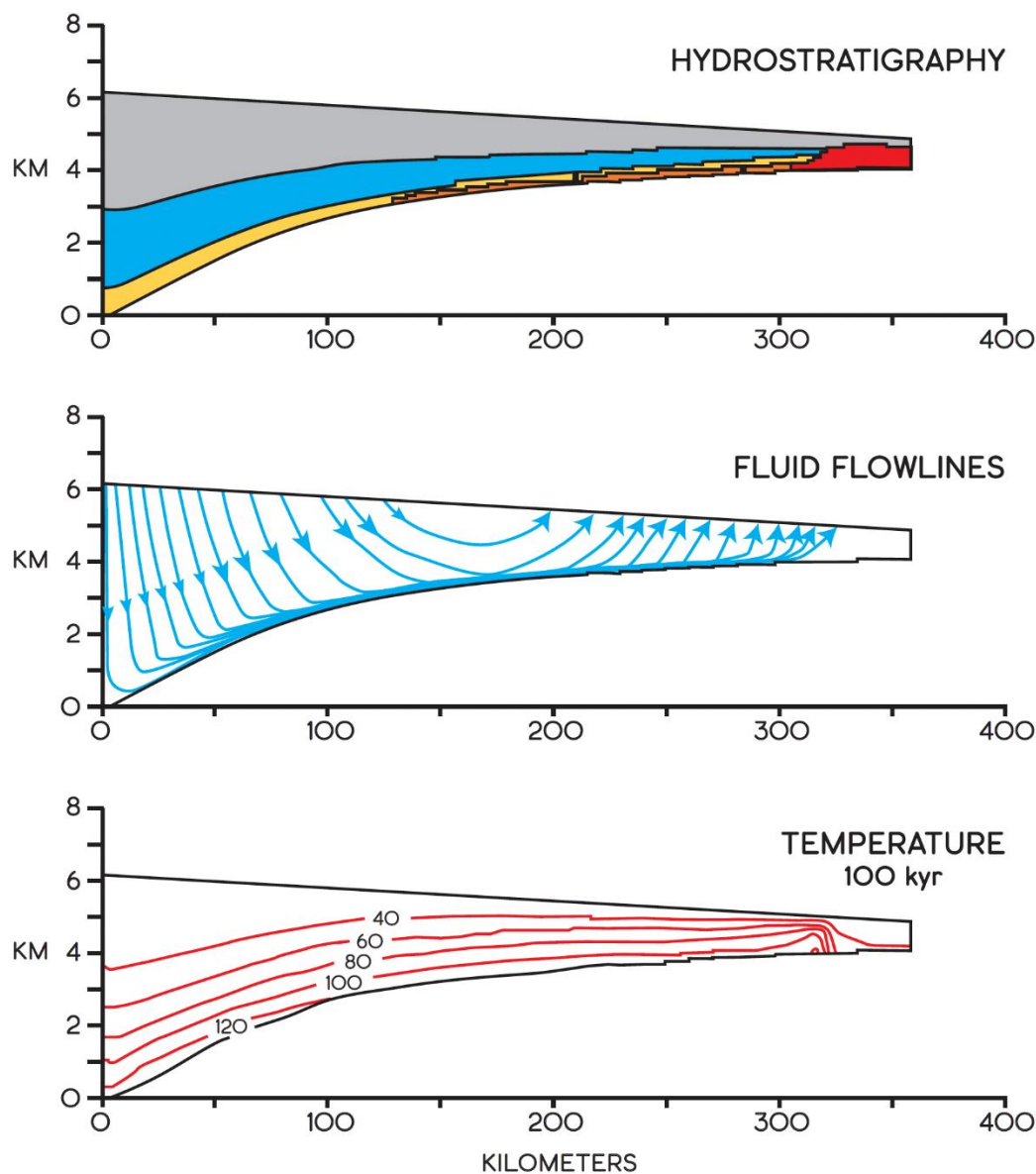


Figure 6 - Topography-driven flow model for MVT ore deposition in the Southeast Missouri district (after Garven et al., 1993). Metal-bearing brines are focused through a sandstone aquifer (yellow) and hydrogen sulfide-bearing brines are focused through a carbonate aquifer (blue) towards the basin margin. There, a low-permeability granitic basement high (red) redirects fluids upward, causing the metal-bearing and hydrogen sulfide-bearing brines to mix, leading to the precipitation of metal-sulfide ore minerals. Blue flowlines represent the calculated stream function, with a contour interval of $50 \text{ m}^3/\text{y}$ per meter width into the page. Red contour lines illustrate the temperature distribution.

The topography-driven flow system that formed the central USA MVT deposits (Figure 7) is an analog for other MVT deposits that formed from deep groundwater discharged from foreland basins. These flow systems evolved over geologically long intervals of time and competed with other mechanisms for driving fluids, though topography-driven flow seems to have dominated.

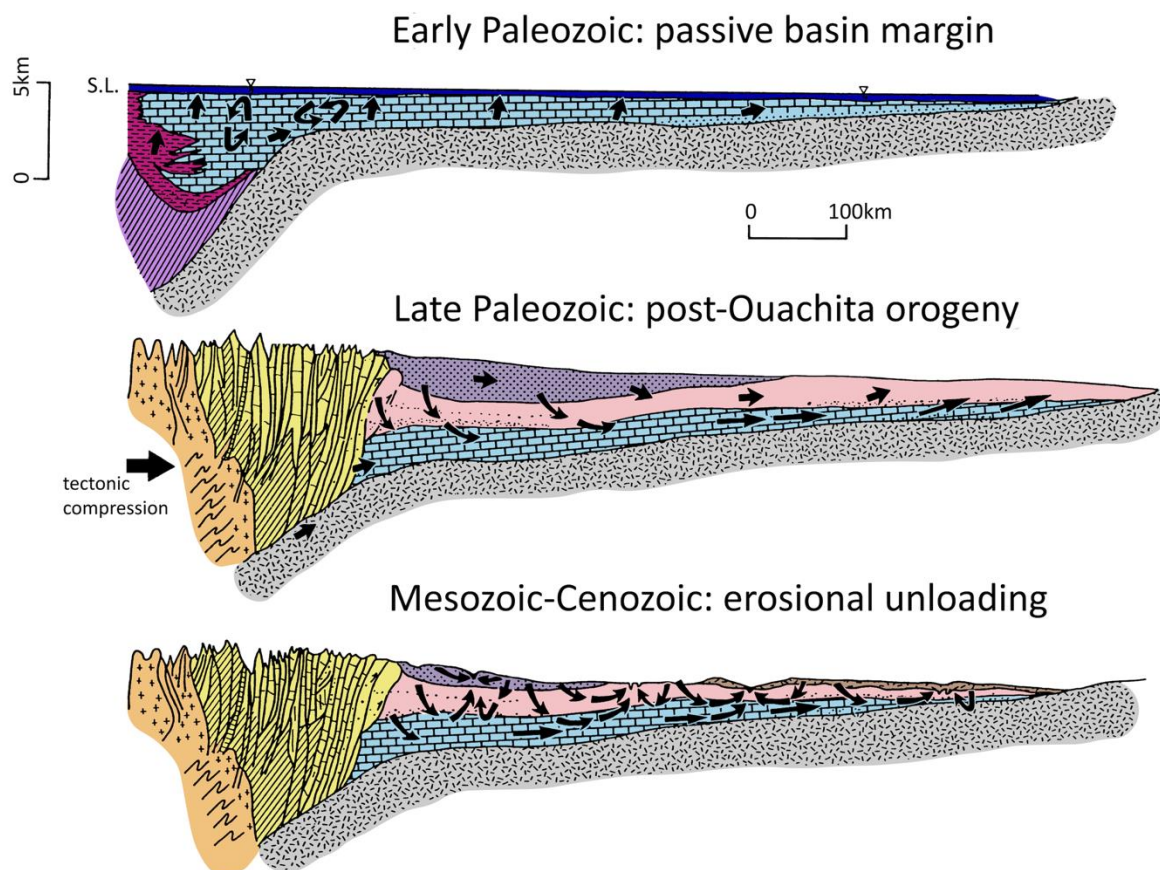


Figure 7 - Hydrogeologic evolution of the Arkoma foreland basin, based on the tectonic history of the Ouachita orogeny. MVT ore deposit formation is known to have peaked in the Late Paleozoic when brines bearing dissolved MVT ore constituents migrated northward due to uplift and subaerial emergence of the Arkoma foreland basin. Redrawn from Garven et al. (1993).

Collision of North America with Gondwanaland during the Alleghanian orogeny in the Pennsylvanian and Permian periods led to uplift of the Ouachita Mountains fold-and-thrust belt. Thickening of the lithosphere in the Ouachita Mountains depressed the surrounding lithosphere, creating space for the formation of the Arkoma Basin, a foreland basin (Figure 8). As the Ouachita Mountains weathered, sediment was shed into the Arkoma Basin and accumulated. The reduced weight of the weathered Ouachita Mountains caused the lithosphere to rebound and the Arkoma Basin to be uplifted, thus initiating topography-driven flow in the Arkoma Basin. Eventually the topographic gradient of the Arkoma Basin would have been diminished by weathering and erosion, though the topography-driven groundwater flow system is likely to have persisted for tens of millions of years (Appold and Garven, 1999).

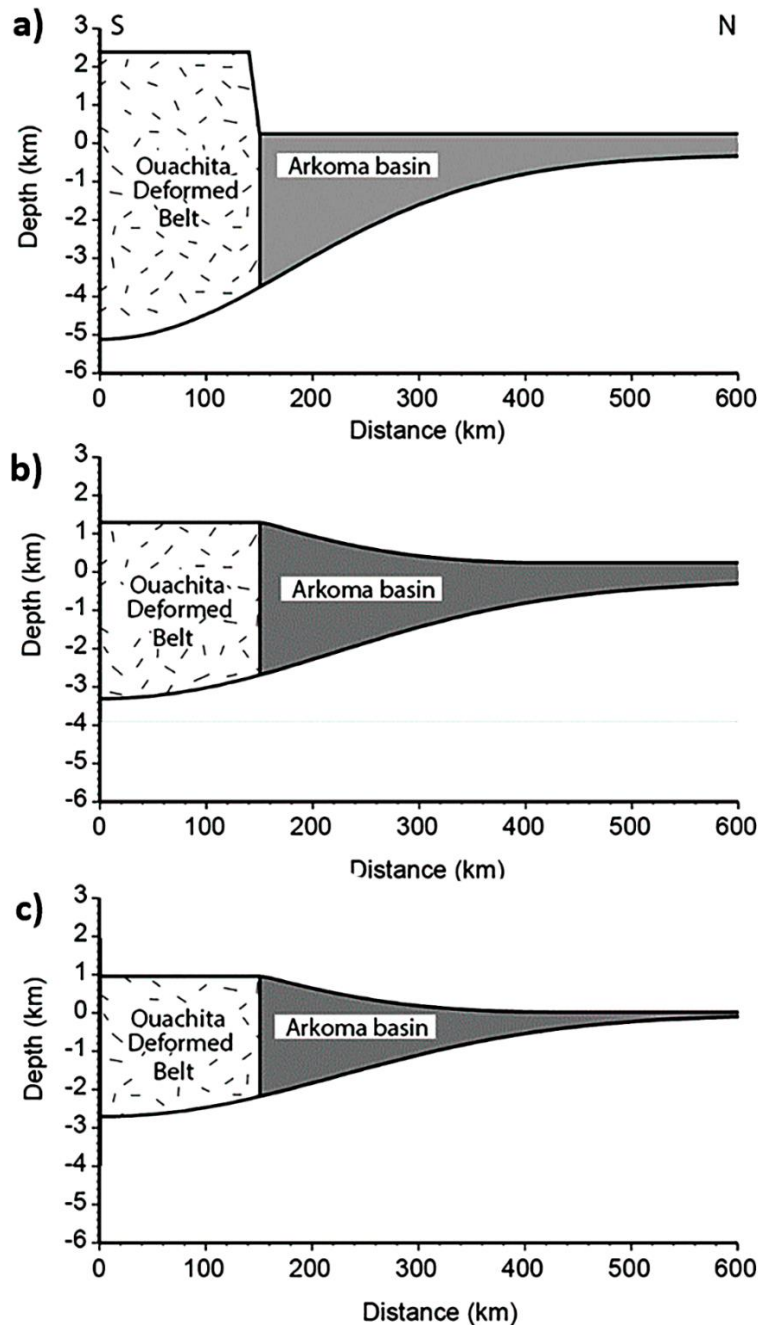


Figure 8 - Conceptual model for the uplift of the Arkoma Basin that initiated the topography-driven flow system likely responsible for the formation of MVT deposits in the central USA (after Nunn and Lin, 2002; with modifications from Appold and Nunn (2005).

- Emplacement of thrust sheets forming the Ouachita Mountains (cross-hatched pattern) leads to down warping in the adjacent crust. Infilling by sediments results in the formation of the Arkoma foreland basin (shaded pattern).
- Erosion of the Ouachita Mountains leads to flexural rebound as the mass is reduced and sediment is transported northward into distal portions of the North American craton, causing tilting and uplift of the Arkoma Basin, which provides the primary driving force for fluid flow. Maximum elevation and topographic gradient in the Arkoma Basin are reached when the elevation of the Ouachita Mountains equals the elevation at the southern margin of the basin.
- Continued uplift and erosion strip the Permian and much of the Pennsylvanian sedimentary cover from the basin.

For topography-driven flow systems to transport heat by advection effectively, permeability must be high not only in the aquifer that conveys the ore-forming groundwater but also in the recharge area. When groundwater velocity is too low in either the aquifer or the recharge area, then the only way to reach MVT ore-forming temperatures at the basin margins is to have anomalously high regional heat flow. To achieve this, either one or more stratigraphic units above the aquifer must provide substantial thermal insulation (e.g., due to high organic shale or coal content, or high porosity); or the depth of MVT deposit formation would need to be significantly greater than previously estimated.

Another mechanism for elevating temperature in topography-driven flow systems has been proposed by Deming (1992), in which transient and episodic groundwater convection cells in basement rocks mine heat from depth and deliver it to shallower groundwater. However, Garven and Raffensperger (1997) questioned whether the high permeability required to form convection cells could exist in deep basement rock on a regional scale.

Although topography-driven flow systems in orogenic settings may persist for tens of millions of years, it is unlikely that much time was available for MVT ore formation. This is because fresh meteoric water recharge entering the flow system tends to flush the connate saline groundwater from the system over shorter time spans, perhaps within only a few million years (Bethke, 1986; Deming and Nunn, 1991; Cathles, 1993; Appold and Garven, 1999; Appold and Nunn, 2005). Thus, eventually the groundwater that arrives at the sites of MVT ore deposition in a topography-driven flow system is too dilute to account for the high ore fluid salinities preserved in fluid inclusions.

In addition, the temperature of groundwater arriving at the ore formation sites on the basin margin initially is not high enough for MVT ore formation but takes time to build to the necessary level as groundwater velocity increases with uplift. Thus, only a relatively narrow window of time exists when groundwater arriving at the basin margin is simultaneously saline and hot enough to form MVT ore deposits. In the MVT district of Southeast Missouri, USA, this window of time may have been on the order of several hundred thousand years (Appold and Garven, 1999) and is likely an analog for other MVT deposits, such as the Polaris Zn-Pb district in Arctic Canada (Mathieu et al., 2022).

If relatively short periods of time on the order of several hundred thousand years were available to form MVT deposits, then this places important further constraints on their origin. Figure 9 is a mass balance diagram that shows the length of time needed to deposit all the lead in the Viburnum Trend MVT deposits of the Southeast Missouri district as a function of average linear velocity of groundwater and the concentration of dissolved lead in the groundwater. The numerical modeling studies cited above suggest that maximum flow rates in topography-driven flow systems are probably on the order of meters per year (m/y). If so, then groundwater entering the Viburnum Trend would have needed dissolved lead concentrations on the order of tens to hundreds of ppm to deposit all of the lead ore

there between 100,000 and 1 million years (the area of the gray triangle in Figure 9. Garven (1985) and Smith-Schmitz and Appold (2018) found that for the Pine Point, Illinois-Kentucky, and Central Tennessee MVT districts, zinc concentrations of ones to tens of ppm in the groundwater entering those districts at average linear velocities of several m/y would have been sufficient to deposit all of the known zinc ore within those districts in under 1 million years.

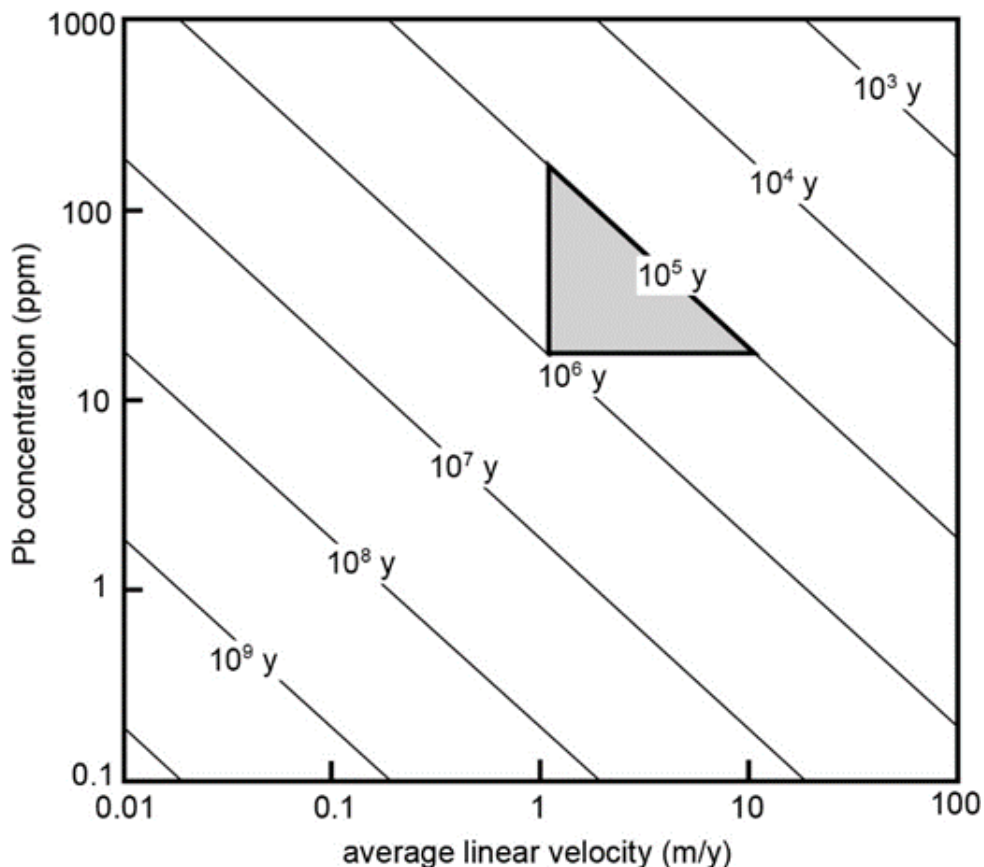


Figure 9 - Contour plot showing the length of time needed to deposit all the lead ore in the Viburnum Trend of the Southeast Missouri district, USA, as a function of average linear velocity and total lead concentration in groundwater if all the lead were precipitated. If between 10^5 and 10^6 years were available for ore formation and groundwater entered the Viburnum Trend at an average linear velocity of 1 to 10 m/y, then the groundwater must have contained tens to hundreds of ppm lead to deposit all the lead in the Viburnum Trend within the available time. The gray triangle delineates the limits of these three constraints (after Appold and Garven, 1999).

This raises the question of what the actual lead and zinc concentrations in MVT ore fluids were during ore formation. Numerous studies have attempted to answer this question through analysis of fluid inclusions and through chemical partitioning theory based on the concentration of zinc in calcite¹. These studies suggest that lead and zinc

¹ Czamanske et al., 1963; Pinckney and Haffty, 1970; Shepherd and Chenery, 1995; Appold et al., 2004; Huizenga et al., 2006; Piqué et al., 2008; Stoffell et al., 2008; Wilkinson et al., 2009; Appold and Wenz, 2011; Wenz et al., 2012; Fusswinkel et al., 2013; Pelch et al., 2015; Bouhlef et al., 2016; Smith-Schmitz and Appold, 2018; Field et al., 2020).

concentrations on the order of ones to hundreds of ppm in MVT deposit-forming groundwater are common and may reach thousands of ppm.

If the time available for ore formation was relatively short and the concentrations of lead and zinc in the ore-forming groundwater were high, then this has implications for the type of precipitation mechanism that was possible. Lead and zinc are not very soluble in the presence of sulfide, meaning that only relatively low concentrations of these solutes can coexist. Consequently, long periods of time are needed to form an ore deposit from groundwater simultaneously carrying lead, zinc, and sulfide (e.g., Anderson, 1975; Sverjensky, 1986). In short, any precipitation mechanisms like cooling, pH increase, or dilution that rely on the simultaneous transport of lead, zinc, and sulfide in a single fluid are unlikely to have been active in forming MVT deposits.

Lead and zinc are much more soluble in the presence of sulfate rather than sulfide, so a more efficient and likely precipitation mechanism would be one in which lead and zinc were transported in groundwater with sulfate, and the sulfate was reduced to sulfide at the site of ore deposition. Another possibility is that lead and zinc were transported in one fluid and sulfide in a second fluid and ore deposition occurred where the two fluids mixed. For all of these precipitation mechanisms, lead and zinc transport are aided by high groundwater salinity, as chloride—one of the most abundant solutes in most saline groundwater—bonds chemically with lead and zinc to form metal-chloride complexes, greatly increasing the solubility of both lead and zinc.

Some other fluid flow mechanisms that have been proposed for MVT ore formation are less capable than topography-driven flow (Figure 10a) of producing the rapid groundwater flow rates (> 1 m/y) and thus the amount of advective heat transport needed to raise temperatures to the levels observed in MVT deposits. Hydrothermal free convection cells may be viable for rift-type basins with ultra-thick sandstone aquifers (Figure 10b). Mechanical compaction of sediment because of rapid burial or thrust fault-loading tectonics in a sedimentary basin (Figure 10c and Figure 10d) can produce temporally continuous regional-scale groundwater flow but at velocities that are about a thousand times too slow to produce temperatures high enough for MVT deposit formation at the basin margin (Cathles and Smith, 1983; Bethke, 1985). However, if overpressure builds in a sedimentary basin (e.g., due to high sedimentation rate, low permeability, high matrix compressibility, sea level rise, or the generation of hydrocarbons) and from time to time the overpressure is released suddenly (e.g., during an earthquake, Figure 10e), then pulses of groundwater flow can be produced that are rapid enough to raise temperatures to MVT levels at the basin margin (Sharp, 1978; Cathles and Adams, 2005). Still, many such pulses of groundwater flow are needed to form large ore deposits, as the volume of each individual pulse of groundwater flow is small.

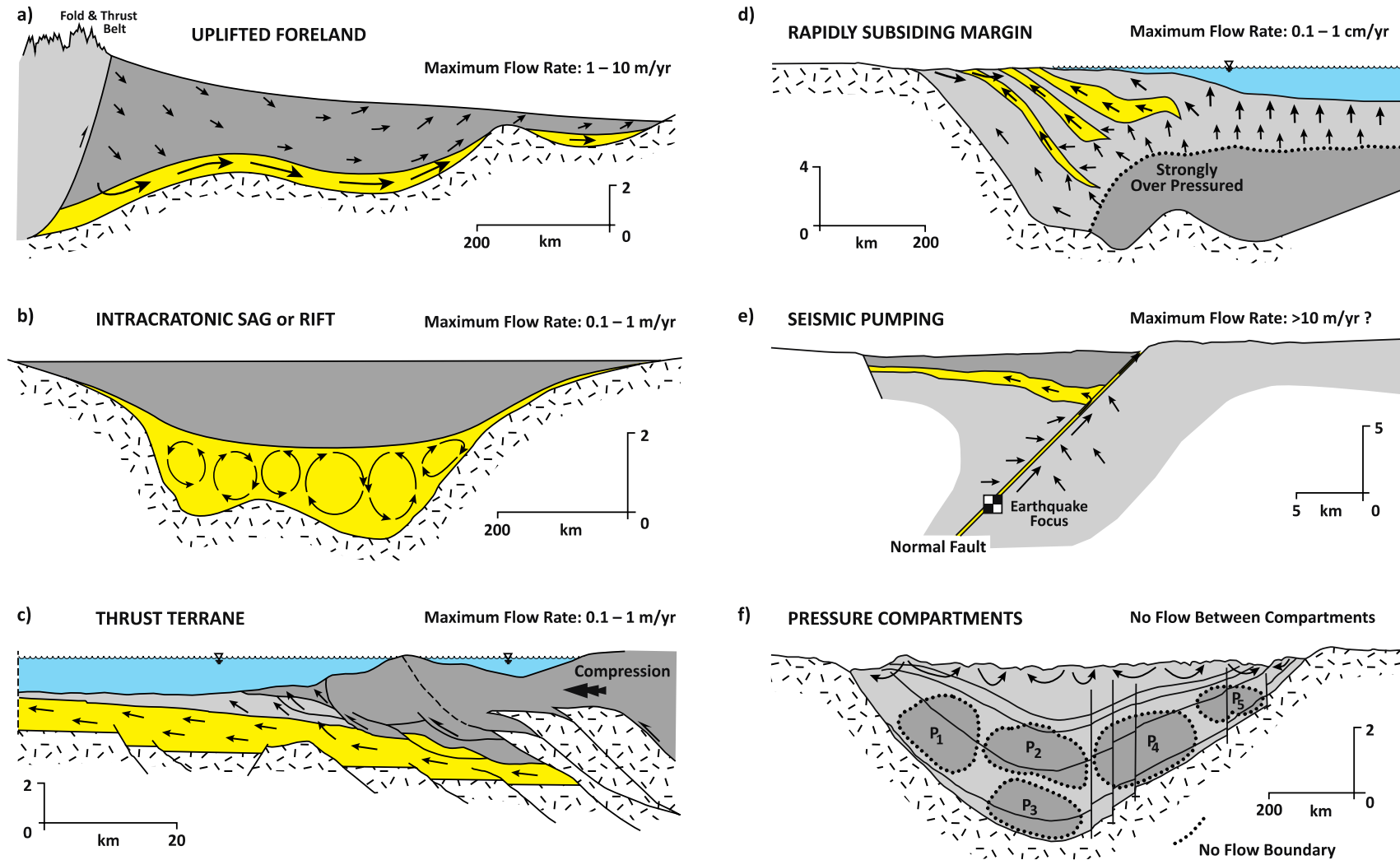


Figure 10 - Mechanisms for fluid flow in sedimentary basins: a) topography, b) thermal convection, c) tectonic deformation, d) sediment compaction, e) seismic pumping, and f) pressure compartmentalization (after Garven, 1995). Yellow units depict aquifers and black arrows represent generalized flow direction/magnitude.

Compaction of a sedimentary basin by lateral tectonic compression may also cause regional scale groundwater flow (Figure 10c). Ge and Garven (1989, 1992, 1994) and Deming and others (1990) found that if compression events were rapid enough, they could cause short-lived pulses of groundwater flow rapid enough to transport the heat needed for MVT deposit formation on the basin's margin. Again, many such pulses would be needed to form a large ore deposit. Thus, the capability of geologic mechanisms to produce and sustain large pressure gradients is vital for the effective advective heat transport required for ore formation. In some settings, high permeability geologic media such as faults and breccias can promote advective heat transport, with heating commonly localized along such features. Contrary to the thinking of most hydrogeologists, some petroleum geologists attribute sediment diagenesis and mineralization in basins as due solely to chemical diffusion, not fluid flow. According to this view, basins undergo "pressure compartmentalization" (Figure 10f) over hundreds of millions of years (Bradley and Powley, 1994)

2.1.2 Evaluating Conditions for MVT Deposit Formation

A series of exercises provides readers an opportunity to learn more about MVT deposit formation and use analytical solutions to the differential equations for groundwater flow and heat transport to explore the conditions needed for MVT ore formation near the shallow margin of a sedimentary basin.

- [Introduction to Part I exercises](#) ↓ that evaluate the influence of temperature on ore deposit formation;
- [Exercise 1](#) ↓ evaluates geothermal gradient;
- [Exercise 2](#) ↓ considers groundwater flow patterns;
- [Exercise 3](#) ↓ provides an analytical solution for calculating hydraulic head in a simplified groundwater flow system;
- [Exercise 4](#) ↓ provides an analytical solution for calculating temperature in a simplified groundwater flow system;
- [Exercise 5](#) ↓ explores temperature distribution in a system with lower hydraulic conductivity than the one considered in Exercise 4;
- [Exercise 6](#) ↓ considers groundwater flow path length and travel time;
- [Exercise 7](#) ↓ evaluates lead concentration necessary to form an MVT deposit; and,
- [Exercise 8](#) ↓ evaluates the pH necessary to form an MVT deposit.

2.1.3 Unconformity-Type Uranium Deposits

Like MVT deposits, unconformity-type uranium deposits form from saline groundwater but with even higher total dissolved solids contents—between about 20 and 35 weight percent (Pagel et al., 1980; Ypma and Fuzikawa, 1980; Wilde et al., 1989).

Unconformity-type uranium deposits form at overall higher temperatures than MVT deposits—between about 110 and 240°C.

Unconformity-type uranium deposits have historically been a major global source of uranium, though the most important examples are limited geographically to the Athabasca Basin in Saskatchewan and Alberta, Canada, and to the McArthur Basin in the Northern Territory, Australia. Unconformity-type uranium deposits obtain their name from the fact that they occur near the unconformity separating Archean to Paleoproterozoic metasedimentary rocks from overlying Mesoproterozoic sediments, mainly sandstone. Mineralization may occur either in the sediment or in the basement but is concentrated where faults intersect the unconformity. Mineralization also tends to be associated with graphite-rich rocks in the basement. The principal ore mineral is uraninite and the principal gangue minerals are chlorite, hematite, quartz, and white mica minerals. Mineralization is generally thought to have formed at depths greater than 5 km, though recent work suggests that mineralization may in fact generally have formed at shallower depths less than about 3 km (Chi et al., 2018).

Unlike MVT deposits, the operative groundwater flow mechanism for unconformity-type uranium deposits need not be effective at heat transport because temperature at the unconformity could have reached ore-forming levels from conductive heat transport alone Figure 11. The operative fluid flow mechanism need only have produced fluid flow rates high enough to allow the ore deposits to form within a geologically reasonable period of time of up to tens of millions of years (Cui et al., 2012).

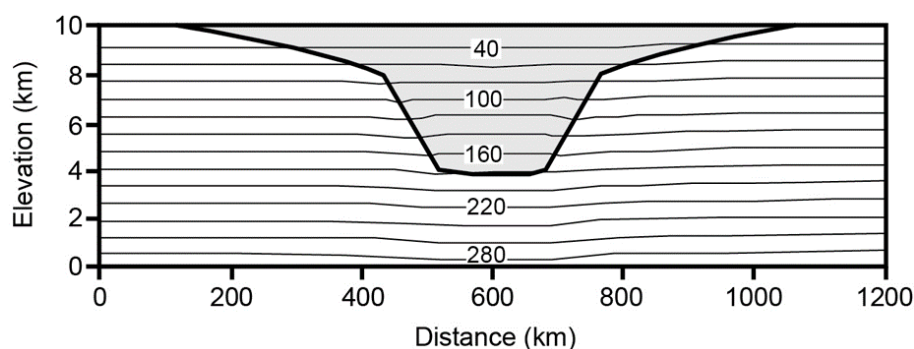


Figure 11 – Predicted temperature field due to conduction in a generic intracratonic sedimentary basin (shown in gray) resembling basins that host unconformity-type uranium ore deposits. The thick black line represents the unconformity and contour lines represent isotherms in degrees Celsius. Sediments in the basin had thermal conductivities ranging from 2.5 to 3.5 $\text{W m}^{-1} \text{K}^{-1}$. The base of the model was assigned a constant heat flux of 60 mW/m^2 while the top of the model was assigned a constant temperature of 20°C (after Raffensperger and Garven, 1995a).

Sedimentary basins in which unconformity type uranium deposits occur are thought to have been submarine at the time of ore formation, thus topography-driven flow is unlikely to have been a viable driving force for ore-forming groundwater. This is because the relatively constant elevation of sea level would not have produced a significant hydraulic head gradient across the basin. Instead, ore-forming groundwater is thought to

have been driven mainly by free convection in response to temperature-related density gradients in the groundwater (Figure 12). In this scenario, hotter groundwater at greater depths would have had lower density than cooler groundwater at shallower depths, causing the shallower groundwater to sink and the deeper groundwater to rise in a circular pattern called a convection cell.

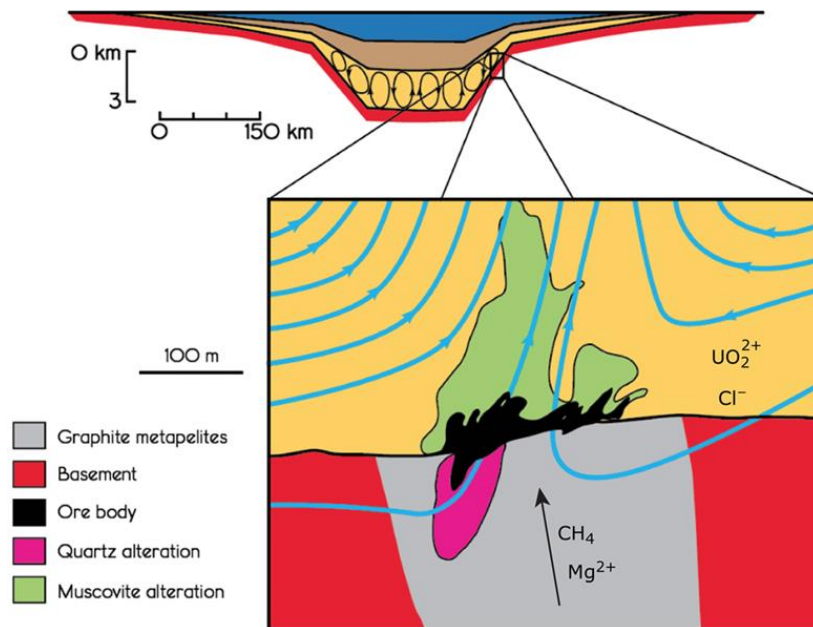


Figure 12 – Conceptual diagram showing the flow of groundwater in free convection cells in a thick sandstone layer at the base of a sedimentary basin corresponding to Figure 7. Some of the groundwater is able to penetrate the upper part of the basement, where dissolved uranium in the groundwater becomes chemically reduced, e.g., by reaction with methane derived from the hydrothermal alteration of graphite, causing the uranium to precipitate near the basement-sandstone contact (after Raffensperger and Garven, 1995b).

Whether or not the conditions for free convection are met can be evaluated by the Rayleigh Number (Ra), which is related to the effective permeability (k') and defined by Equation (1).

$$Ra = \frac{g\rho\beta_T k' \Delta T H}{\mu D} \quad (1)$$

where:

g = gravitational acceleration (m/s^2) (LT^{-2})

ρ = groundwater density (kg/m^3) (ML^{-3})

β_T = thermal expansivity of the groundwater (K^{-1})

k' = effective permeability defined in Equation (2), (L^2)

ΔT = temperature difference across an interval of thickness H (K)

H = thickness H (L)

μ = dynamic viscosity ($\text{kg m}^{-1} \text{s}^{-1}$) ($\text{ML}^{-1}\text{T}^{-1}$)

D = thermal diffusivity (m^2/s) (L^2T^{-1})

$$k' = \frac{4k_x k_z}{(\sqrt{k_x} + \sqrt{k_z})^2} \quad (2)$$

where:

k_x and k_z = intrinsic permeabilities (m^2) (L^2)

x and z = Subscripts indicating coordinate directions

The Rayleigh Number formulation in Equation (1) was derived for a saturated, homogeneous, anisotropic, laterally infinite, and horizontal porous medium; free convection should develop when $Ra \geq 4\pi^2$.

The conditions for which Equation (1) was derived involve simplifying assumptions that cannot be attained in nature. Heterogeneity is one example of a complicating factor (Simmons et al., 2001, 2008; Nield and Simmons, 2007). High permeability can trigger free convection at lower Rayleigh numbers than the critical $4\pi^2$ value noted above by promoting instabilities like fingering along interfaces between fluids of different densities. However, more randomly distributed heterogeneity is more likely to dissipate convection through dispersive mixing. In contrast, ordered heterogeneity, such as produced from regularly spaced fracture sets, facilitates convection. Nonetheless, at a minimum, Equation (1) is qualitatively useful in that it shows that free convection is promoted by high parameter values in the numerator and low parameter values in the denominator.

Numerous numerical hydrologic modeling studies have been conducted to understand the origin of unconformity-type uranium deposits, evaluating various possible hydrologic flow and precipitation mechanisms (Raffensperger and Garven, 1995a,b; Cui et al., 2010, 2012; Li et al., 2016; Chi et al., 2018). These studies confirmed that free convection was likely the dominant mechanism of fluid flow in the formation of unconformity-type uranium deposits. In addition, they found that sedimentary basins having a total thickness of at least 3 km containing a permeable basal sandstone with a thickness on the order of 2 km and a horizontal hydraulic conductivity of at least 50 m/y can sustain convection cells that drive groundwater at velocities on the order of centimeters to meters per year, even for high levels of anisotropy in the sandstone. Given that uranium concentrations in the ore-forming groundwater may have reached 600 ppm (Richard et al., 2016), these flow rates would easily have allowed the world's major unconformity-type uranium deposits to have formed within tens of millions of years, and possibly in as little as thousands to tens of thousands of years (Raffensperger and Garven, 1995b). Geochronologic data from Kyser and others (2000) for several unconformity-type uranium deposits suggest that they formed in tens to hundreds of millions of years.

Convection cells were largely confined to the sandstone layer if its hydraulic conductivity was at least two orders of magnitude greater than that of the basement. However, even for large sandstone-basement hydraulic conductivity contrasts (i.e., greater than two orders of magnitude) some groundwater could penetrate the basement to depths of 1 to 2 km below the unconformity, though at very low velocities (Figure 13). Free convection in sedimentary basins that host unconformity-type uranium deposits did not require unusual thermal conditions but could occur for typical modern continental heat flow values of around 60 mW/m^2 and geothermal gradients of 25 to 35° C/km (Raffensperger and Garven, 1995a; Cui et al., 2010). Free convection may have been more achievable in the Proterozoic because the interior of the Earth was hotter in the past than it is now, though the quantitative evolution of heat flow and the temperature of Earth's interior over time remains uncertain because of large uncertainties in the distribution of sea floor ages and the rate of growth of the continents (Jaupart and Mareschal, 2011).

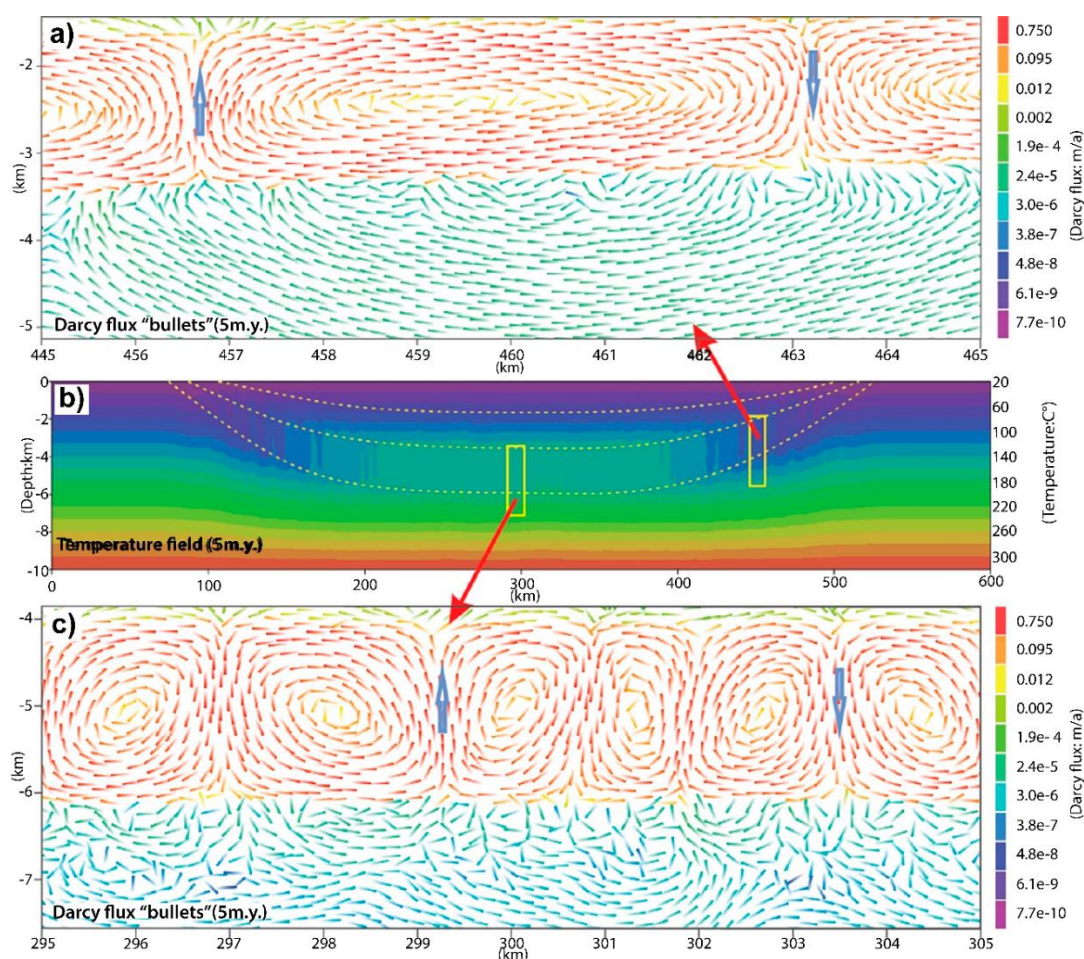


Figure 13 - Groundwater velocity and temperature field predicted from numerical modeling of Cui and others (2012) for a generic sedimentary basin resembling those that host unconformity-type uranium deposits. a) Groundwater velocity field centered on the basement unconformity near the right margin of the basin surrounded by the right yellow rectangle in (b). b) Groundwater temperature field. Yellow dashed lines represent major hydrostratigraphic divisions within the basin. c) Groundwater velocity field near the basement unconformity and depocenter of the basin surrounded by the central yellow rectangle in (b). Velocity vectors are represented as bullets where the thicker end of the bullet points is the direction of flow and the color represents the magnitude of the velocity.

Sediment compaction is unlikely to have made much of a contribution to groundwater flow in unconformity-type uranium ore formation, producing only small overpressures (i.e., small increases in fluid pressure above hydrostatic pressure) where permeability is sufficiently low, and thus producing only small pressure gradients to drive flow (Chi et al., 2013). Much larger overpressures and pressure gradients could have been caused by tectonic compression, provided that the strain rate was high enough, i.e., greater than about $7 \times 10^{-11} \text{ s}^{-1}$ (Li et al., 2020). The high overpressures caused by tectonic compression are likely to have destroyed any convection cells but could have increased the permeability of basement fault zones. Thus, unconformity-type uranium ore formation may have been characterized by alternating intervals of tectonic compression and quiescence. During intervals of tectonic compression, the formation of convection cells and thus uranium ore formation would have been inhibited but fault permeability would have been increased. During intervals of tectonic quiescence, overpressures would have dissipated, and convection cells would have formed, resulting in uranium mineralization.

The solubility of uranium is a strongly dependent on redox potential, with uranium in the +6 state being much more soluble than uranium in the +4 state. Thus, genetic models for uranium transport and ore precipitation center on mechanisms that alter the redox potential of the ore fluid. In the case of unconformity-type uranium deposits, convection of oxidizing meteoric groundwater would have leached high concentrations of uranium from sandstone. Some of this uranium-rich meteoric groundwater would then have descended into upper basement rock, where it may have dissolved additional uranium (Cui et al., 2012); upon encountering vertically faulted graphite-rich zones in the basement, the groundwater would have been channeled upward toward the unconformity.

Methane, produced from deeper hydrothermal alteration of graphite, would also have ascended the faulted zones. Numerical modeling by Raffensperger and Garven (1995b) shows that this methane would have reduced and precipitated uranium in greatest amounts near the unconformity. Iron in aluminosilicate minerals may have served as a further reductant of the uranium (Komninou and Sverjensky, 1996). Raffensperger and Garven's (1995b) model also produced a halo of chlorite and muscovite alteration around the uranium mineralization, consistent with field observations.

2.1.4 Sediment-Hosted Stratiform Copper Deposits

Sediment-hosted stratiform copper (SHSC) deposits are the second largest global copper resource after porphyry copper deposits (Sillitoe, 2012). The deposits are characterized by mineralization consisting of fine-grained, disseminated copper sulfide minerals occurring in thin—generally less than several meters thick—layers oriented parallel to the bedding of the host rock and extending for up to several kilometers laterally. The deposits tend to occur in carbonaceous, chemically reducing, fine-grained clastic or carbonate rocks near their contact with underlying oxidizing red beds and evaporites in rift basins.

Numerous significant SHSC deposits around the world containing at least one million tons of ore have been documented (Kirkham, 1989; Misra, 2000). However, three deposits or deposit groups (districts) predominate in size: the Central African copper belt, the Udokan deposit (Russia), and the Kupferschiefer (Poland-Germany).

SHSC deposits formed from saline groundwater with total dissolved solids contents ranging from about 20 to 45 weight percent and at temperatures between about 80° and 380° C (Strengel-Martinez et al., 1993; Heijlen et al., 2008). The groundwater likely acquired its high salinity by dissolving evaporites. This high salinity enabled the groundwater to leach copper effectively from red beds that it subsequently encountered along its flow path. In addition, interaction with red beds raised the redox potential of the groundwater, increasing its ability to oxidize minerals. When the copper-enriched groundwater then encountered organic-rich sediments, sulfate in the groundwater became reduced, leading to the precipitation of copper and other metal sulfide minerals. These minerals typically have a zoned distribution, probably governed by differential rates of diffusion of the aqueous metal ions in the pore water of the fine-grained, organic-rich sediments (Large and Small, 2000).

Various models have been proposed for how groundwater was driven through this sequence of lithologies. In the following part of this section, three possible mechanisms are discussed: thermally driven free convection, sediment compaction, and deep-fault seismic activity (Figure 10).

Because of the common occurrence of SHSC deposits in rift basins—which tend to have high heat flow and thus high temperature gradients that promote high Rayleigh numbers as defined by Equation (1)—free convection is widely regarded as the likely mechanism for groundwater flow. A conceptual diagram of SHSC ore formation by free convection is shown in Figure 14.

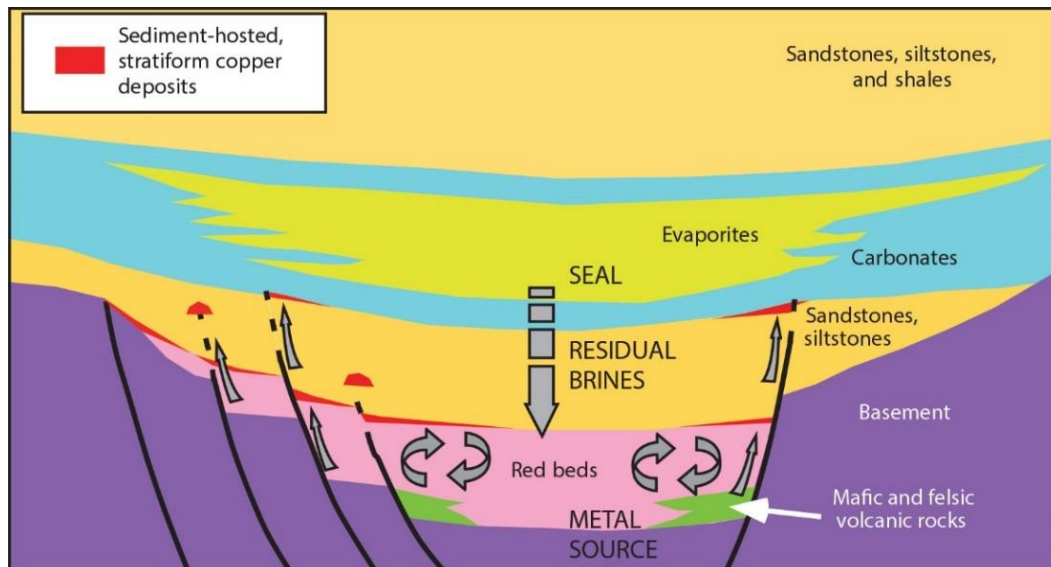


Figure 14 – Conceptual diagram for the hydrodynamics of SHSC ore formation in a rift basin. Groundwater likely acquired its high salinity to become brine by dissolving evaporite minerals from the seal, causing the groundwater to sink due to its increased density. As the saline groundwater descended, its temperature gradually increased, causing its density to decrease until it became low enough for the groundwater to rise, initiating free convection. In some SHSC deposits, free convection may have been confined to the red bed layer, as shown in the diagram. In other SHSC deposits, the convection cells may have extended higher to the base of the evaporite seal (from Hitzman et al., 2010).

In the Kupferschiefer, this high heat flow combined with lateral contrasts in thermal conductivity between the rift-filling volcanic rocks and red beds and rift-bounding basement horsts may have been sufficient to generate kilometer-scale convection cells with flow rates on the order of 10 cm/y (Jowett, 1986). Convection was also shown to be possible in the Central African Copper Belt by Koziy and others (2009). In their numerical models, convection cells extended upward to the base of the evaporite seal, dissolving some of it, and thereby progressively increasing the salinity and density of the groundwater, further promoting convection. Indeed, without this increase in the shallower groundwater salinity by ongoing evaporite dissolution, fluid flow rates in the convection cells would decrease by about an order of magnitude. The increased salinity and density of the groundwater caused by evaporite dissolution helped the convection cells penetrate the low permeability basement by giving the groundwater a stronger propensity to sink, allowing it to leach the extra copper needed to account for the size of the Central African Copper Belt ore deposits. The red beds in this region are too thin to have been the sole source of copper in the ore deposits.

Another mechanism for fluid flow in the Kupferschiefer may have been compaction of red bed sediments by deposition of the overlying fine-grained clastic sediments and evaporites (Cathles et al., 1993). The fluids expelled by the compaction may have ascended rift basin-bounding faults until they reached the chemically reducing fine-grained sediments, through which they then migrated sub-laterally. The permeability of these fine-grained sediments may have been increased by overpressures that built beneath the evaporite seal, causing the pores of the sediments to become enlarged.

Compaction-driven groundwater flow in the red bed sequence because of loading by overlying sediments may also have led to SHSC ore formation in the White Pine district in northwestern Michigan, USA (Swenson et al., 2004). The possible evolution of this groundwater flow system is shown in Figure 15.

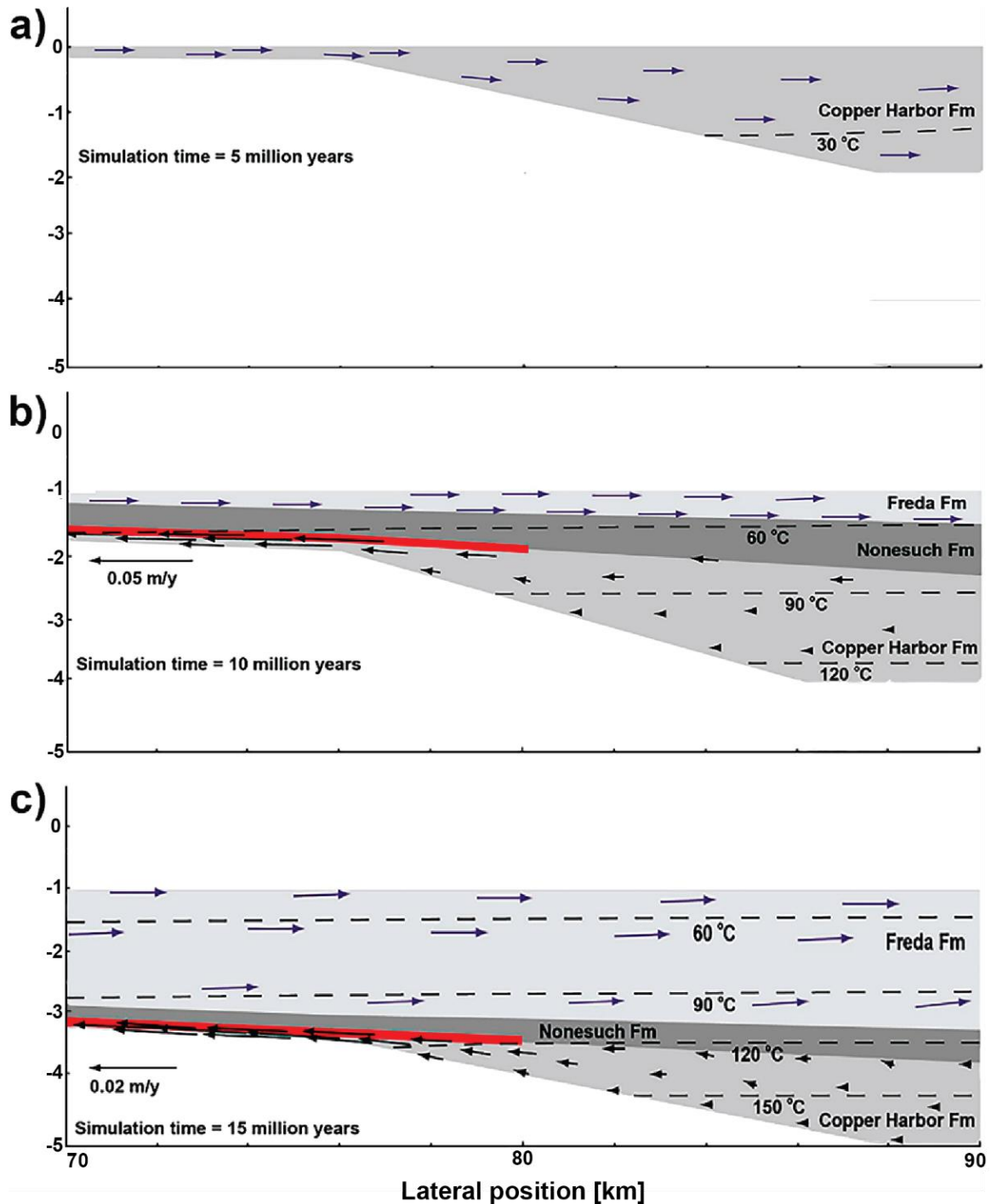


Figure 15 - Evolution of groundwater flow in the White Pine district after a) 5 million years, b) 10 million years, and c) 15 million years of simulation time during successive deposition of the Copper Harbor, Nonesuch, and Freda Formations. Topography-driven flow directed toward the rift center predominates in the Freda Formation, whereas compaction-driven flow directed toward the rift margin predominates in the Copper Harbor Formation. The red band represents the approximate location of the SHSC mineralization (after Swenson et al., 2004).

During deposition of the permeable red bed sequence, called the Copper Harbor Formation in the White Pine district, groundwater would have been driven by topographic gradients from the uplifted rift margin toward the basin center. Deposition of the low-permeability, chemically reducing, fine-grained clastic sediments of the Nonesuch Formation would have confined the Copper Harbor Formation aquifer and insulated it from the ongoing topography-driven flow system in the shallower, later deposited sediments. The loading produced by these later-deposited sediments, the Nonesuch Formation and the overlying fluvial clastic rocks of the Freda Formation, would have produced compaction-driven flow that was directed opposite to the shallower topography-driven flow—i.e., toward the rift margin rather than toward the rift center.

As is generally the case for compaction-driven flow, groundwater velocities were low: on the order of cm/y, too low to generate significant advective heat transport. However, heat flow in the rift was high enough for ore-forming temperatures to have been reached by conductive heat transport. Ore in the White Pine district was probably localized by an abrupt degree of thinning of the Copper Harbor Formation near the basin margin, which focused fluid and solute flux.

A distinctive feature of the White Pine district is that mineralization is greatest above a volcanic dome within the rift basin. Resurgent igneous activity within the dome during the time of SHSC ore formation may have caused localized heating that influenced groundwater flow (Figure 16). According to Brown (2014), groundwater in the Copper Harbor and Nonesuch Formations had a strong upward component, probably caused mainly by compaction. The greater heat above the dome would have lowered the viscosity of groundwater in the Copper Harbor Formation relative to cooler regions distal to the dome. The lower groundwater viscosities would have led to higher groundwater flow rates and thus solute fluxes above the dome, leading to enriched mineralization. This differential rate of groundwater flow would have had the greatest effect on mineralization during the early diagenesis of the Nonesuch Formation before it had become greatly compacted and before its porosity and permeability had been significantly reduced, allowing rising fluids from the Copper Harbor Formation to penetrate the fine-grained clastic sediments of the Nonesuch Formation more easily.

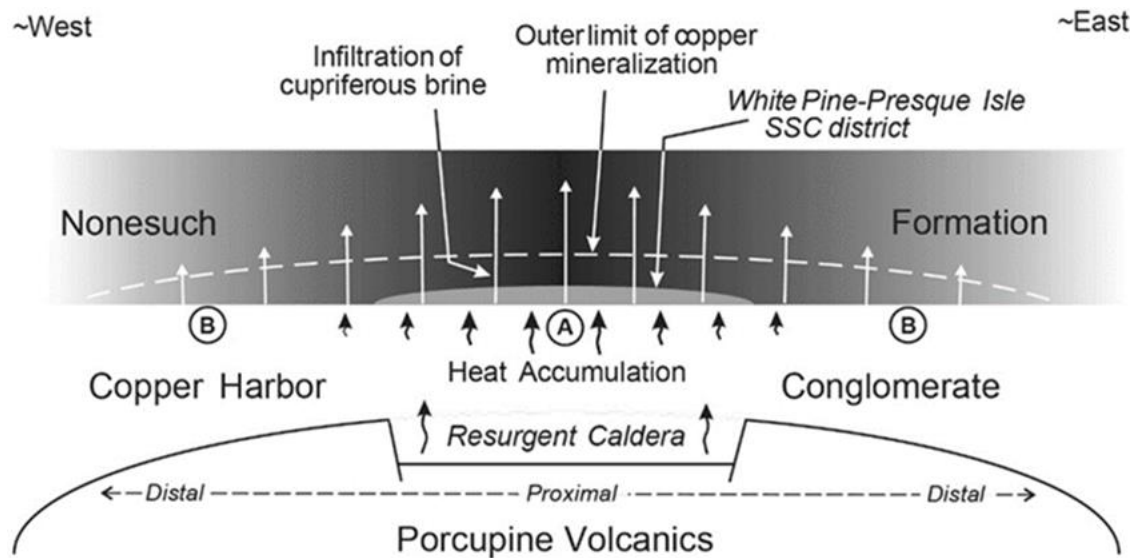


Figure 16 - Conceptual diagram of groundwater flow in the White Pine district according to the model of Brown (2014). Higher temperatures in the resurgent caldera within the Porcupine Volcanics dome would have lowered the viscosity of the groundwater above the dome (region A), therefore increasing its velocity relative to cooler groundwater further from the caldera (regions B), leading to higher solute flux penetrating the Nonesuch Formation above the caldera (from Brown, 2014).

A third possible mechanism for the flow of ore-forming groundwater in the Kupferschiefer region may have been seismic activity as illustrated in Figure 17 (Blundell et al., 2003). The tensional stress that prevailed in the rift setting would have formed cracks that dilated over time. This dilation would have lowered the fluid pressure inside the cracks, causing groundwater to be drawn into them. When an earthquake occurred, the stress and accompanying strain that had accumulated near the fault would have been relieved, causing cracks near the fault to shrink rapidly, expelling the groundwater they contained. This mechanism may have generated fluid flow rates on the order of tens of m/y. If earthquakes in the Kupferschiefer region recurred every 100 to 200 years, and if the groundwater had a relatively modest copper concentration of 60 ppm, then the Kupferschiefer ore deposits could have been formed within about 12 million years.

The formation of SHSC deposits does not appear to have been dependent on high copper concentrations in the ore-forming groundwater. This is because available evidence suggests that SHSC deposits tend to have formed over very long periods of time, perhaps exceeding 100 million years (Hitzman et al., 2010, 2012), allowing the deposits to have formed from groundwater containing low copper concentrations. If SHSC flow systems were indeed long-lived, then SHSC ore formation would have been favored by free convection groundwater flow regimes that recycle basinal fluids, rather than by single-pass flow regimes driven by topography or compaction that gradually flush the basin of its saline groundwater, unless the salinity of the groundwater was replenished by dissolving evaporites.

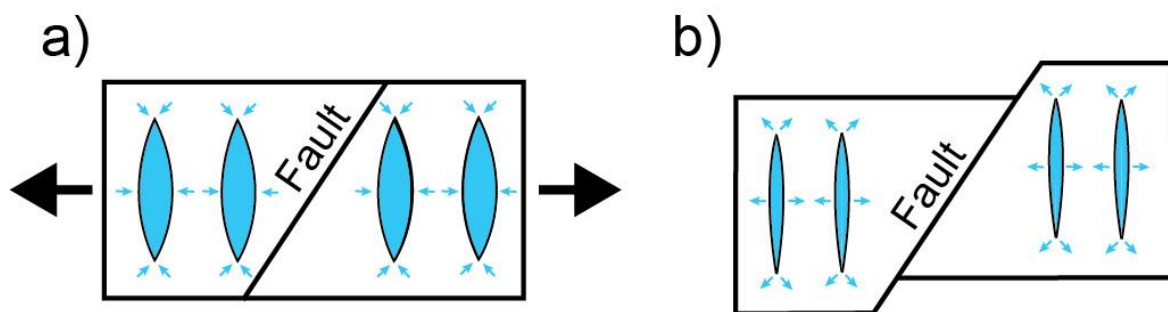


Figure 17 – a) During times of extension, when geologic media are being stretched, pores (blue pointed ellipses) in geologic media will expand and fill with groundwater. b) During an earthquake, the extension ceases and the deformation of the geologic media that occurred during extension is at least partially reversed, causing pores in the geologic media to shrink, expelling groundwater. This expelled groundwater is commonly directed along faults. Blue arrows show the direction of groundwater flow. After Blundell et al. (2003) and Muir-Wood and King (1993).

2.2 Magmatic Hydrothermal Ore Deposits: The Porphyry Copper Example

Magmatic hydrothermal ore deposits precipitate from groundwater that has been affected by heat, solute, and water derived from magma. In continental settings, magmatic hydrothermal ore deposits most commonly form near convergent plate boundaries and are important sources of copper, molybdenum, gold, silver, tin, and tungsten. In oceanic settings, magmatic hydrothermal ore deposits most commonly form near divergent plate boundaries and are important sources of copper, zinc, lead, silver, gold, and to a lesser degree tin, cadmium, antimony, and bismuth. In this section we profile porphyry copper deposits, which are a type of magmatic hydrothermal ore deposit that has received significant hydrogeologic study.

Porphyry copper deposits account for about 60 percent of global copper resources (Johnson et al., 2014). They are characterized by large masses of at least 20 million tons of ore (Lowell, 1974) occurring within large volumes of hydrothermally altered rock exceeding 10 km^3 , but with relatively low Cu grades between 0.5 and 1.5 percent (Lowell, 1974; Sillitoe, 2010). Porphyry copper deposits are strongly associated with convergent plate boundaries. Major provinces of porphyry deposits include the North American Cordillera, the Andes, the Alpine-Tethyan belt, and the Southwest Pacific belt (Misra, 2000; Seedorf et al., 2005).

The genesis of porphyry copper deposits has been outlined by numerous researchers (e.g., Seedorf, 2005; Sillitoe, 2010; Kouzmanov and Pokrovski, 2012; Lee and Tang, 2020; Rezeau and Jagoutz, 2020). Porphyry copper deposits form in magmatic arcs (Figure 18), particularly in continental magmatic arcs where the crust is thick (35 to 80 km).

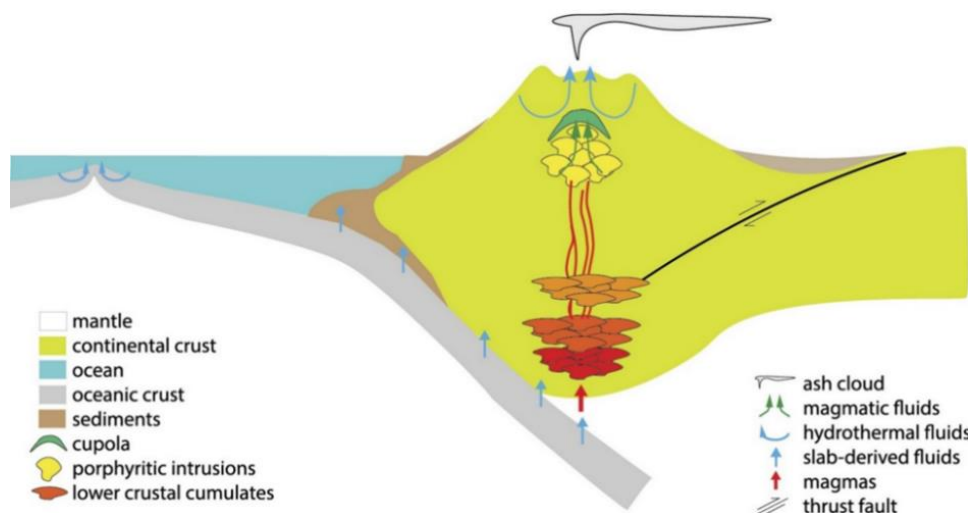


Figure 18 - Cross section of a continental magmatic arc. Magma is generated in the lower part of the arc as water vapor leaves the subducting oceanic plate and infiltrates overlying rock, lowering its melting temperature. The magmas rise through the crust, cooling and crystallizing to form cumulate rocks. Magmas that rise to depths of 2 to 5 km typically form rocks with porphyritic texture and may produce copper mineralization that tends to be concentrated in cupolas at the top of the porphyritic intrusions (from Lee and Tang, 2020).

A conceptual diagram of porphyry copper ore formation is depicted in Figure 19. The ore formation process begins with the formation of silicic magma that is rich in water (> 4 weight percent) and sulfur (up to 0.9 weight percent). As this silicic magma evolves chemically while ascending from its mantle source, the melt (i.e., the liquid portion of the magma) becomes depleted in iron. In thick magmatic arcs where the onset of magma formation occurs at high pressures, iron depletion in the melt may be caused by crystallization of the high-pressure mineral garnet, which simultaneously oxidizes the melt by removing Fe^{2+} , causing the remaining iron to become enriched in Fe^{3+} . At depths between 2 and 5 km, the magma stalls in its ascent and cools, exsolving saline liquid water containing 2 to 10 weight percent NaCl. If the magma has become sufficiently oxidizing, then sulfur will be in the form of sulfate and SO_2 , making copper soluble in the exsolved water and promoting the extraction of copper from the magma. If the magma remains sufficiently reducing for sulfur to be present as sulfide, then the sulfide sequesters the copper in the magma at relatively low concentrations, inhibiting copper's release into the exsolved liquid water. Once exsolved from the magma, copper-bearing liquid water ascends, undergoing a decrease in temperature and pressure that causes it to fractionate into a low-density, low-salinity water vapor and a high-density brine with salinities between 26 and 80 weight percent NaCl equivalent. As the exsolved fluids ascend, their pH commonly decreases from near neutral to acidic as SO_2 speciates into H_2S and sulfuric acid (H_2SO_4). The formation of H_2S contributes to the precipitation of sulfide minerals like chalcopyrite; sulfate from the sulfuric acid contributes to the formation of anhydrite. Copper precipitation coincides with a decrease in temperature from about 600 to 700° C to about 350 to 450° C.

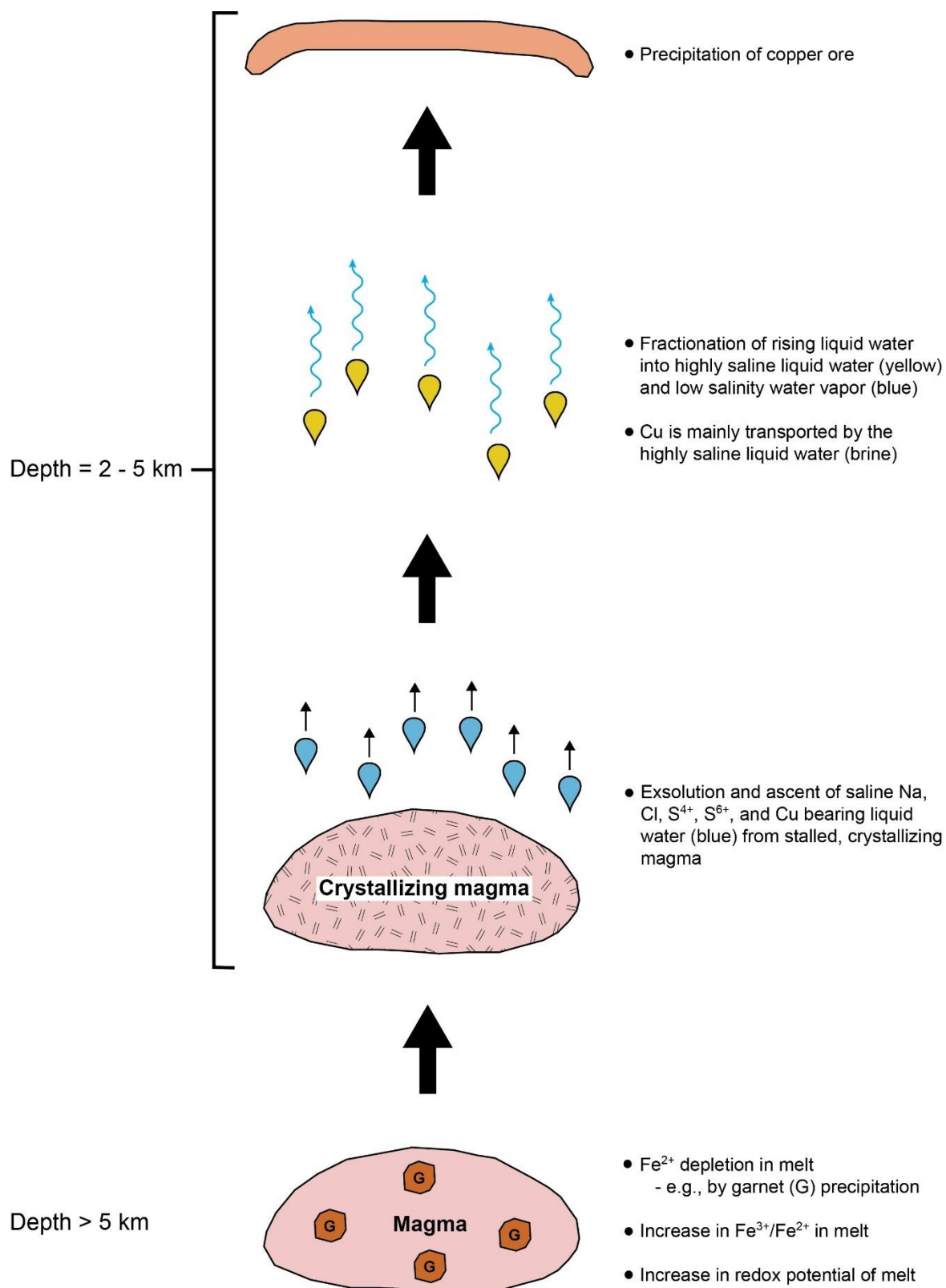


Figure 19 – Conceptual diagram of porphyry copper ore formation. The magma consists of a liquid melt, solid mineral crystals suspended in the melt, and gases dissolved in the melt.

The dynamics of groundwater behavior in porphyry copper ore-forming environments have been studied by numerous researchers. Pioneering numerical modeling studies by Cathles (1977) and Norton and Knight (1977) demonstrated that convection would be initiated in groundwater surrounding a pluton, leading to a focused plume of upward flow above the pluton and downward flow further from the pluton. Groundwater temperature was correspondingly increased in the up-flow zone and decreased in the downflow zones. The rate of fluid flow, size of the temperature perturbations, and lifespan of the hydrothermal system were found to be sensitive to the permeability of the country rock and pluton, as well as the burial depth and size of the pluton. Steam may temporarily form in the up-flow zone and the fluid fluxes in these convective groundwater flow systems were found to be sufficient to form large porphyry copper deposits.

Generally, these results have been upheld by subsequent studies that added complexity and greater geologic realism to the model. These subsequent studies have also produced important further insights. For example, models by Hayba and Ingebritsen (1997) extended those of Cathles (1977) and Norton and Knight (1977) by incorporating the multi-phase flow physics of both steam and liquid water, a more complete treatment of the variability of fluid density, the variability of permeability as a function of temperature, the effects of topography, and the presence of a low permeability caprock above the pluton. Hayba and Ingebritsen (1997) identified a host rock permeability of 10^{-15} m^2 to optimize heat transport and the longevity of the hydrothermal system. When host rock permeability is significantly less than 10^{-15} m^2 , little heat is advected beyond the immediate vicinity of the pluton, with most of the heat transfer occurring by the less efficient process of conduction. In contrast, when host rock permeability is significantly greater than 10^{-15} m^2 , the hydrothermal system likely becomes too cool, short-lived, and lacks the vapor needed for porphyry copper ore formation.

Studies by Weis and others (2012, 2014), Weis (2015), Lamy-Chapuis and others (2020), Korges and others (2020), and Stoltnow and others (2023) provide further insights. The mineralizing magmatic hydrothermal system originates with the exsolution of water vapor from the magma intrusion as it cools a few kilometers below the Earth's surface. A two-dimensional numerical model by Lamy-Chapuis and others (2020) for the evolution of water vapor expulsion for an elliptical intrusion is shown in Figure 20.

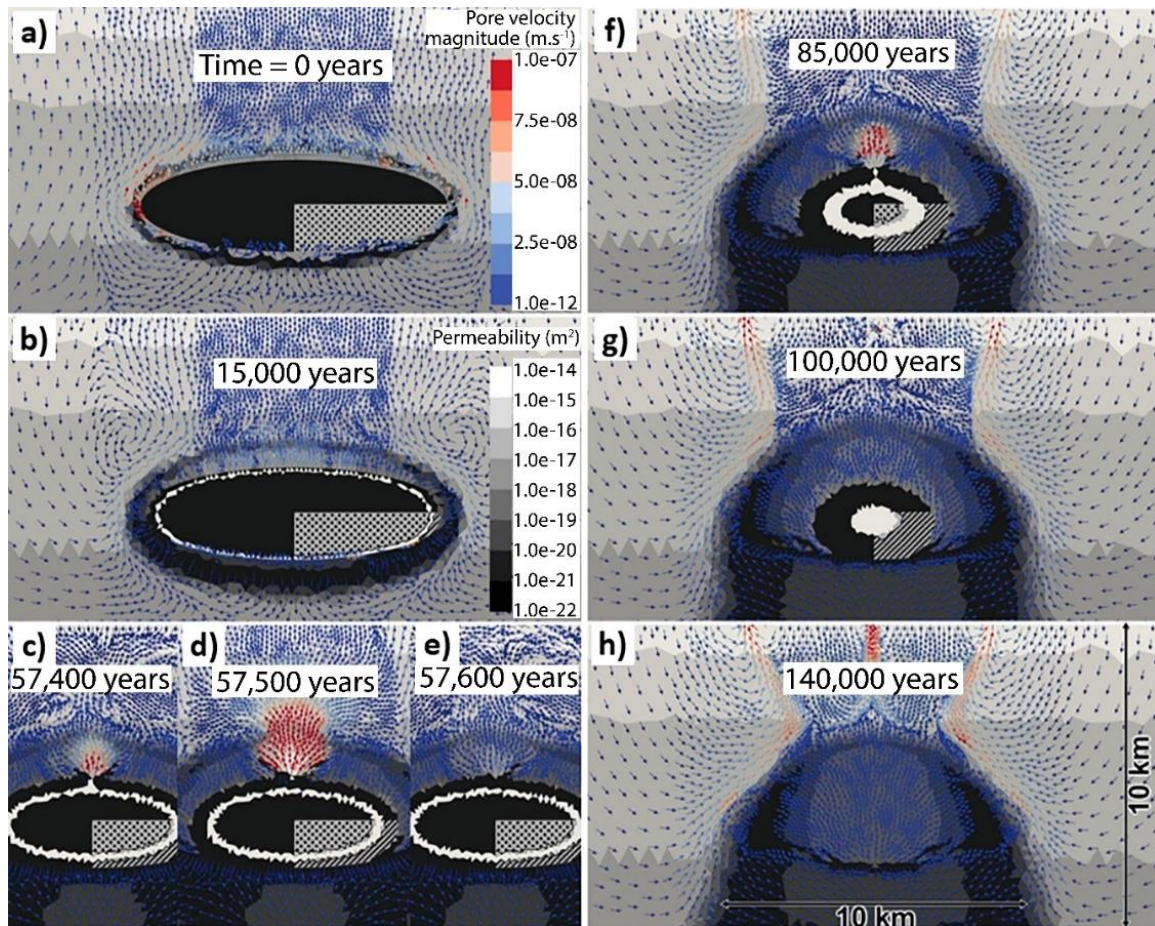


Figure 20 - Representative time series of the hydrologic regime produced by a cooling magmatic intrusion. At early times of a) 0 and b) 15,000 years, magmatic water vapor is broadly expelled across the roof of the intrusion. At later times shown by c) 57,400 years, d) 57,500 years, e) 57,600 years, and f) 85,000 years, when the intrusion has differentiated into concentric zones, magmatic water vapor is episodically expelled through a narrow rupture zone at the apex of the intrusion. g) By 100,000 years the intrusion has cooled enough such that fluid pressures sufficient to rupture the fracturable mush layer can no longer be reached. By 140,000 years, h) the intrusion has completely crystallized (from Lamy-Chapuis et al., 2020).

Initially, before the magma has cooled enough to form a solid outer shell, exsolved water vapor that is near lithostatic pressure freely leaves the magma body and flows into the surroundings, which are near hydrostatic pressure. The magmatic water vapor flows radially outward, but initially most of the flow is broadly distributed across the roof of the intrusion. As the magma intrusion cools, solidification proceeds radially inward from the surface of the intrusion, temporarily leading to four concentric zones: an outermost layer of solid rock, a mush containing a high crystal-melt ratio that is brittle enough to be fractured, a ductile mush with a low crystal-melt ratio that allows tubes of water vapor to form (Parmigiani et al., 2016, 2017), and a mostly molten core containing a sparse suspension of crystals and water vapor bubbles (Figure 21).

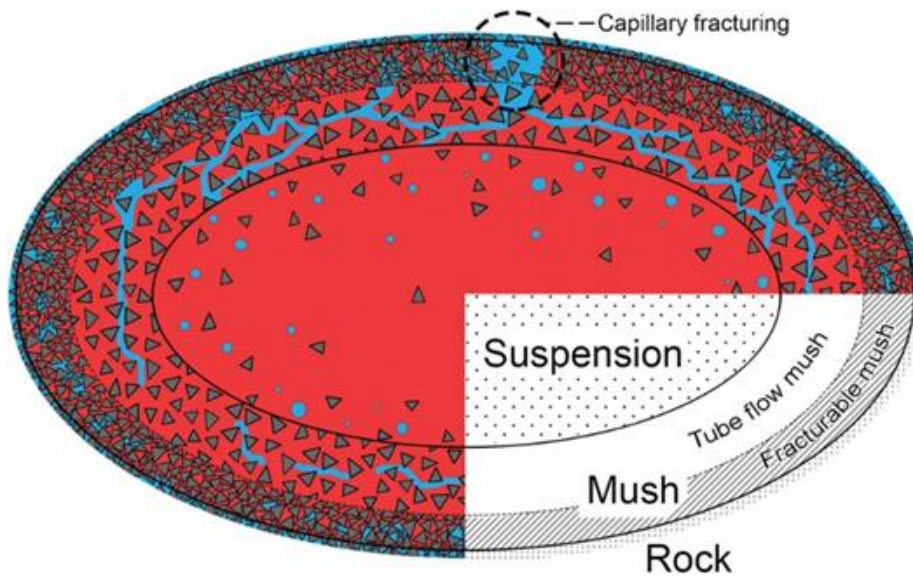


Figure 21 - Conceptual model of a cooling magmatic intrusion as employed in the numerical modeling shown in Figure 20. The intrusion shown here corresponds to the ellipses shown in Figure 20a-g (from Lamy-Chapuis et al., 2020). The magmatic intrusion is conceptualized to have risen from depth, as illustrated in Figure 19.

The fracturable mush has very low permeability, inhibiting the flow of magmatic water vapor into the country rock from its main source in the tube flow mush layer. Over time, as the pressure of the magmatic water vapor increases and because of its buoyancy, the fracturable mush is ruptured near the top of the intrusion, allowing a focused flow of magmatic water vapor into the surroundings and decreasing its pressure within the intrusion. Ongoing exsolution of magmatic water vapor with continued cooling of the intrusion leads to episodic cycles of pressure increase, intense fluid outbursts through the fracturable mush, and pressure release over times as long as on the order of hundreds of years, slowing over time and eventually stopping after the intrusion has largely solidified. These magmatic water vapor expulsion patterns were found by Lamy-Chapuis and others (2020) to be consistent over a wide range of conditions but favored by high initial water content in the magma and shallow burial depths. The expulsion patterns were not found to be strongly sensitive to variations in intrusion size or shape.

Figure 20 also provides insights into the nature of the hydrologic regime that develops in the country rock outside the magma intrusion. The hydrologic regime self organizes into an inner zone centered above the apex of the intrusion (i.e., the cupola) consisting of ascending magmatic fluid at near lithostatic pressure and two adjacent outer zones consisting of convecting, cooler meteoric water at near hydrostatic pressure. The magmatic fluid that ascends through the country rocks in the inner zone is hot enough (350 to $>600^{\circ}$ C) to maintain a ductile rheology in the rocks whereas the cooler outer zones have a brittle rheology. However, the ductile rheology of the rocks in the inner zone is too low to allow continuous rapid fluid flow. Instead, flow through the inner zone is episodic and wavelike, flowing as a succession of pulses called permeability waves that form each time the fluid pressure immediately above the cupola builds to a level that exceeds the failure

pressure of the rock, increasing the rock's porosity and permeability. This is shown in Figure 22, which provides a snapshot of a model hydrothermal system at about 5,000 years after initial magma emplacement.

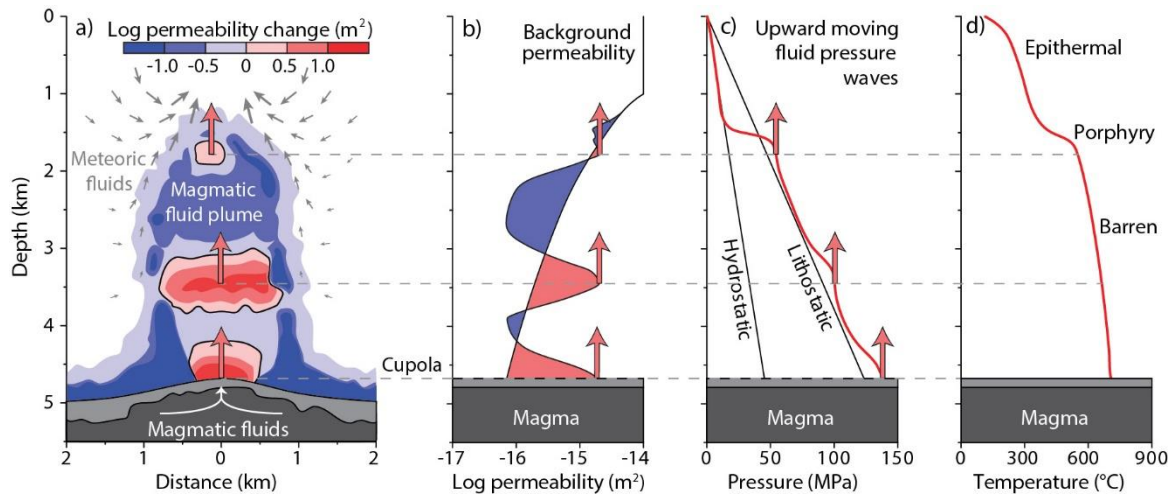


Figure 22 - Numerical model results after 5,000 years. a) Succession of episodically released permeability waves, marked by increased permeability b) and fluid pressure c) relative to the surroundings. d) Predicted temperature profile with depth. The red arrows represent the direction of movement of the permeability waves. The permeability, pressure, and temperature profiles in b), c), and d) are centered above the cupola (from Weis et al., 2012).

Three distinct permeability waves are visible as red-colored zones in Figure 22a and Figure 22b, which correspond to locally elevated fluid pressure in Figure 22c; Figure 22d shows the temperature profile with depth. Thus, the velocity of fluid flow, porosity, fluid pressure, and permeability are intimately coupled in the ore-forming system. The permeability waves that erupt from the cupola increase the porosity and permeability of the rock in which they are contained because of their high (greater than lithostatic) fluid pressure. The increased porosity of the permeability waves enhances their ability to transport fluid. The high pressure inside the permeability waves increases permeability inside the waves, allowing them to sustain high velocities. The transient evolution of the hydrothermal system is shown in Figure 23.

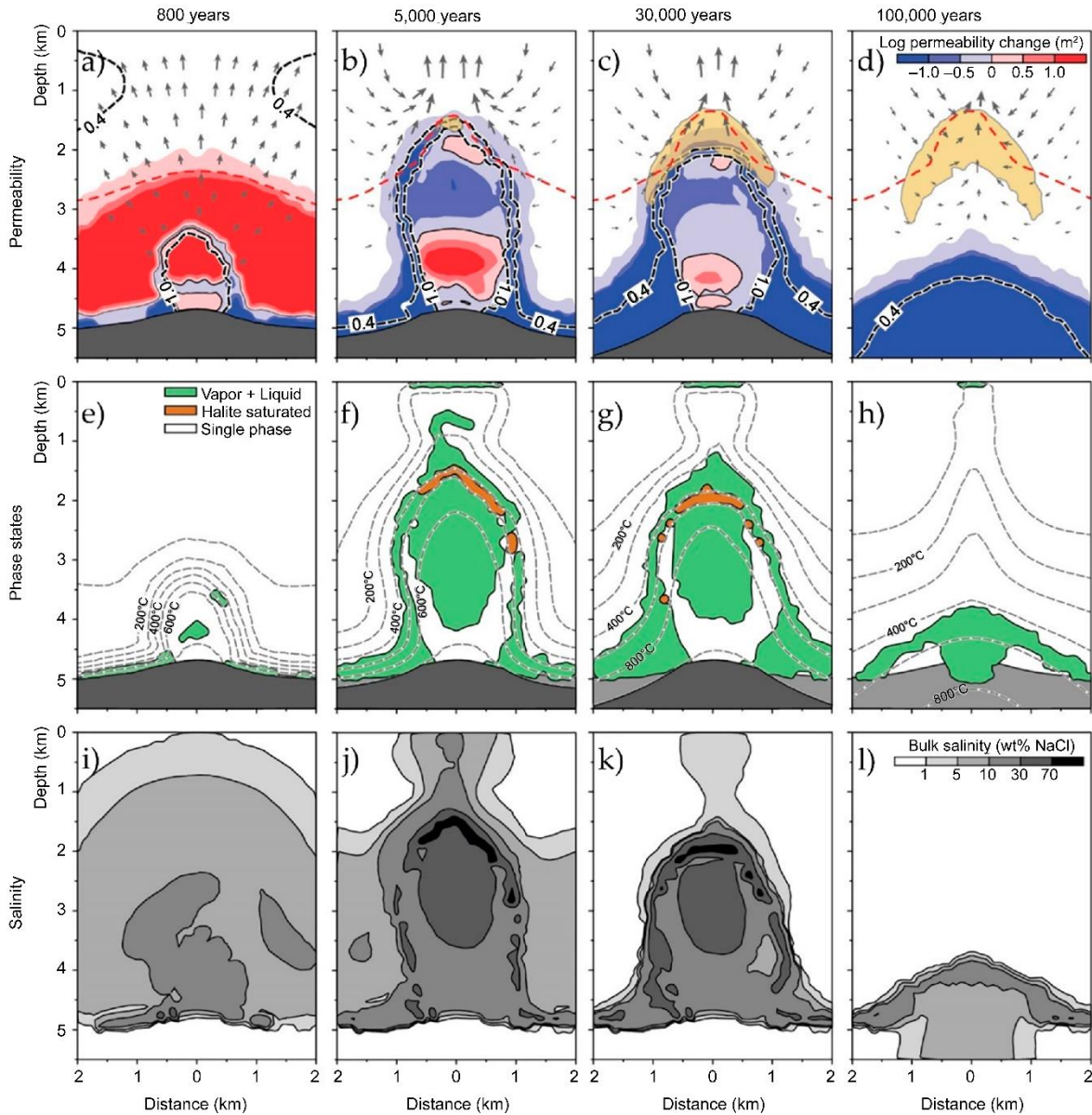


Figure 23 - Time series of simulated permeability (a-d), phase states (e-h), and salinity (i-l) after 800, 5,000, 30,000, and 100,000 years. Black dashed lines represent a *pore fluid factor*, defined to be the fluid pressure divided by lithostatic pressure. Pore fluid factor of 0.4 represents near hydrostatic pressure and a pore fluid factor of 1.0 represents near lithostatic pressure. Gray arrows represent fluid velocity. The gray dashed lines represent isotherms, i.e., lines of constant temperature. The red dashed line represents a maximum possible mineralized vein density (i.e., volume percent of veins within a volume of bulk rock) of 10 percent. The yellowish zones represent a copper enrichment potential of 500. In a-h, the dark gray area represents magma and the light gray represents solidified pluton (from Weis, 2015).

Initial emplacement of the magma leads to broad upward fluid flow and pressurization of the immediately overlying rock, causing the rock to fracture and greatly increasing its permeability, as shown in Figure 23a. By 5,000 years, the permeability wave magmatic fluid flow regime described above has developed, which persists for on the order of tens of thousands of years, while in the surrounding rock convective circulation of meteoric water develops. The shape, height, and temperature profile of the ascending magmatic fluid plume remain relatively constant while the magma is hot enough to exsolve fluids (Weis et al., 2012). The height of the plume is truncated by the actively upward

convecting meteoric water, which leads to a sharp drop in temperature and pressure at the top of the plume and promotes copper mineralization, as shown in Figure 23d and Figure 24. The results shown in Figure 22 and Figure 23 are for a model in which the land surface topography is flat (horizontal).

Meteoric water flow above the magmatic plume can be downward if the topographic relief of the overlying volcano is great enough, creating a shallow meteoric topography-driven flow system (Figure 24). However, in cases of both high and low volcanic topographic relief, a hydraulic divide between meteoric and magmatic fluid flow is created that leads to copper mineralization.

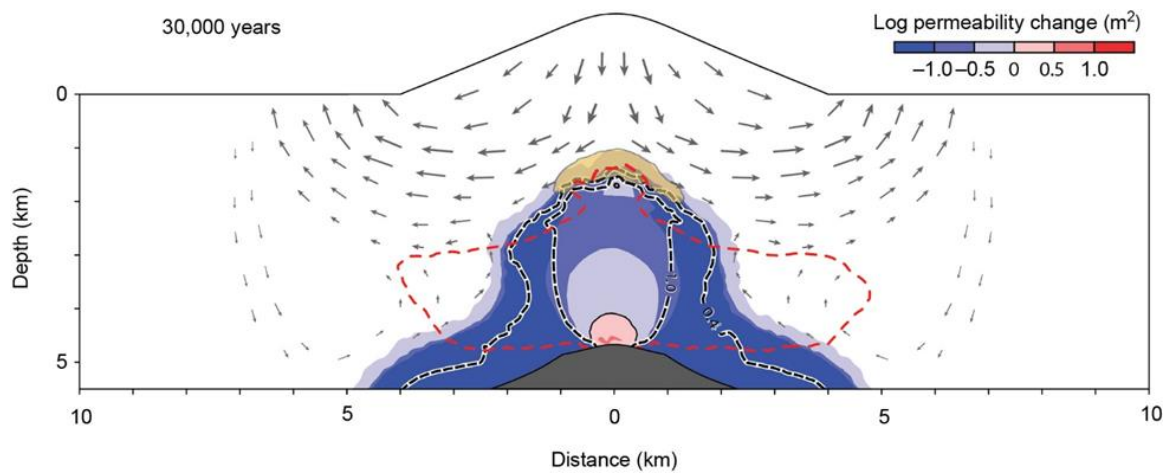


Figure 24 - Effects of volcano topography on the hydrology of a porphyry copper hydrothermal system shown after 30,000 years of simulation time. The red dashed line encloses a region within which hydraulic fracturing is sufficiently intense to cause at least 10% of the volume of the rock to consist of fractures. Outside this region, fractures constitute a smaller percentage of the rock volume (from Weis et al., 2015).

Copper mineralization coincides with a region where the potential for fracture formation is high, as indicated by the red dashed lines in Figure 23a to Figure 23d. Continued decreasing temperature with decreasing depth leads to an environment favorable for the formation of epithermal deposits at a depth within about a kilometer from the Earth's surface. By about 100,000 years, the pluton has cooled to the level that further discharge of magmatic fluid does not occur.

The magmatic fluid initially exsolved is hot enough to exist entirely in the liquid state. As the fluid pressure in the inner zone fluctuates, the phase state of the fluid also fluctuates between a single liquid phase and a two-phase fluid consisting of dilute water vapor and brine containing 30 to 70 weight percent NaCl. Fluid pressure gradients inside the magmatic fluid plume are great enough to drive the dense brine upward such that most of the highest salinities are in the upper part of the plume, reaching halite saturation near the hydrologic divide that separates the magmatic fluid from the convecting meteoric water. The upward convecting meteoric water above the hydraulic divide is prone to boil. The fluctuations in fluid pressure and phase state may give rise to the oscillatory patterns

of quartz precipitation and dissolution that are observed in many porphyry copper deposits (Weis et al., 2012).

Porphyry copper ore formation is also sensitive to the rate and frequency of magma emplacement (Figure 25). Ore formation is optimized when magma is emplaced as a succession of smaller sills (both in vertical thickness and horizontal width) rather than a single larger pluton, and in which the rate of magma cooling is about equal to the rate of magma injection as sills. This allows a continuous flux of magmatic fluid to be maintained. When the rate of sill injection is low, this causes the magmatic fluid plume to collapse between injection events, leading to more episodic and dispersed mineralization. Such episodic fluid flow leads to multiple generations of overprinting of lower temperature alteration minerals by higher temperature alteration minerals, which is not typical of porphyry copper deposits (Korges et al., 2020). When the rate of sill injection is too high, then magmas do not have as much opportunity to cool, thus less magmatic fluid is exsolved. High rates of magma emplacement also promote volcanic eruptions, which tend to result in weakly mineralized porphyry environments.

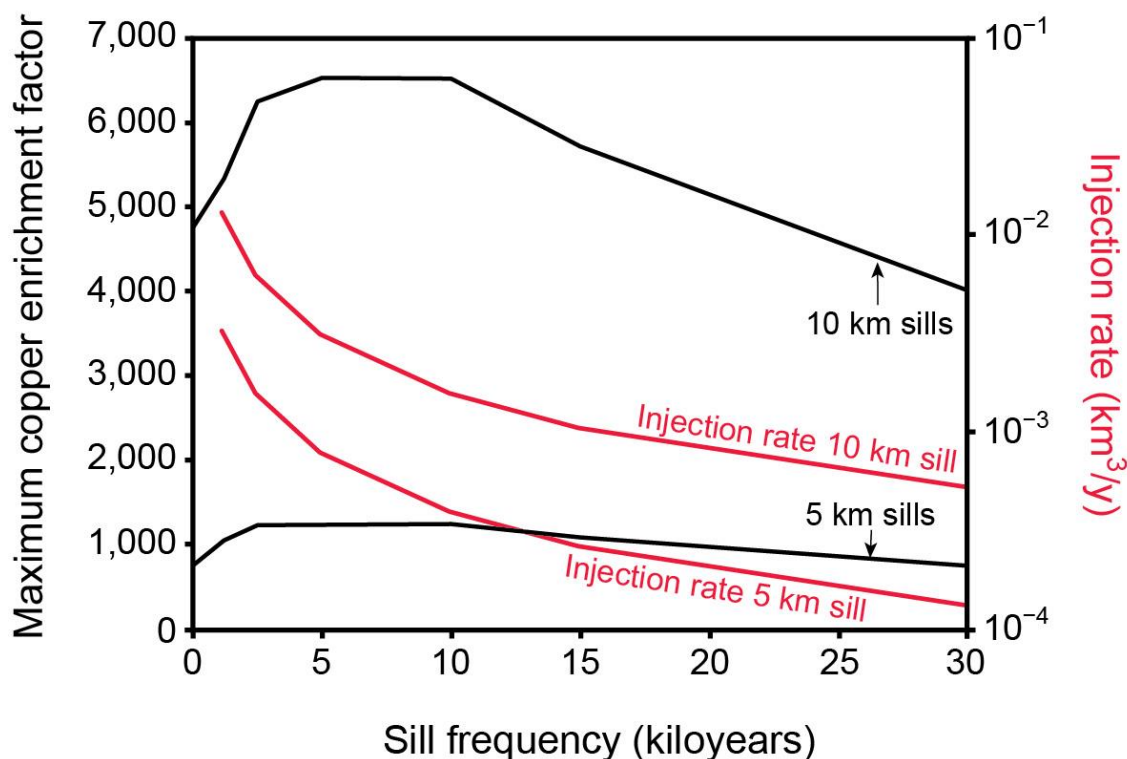


Figure 25 - Maximum copper enrichment factor and magma injection rate computed as a function of sill emplacement frequency for a 5 km and 10 km sill width (from Korges et al., 2020).

2.2.1 Evaluating Conditions for Hydrothermal Ore Deposit Formation

A further series of exercises (Parts II and III) provides readers an opportunity to explore further principles of hydrothermal ore formation in both magmatic and sedimentary basinal settings.

- [Introduction to Part II exercise](#) ↴ that evaluates solute transport in a magmatic hydrothermal environment;
- [Exercise 9](#) ↴ evaluates solute transport to the location of ore deposit formation;
- [Introduction to Part III exercises](#) ↴ that evaluate subsurface fluid dynamics and heat transfer;
- [Exercise 10](#) ↴ considers coupled heat and fluid flow as they relate to free convection; and,
- [Exercise 11](#) ↴ explores the heat generated by groundwater flow and its contribution to heat flux at the ground surface.

3 Wrap Up

Hydrogeology is a powerful science for quantifying the behavior of ore-forming fluids and thus for assessing the conditions under which potential ore-forming mechanisms are achievable in nature. In this sense, hydrogeology is valuable for testing hypotheses about ore fluid behavior that are commonly inferred from patterns of geochemical, isotopic, or geophysical data.

Hydrogeology has made fundamental contributions to our understanding of hydrothermal ore deposits. For example, hydrothermal ore deposits were once thought to require a magmatic heat source. However, hydrogeologic studies have shown that high ore formation temperatures significantly greater than those expected from typical geothermal gradients can be achieved through advective transport of heat from deeper in the crust by groundwater. Also, hydrogeologic studies have revealed details about the structure and evolution of magmatic hydrothermal flow systems that help explain the locations of porphyry copper ore deposits.

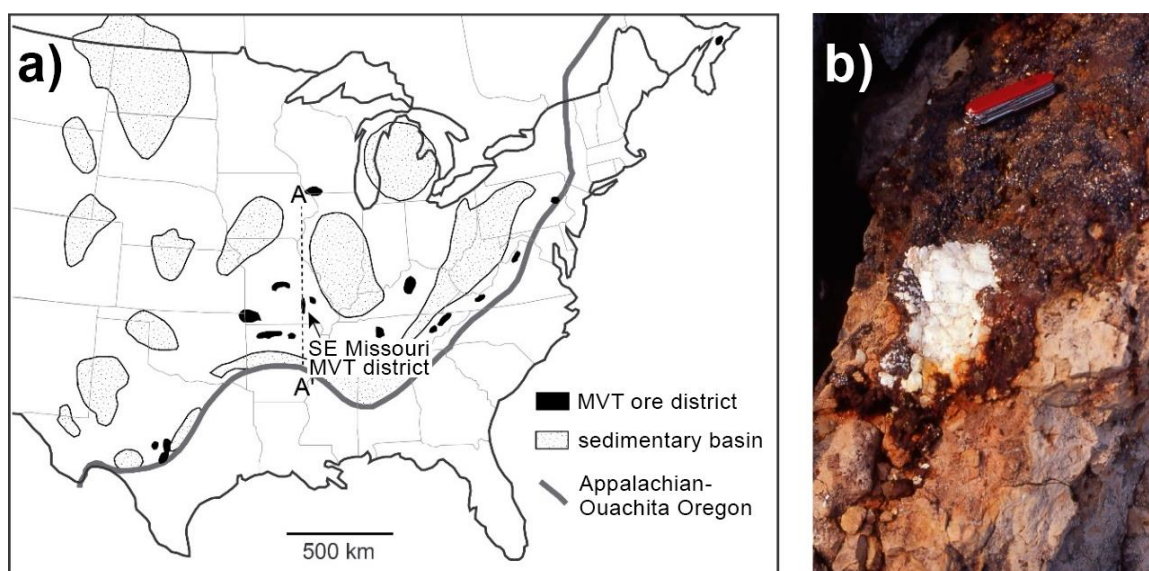
Hydrogeology has the potential to contribute much more to our understanding of hydrothermal ore deposits, but many types of hydrothermal ore deposits have received little hydrogeologic study. Many hydrogeologic modeling studies require important simplifying assumptions, and as computing power and theoretical algorithms improve, hydrogeologic models will be better able to represent field conditions. The ability of hydrogeologic modeling to treat couplings among transport processes, chemical reaction, and rock deformation offers opportunities for insights that are difficult to learn from other methods. Thus, hydrogeology should remain an integral tool in future studies of hydrothermal ore deposits.

4 Exercises

Part I - Constraints and Implications of Groundwater Temperature on the Formation of Mississippi Valley-type Zn-Pb Deposits

Introduction

Groundwater is fundamentally involved in the formation of numerous types of economic mineral deposits in the Earth's crust. One notable example is the Mississippi Valley-type (MVT) class of Zn-Pb deposits, named after several prominent occurrences in the Mississippi River watershed in the central USA as shown in part (a) of the image below. The principal economic commodities are typically the zinc and lead sulfide minerals sphalerite and galena, which are typically accompanied by significant amounts of calcite, dolomite, and quartz as shown in part (b) of the image below. Evidence from fluid inclusions—tiny samples of the ore fluid trapped in the mineral during precipitation—indicates that the deposits were formed from highly saline groundwater at temperatures around 100° C or more.



Mississippi Valley-type (MVT) class of Zn-Pb deposits. a) Map of major MVT ore districts in the eastern USA and their proximity to sedimentary basins. The transect A-A' corresponds to the vertical profile shown in Exercise 2. Map modified from Cathles and Smith (1983). b) Photograph of MVT sphalerite (dark reddish-brown mass around pocketknife) and calcite spar (white) hosted by Ordovician limestone at the Mulcahey mine in southwestern Wisconsin.

The high temperatures of ore deposit formation presented a puzzle as MVT deposits appear to have formed at depths of no more than 1.5 km either at or beyond the margins of sedimentary basins and generally not close to any local heating sources such as igneous intrusions. Contributions from groundwater hydrology (e.g., Domenico and Palciauskas, 1973; Garven and Freeze, 1984a, 1984b) played an important role in ultimately solving the

puzzle by showing that groundwater driven by regional gradients in the water table could have advected enough heat from deep parts of sedimentary basins to raise temperatures at shallow depths even well beyond the basin margin to levels needed for MVT ore formation.

The objective of exercises in Part I is to use analytical solutions to the differential equations for groundwater flow and heat transport published by Domenico and Palciauskas (1973) to explore the conditions needed for MVT ore formation near the shallow margin of a sedimentary basin.

[Click to return to where text linked to the Introduction of Part I Exercises](#) ↗

[Or click to continue to Exercise 1](#) ↗

Exercise 1

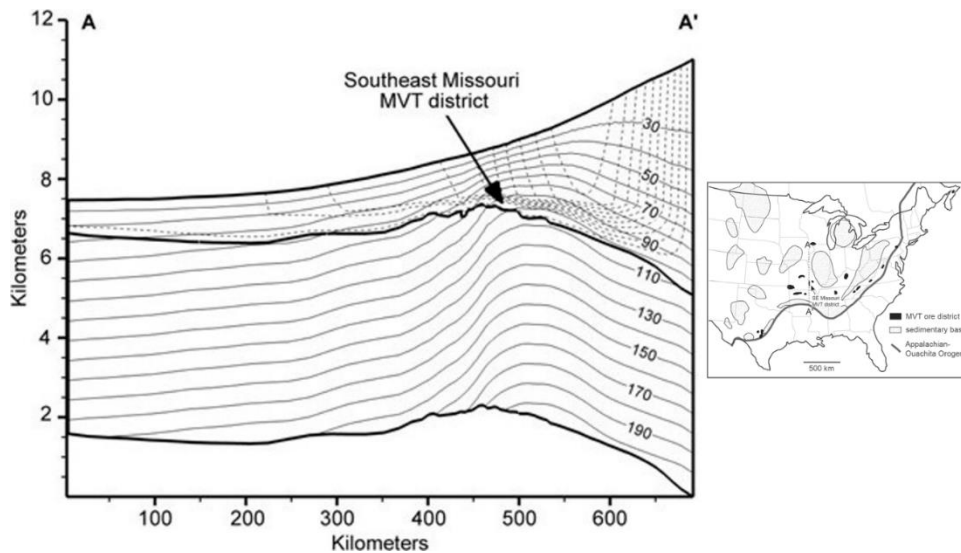
Typical geothermal gradients in the Earth's crust range from about 25° to 35° C per kilometer. Using these values and assuming an average surface temperature of 20° C, what range of temperatures would typically be expected at MVT ore-forming depths of about 1.5 km?

[Click to return to where text linked to Exercise 1 ↑](#)

[Click for solution to Exercise 1 ↓](#)

Exercise 2

The image below shows the results of a numerical model of steady-state groundwater flow and temperature along a transect A-A' extending from the Arkoma Basin through the Southeast Missouri MVT district for the Late Pennsylvanian or Early Permian as shown in the introduction to these exercises and on the inset map.



Steady-state groundwater flow and temperature field along a transect A-A' (Appold and Garven, 1999).

Solid contour lines are isotherms in degrees Celsius and the dashed lines are streamlines (i.e., groundwater flow lines). The direction of flow is not indicated on the streamlines, so it is important to know that the topographically driven flow starts at the surface near A' and proceeds northward. The vertical dimension of the cross section is exaggerated by roughly a factor of 50 so the streamlines appear to bend more than they would in the natural setting. Groundwater flux is the same between any two adjacent streamlines. Thus, the greater the density of streamlines in an area, the greater the flux of groundwater in that area.

Topographic relief was caused by uplift during the Appalachian-Ouachita orogeny and created the driving force for a regional-scale northward movement of groundwater. The heavy bold line in the interior of the cross section represents the top of the Precambrian basement, which was considered to have low permeability in the model and thus through which very little groundwater flow occurred.

Above the bold line is a package of more permeable Paleozoic sedimentary rocks. Describe the pattern of groundwater flow in the model. How does groundwater flow seem to affect the temperature distribution in the model?

[Click to return to where text linked to Exercise 2 ↑](#)

[Click for solution to Exercise 2 ↓](#)

Exercise 3

Domenico and Palciauskas (1973) published an analytical solution for steady-state groundwater flow over a two-dimensional rectangular domain that is given by the equation shown here.

$$h(x, z) = A - \left[\frac{B \cosh\left(\frac{\pi z}{L}\right)}{\cosh\left(\frac{\pi z_0}{L}\right)} \right] \cos\left(\frac{\pi x}{L}\right)$$

where:

h = hydraulic head (L)

A = height of inflection point of the water table (L)

B = distance between the top of the rectangular domain over which flow is calculated and A (L)

x = horizontal coordinate (L)

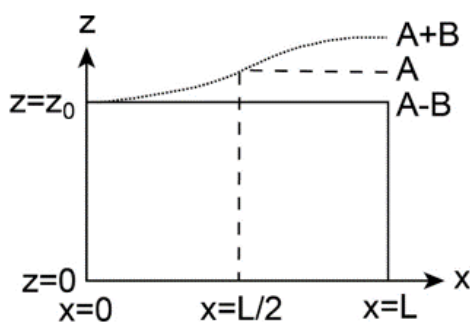
z = vertical coordinate (L)

z_0 = height of the rectangular problem domain (L)

L = horizontal length of the rectangular problem domain (L)

$\pi = 3.14159\dots$

This equation assumes that the entire problem domain is homogeneous and isotropic, no fluid flow occurs across the bottom or side boundaries, and the hydraulic head (h) across the top boundary varies as shown by the dotted curve $A+B$ in the image below which corresponds to the water table elevation.



Boundary conditions for the flow equation presented in this exercise (after Domenico and Palciauskas, 1973).

Calculate and draw contours of the hydraulic head in a hypothetical sedimentary basin for the following conditions selected as a rough approximation of the MVT district between a distance of 500 and 600 km on the MVT cross section as illustrated in Exercise 2.

$$z_0 = 10,000 \text{ m}$$

$$L = 100,000 \text{ m}$$

$$B = 500 \text{ m}$$

The calculations and plotting of head values to be contoured can be conveniently carried out using a spreadsheet program. Subdividing each coordinate direction by 10 to 20 nodes should provide sufficient detail to generate an accurate contour plot.

Print out the hydraulic head contour plot and draw in the flowlines by hand. What is the pattern of flow and how does it compare to the flow system illustrated by Appold and Garven (1999) and provided in Exercise 2?

[Click to return to where text linked to Exercise 3 ↑](#)

[Click for solution to Exercise 3 ↓](#)

Exercise 4

Domenico and Palciauskas (1973) also published an analytical solution for steady-state heat transport over a two-dimensional rectangular domain that allows the prediction of temperature according to the following equation.

$$T(x, z) = T_1 + T'_0(z - z_0) - \frac{T'_0KB}{2\kappa} \left(\frac{\cos\left(\frac{\pi x}{L}\right)}{\cosh\left(\frac{\pi z_0}{L}\right)} \right) \left\{ (z_0 - z) \cosh\left(\frac{\pi z}{L}\right) + \frac{L}{\pi} \left[\frac{\sinh\left(\frac{\pi(z - z_0)}{L}\right)}{\cosh\left(\frac{\pi z_0}{L}\right)} \right] \right\}$$

where:

T_1 = temperature along the top boundary (Θ)

T'_0 = vertical temperature gradient due solely to conduction (ΘL^{-1})

K = hydraulic conductivity (LT^{-1})

κ = thermal diffusivity of the bulk porous medium (L^2T^{-1})

The solution assumes the existence of a U-shaped groundwater flow field as described in Exercise 3. Further assumptions are that no lateral heat flow occurs through the side boundaries, a prescribed temperature gradient occurs at the bottom boundary, and the temperature along the top boundary is constant (isothermal).

- a) Calculate and contour the temperature field for the hypothetical sedimentary basin and conditions used in Exercise 3, along with the additional conditions listed below.

$$T_1 = 20^\circ \text{C}$$

$$T'_0 = -0.030^\circ \text{C/m}$$

$$K = 5 \times 10^{-8} \text{ m/s}$$

$$\kappa = 1 \times 10^{-6} \text{ m}^2/\text{s}$$

- b) Describe the temperature pattern predicted by your calculation and the way in which it is influenced by the flow of groundwater in the basin.
- c) What is the temperature at the basin margin ($x = 0$) at a depth of 1.5 km? Does this temperature meet MVT ore-forming temperatures?
- d) How does the temperature gradient near the top of the problem domain at $x = 0$ and $x = 100,000$ m compare to the original background temperature gradient that was due solely to conduction? What implications might this have for the geologic exploration for MVT mineral deposits?

[Click to return to where text linked to Exercise 4 ↴](#)

[Click for solution to Exercise 4 ↴](#)

Exercise 5

Repeat the calculation in Exercise 4 using a lower hydraulic conductivity value of $K = 5 \times 10^{-9}$ m/s while keeping all other parameter values the same.

- a) How did lowering the hydraulic conductivity of the basin affect the temperature profile?
- b) Is the temperature at $x = 0$ at a depth of 1.5 km still sufficient for MVT ore formation?
- c) At approximately what rate must groundwater flow in the basin to allow MVT ore-forming temperatures to be reached?

[Click to return to where text linked to Exercise 5 ↑](#)

[Click for solution to Exercise 5 ↓](#)

Exercise 6

Highly saline fluids initially present in the sedimentary basin would gradually be displaced by fresh meteoric water unsuitable for MVT deposit formation that is entering the basin in the recharge zone, though some saline fluids may persist in stagnant areas in some sedimentary basins where flow velocities are low. The advance of this freshwater plume is complicated by dispersion of solutes, but on average the fresh water front moves at the rate of the average linear velocity of the groundwater.

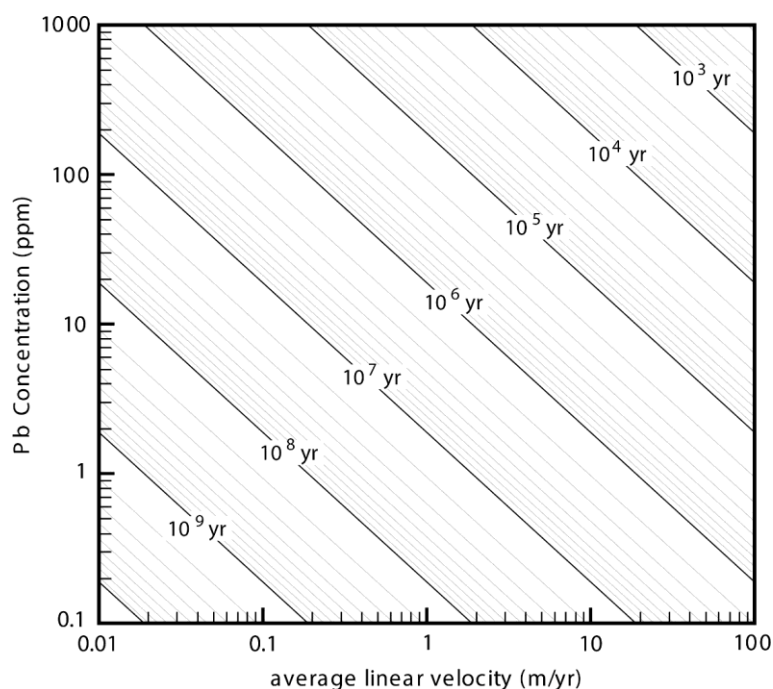
- a) Referring to your results from Exercises 3 and 4, estimate the distance that freshwater entering the recharge zone would travel before reaching a suitable site of MVT deposition at a depth of about 1.5 km near the margin of the basin.
- b) Approximately how long would it take for the freshwater plume to arrive at the site of MVT deposition, assuming that no additional sources of salinity (e.g., evaporites) exist in the basin? Assume an average basin porosity of 20 percent.

[Click to return to where text linked to Exercise 6 ↑](#)

[Click for solution to Exercise 6 ↓](#)

Exercise 7

The image below shows the result of a mass balance calculation that indicates the length of time needed to deposit all of the Southeast Missouri lead located on the transect A-A' as a function of average linear velocity and dissolved lead concentration of the mineralizing groundwater. Based on your results from the Exercise 6 and the image below, estimate the concentration of lead that the groundwater would need to carry to deposit all the lead metal located in the Southeast Missouri deposits on A-A' in the time available once meteoric recharge of the basin has begun, as calculated in Exercise 6b.



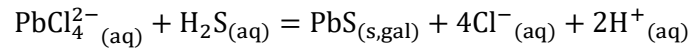
Contour plot showing the length of time needed to deposit all of the Pb in the part of the Southeast Missouri district lying on transect A-A' as a function of average linear velocity and Pb concentration of groundwater (Appold and Garven, 1999).

[Click to return to where text linked to Exercise 7](#)

[Click for solution to Exercise 7](#)

Exercise 8

At the temperature and salinity of MVT ore-forming groundwater, lead is transported primarily as the complex PbCl_4^{2-} and may precipitate as galena (PbS) according to the reaction described by the following equation.



If the chloride concentration is 3 mol/kg and dissolved lead and sulfur are present in the same molar concentrations, compute the pH that the groundwater required to transport the concentration of lead determined from Exercise 7. The equilibrium constant for this reaction at a temperature of 100° C and a pressure of 16 MPa is $K = 7603$. Assume the galena is composed purely of *PbS*. The activity coefficients for the aqueous species are provided below.

$$\gamma_{\text{PbCl}_4^{2-}} = 0.110$$

$$\gamma_{\text{H}_2\text{S}} = 1.0$$

$$\gamma_{\text{Cl}^-} = 0.873$$

$$\gamma_{\text{H}^+} = 0.873$$

Compare your result to known ranges of typical pH values in natural groundwater and discuss the geologic implications.

[Click to return to where text linked to Exercise 8 ↑](#)

[Click for solution to Exercise 8 ↓](#)

Part II – Solute Transport in a Magmatic Hydrothermal Environment

Introduction

Groundwater's ability to transport solute as well as heat is another factor in groundwater's efficacy as an agent of ore formation. The concentration of solute in groundwater is a function of numerous factors, including temperature, pressure, and the concentrations of other solutes in the groundwater, which directly affect the solubility of the solute, i.e., the amount of solute that the groundwater is capable of dissolving.

The concentration of solute in groundwater is also a function of the distance from the solute source, the velocity at which the groundwater is flowing, and the degree to which the porous medium through which the groundwater is flowing disperses the solute. These latter three factors are considered in the following exercise.

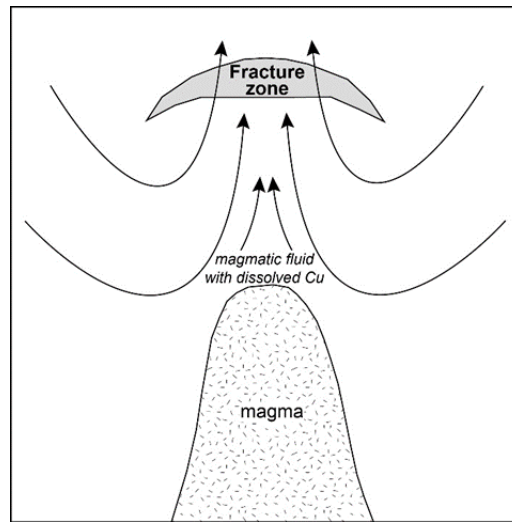
The objective of Exercise 9 is to predict how much time would be needed for copper concentrations in groundwater exsolved from magma in a porphyry copper ore-forming environment to become high enough for copper mineral precipitation to begin. This is accomplished by using an analytical solution to the differential equation for solute transport published by Ogata and Banks (1961).

[Click to return to where text linked to the Introduction of Part II Exercises ↑](#)

[Or click to continue to Exercise 9 ↑](#)

Exercise 9

The image below is a schematic cross section through a magmatic hydrothermal system. Water containing dissolved copper is being exsolved from the magma as it cools and crystallizes. This magmatic water ascends and becomes entrained within convection cells that transport meteoric water from the surroundings. Dissolved copper is transported upward until it reaches a fracture zone where it precipitates as copper minerals.



Schematic cross section of a hypothetical magmatic hydrothermal system. Solid back lines with arrowheads represent groundwater flow lines.

The concentration of dissolved copper in the upward flowing groundwater as a function of time and distance can be modeled with the Ogata-Banks (1961) analytical solution to the solute transport equation as shown here.

$$C = \frac{C_0}{2} \left[\operatorname{erfc} \left(\frac{z - v_z t}{2\sqrt{D_L t}} \right) + \exp \left(\frac{v_z z}{D_L} \right) \operatorname{erfc} \left(\frac{z + v_z t}{2\sqrt{D_L t}} \right) \right]$$

where:

- C = solute (Cu) concentration at position z
- C_0 = initial concentration at the solute source, which is constant for all time, t
- z = distance from the source in the vertical coordinate direction
- v_z = average linear groundwater velocity in the vertical (z) direction
- t = time
- D_L = longitudinal dispersion coefficient
- erfc = complementary error function

Suppose the top of the magma body continuously exsolves water with a copper concentration of 5 ppm. If fluid arriving in the fracture zone must have a concentration of

at least 1 ppm to precipitate copper minerals, how long (in years) will it take for copper mineral precipitation to begin once the magma begins exsolving water?

To answer this question, use a spreadsheet to solve copper concentration (C) as a function of time and plot the values with C on the vertical axis and t on the horizontal axis. The fracture zone is located 1.5 km above the top of the magma body. The average linear upward velocity (v_z) above the magma is 10 m/y. The longitudinal dispersion coefficient is $50 \text{ m}^2/\text{y}$. Assume that water rising from directly above the top of the magma body is not diluted by meteoric water in the surrounding convection cells.

[Click to return to where text linked to Exercise 9↑](#)

[Click for solution to Exercise 9↴](#)

Part III – Subsurface fluid dynamics and heat transfer

Introduction

Groundwater and heat flow are coupled because groundwater can flow in response to heat and groundwater can transport heat. Heat-driven groundwater flow can lead to free convection and, in turn, to the formation of ore deposits. For example, free convection appears to be key to the formation of unconformity-type uranium deposits in sedimentary basins and is intrinsic to most magmatically-driven groundwater flow systems, including those that form porphyry copper deposits. The heat gained or lost by groundwater as it flows affects its ability to form ore deposits.

The objective of Exercises 10 and 11 is to explore the conditions that lead to free convection in porous media and the transfer of heat that can be caused by flowing groundwater systems.

[Click to return to where text linked to the Introduction of Part III Exercises](#) ↗

[Or click to continue to Exercise 10](#) ↗

Exercise 10

In a homogeneous and horizontal aquifer, we may assume that groundwater will flow in response to a hydraulic gradient, with no *free convection* (Bear, 1972), until the thermal gradient exceeds the adiabatic gradient by an amount β ($^{\circ}\text{C}/\text{m}$) called the *critical thermal gradient* by Lapwood (1948). To calculate β , Birch (1958) derived the following equation.

$$\beta = \frac{4\pi^2\kappa\nu}{H^2\alpha gk}$$

where:

- κ = thermal diffusivity (L^2T^{-1})
- ν = kinematic viscosity (L^2T^{-1})
- H = thickness of the aquifer (L)
- α = coefficient of thermal expansion (Θ^{-1})
- g = acceleration of gravity (LT^{-2})
- k = intrinsic permeability (L^2)

- a) Assume a horizontal, homogeneous, and isotropic aquifer with the following characteristics and calculate the value of the critical thermal gradient, β .

$$\kappa = 0.01 \text{ cm}^2/\text{s}$$

$$\nu = 0.01 \text{ cm}^2/\text{s}$$

$$H = 100 \text{ m}$$

$$\alpha = 2.5 \times 10^{-4} \text{ }^{\circ}\text{C}^{-1}$$

$$k = 5.9 \times 10^{-7} \text{ cm}^2$$

- b) Assume that hot magmatic fluid is injected into a confined aquifer raising the critical thermal gradient to $6.5 \text{ }^{\circ}\text{C}/100 \text{ m}$. The aquifer is homogeneous but anisotropic, where $k_x = 5.90 \times 10^{-7}$ and $k_z = 2.95 \times 10^{-7} \text{ cm}^2$. The formation parameter values of κ , ν , and α are the same as those given in part (a). What would be the maximum thickness of the aquifer H_{max} in which no free convection occurs? H_{max} can be calculated using the following equations provided by Combarous and Bories (1975).

$$H_{max} = \left(\frac{4\pi^2\nu D}{g\alpha\beta k'} \right)^{1/2}$$

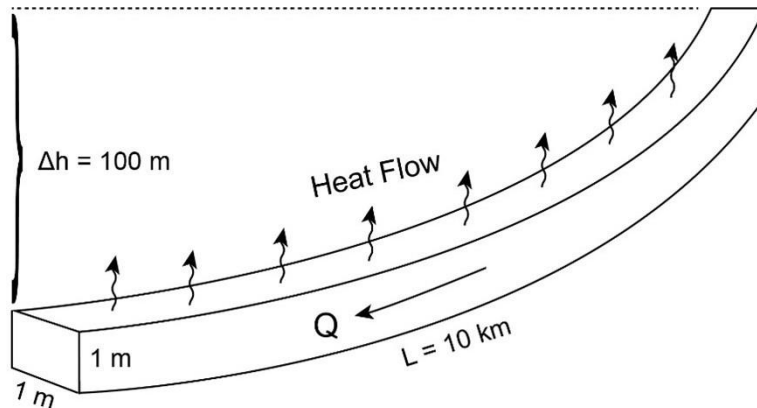
$$k' = \frac{4k_x k_z}{(\sqrt{k_x} + \sqrt{k_z})^2}$$

[Click to return to where text linked to Exercise 10↑](#)

[Click for solution to Exercise 10↓](#)

Exercise 11

Assume a confined aquifer shown in the image below in which the average flow distance from a point of recharge to a point of discharge is $L = 10$ km, and the hydraulic head drop over this distance is $\Delta h = 100$ m.



Schematic diagram of groundwater flow through a $1\text{ m} \times 1\text{ m} \times 10\text{ km}$ section of a confined aquifer.

- If all of the energy loss due to fluid flow is converted to heat, how much heat is produced per kilogram of water moving from the recharge to the discharge area?
- If the average linear velocity of the groundwater $v_s = 1$ m/day, the porosity $n = 0.15$, the density of the groundwater is $1,000\text{ kg/m}^3$, and all of the generated heat travels upward, what is the heat flux q_h (in units of $\text{J m}^{-2} \text{y}^{-1}$) at the land surface produced by groundwater flow alone?
- If the crustal heat flux is on the order of 70 mW/m^2 , and the aquifer thickness in part b) of this exercise is 100 m , what fraction (percentage) of this crustal heat flux can be attributed to groundwater flow?

[Click to return to where text linked to Exercise 11](#) ↴

[Click for solution to Exercise 11](#) ↴

5 References

- Anderson, G.M., 1975, Precipitation of Mississippi Valley-type ores: *Economic Geology*, volume 70, issue 5, 6 pages, doi.org/10.2113/gsecongeo.70.5.937.
- Appold, M.S. and G. Garven, 1999, The hydrology of ore formation in the Southeast Missouri district: Numerical models of topography-driven fluid flow during the Ouachita orogeny. *Economic Geology*, volume 94, issue 6, 24 pages, doi.org/10.2113/gsecongeo.94.6.913.
- Appold, M.S., T.J. Numelin, T.J. Shepherd, and S.R. Chenery, 2004, Limits on the metal content of fluid inclusions in gangue minerals from the Viburnum Trend, Southeast Missouri, determined by laser ablation ICP-MS. *Economic Geology*, volume 99, 15 pages, doi.org/10.2113/gsecongeo.99.1.185.
- Appold, M.S. and J.A. Nunn, 2005, Hydrology of the Western Arkoma basin and Ozark platform during the Ouachita orogeny: Implications for Mississippi Valley-type ore formation in the Tri-State Zn-Pb district. *Geofluids*, volume 5, 19 pages, doi.org/10.1111/j.1468-8123.2005.00122.x.
- Appold, M.S. and P.I. Nabelek, 2009, Introduction to the Special Issue on Numerical Modeling of Hydrothermal Fluids. *Geofluids*, volume 9, 7 pages, doi.org/10.1111/j.1468-8123.2009.00248.x.
- Appold, M.S. and Z.J. Wenz, 2011, Composition of ore fluid inclusions from the Viburnum Trend, Southeast Missouri District, United States: Implications for transport and precipitation mechanisms. *Economic Geology*, volume 106, 25 pages, doi.org/10.2113/econgeo.106.1.55.
- Bear, J, 1972, *Dynamics of Fluids in Porous Media*. Dover Publications, Incorporate, 800 pages, New York, USA.
- Benoit, W.R. and R.W. Butler, 1983, A review of high-temperature geothermal developments in the northern Basin and Range province. Geothermal Resources Council, Special Report 13, 25 pages, <https://publications.mygeoenergynow.org/grc/1005447.pdf>.
- Bethke, C.M., 1985, A numerical model of compaction-driven groundwater flow and its application to the paleohydrology of intracratonic sedimentary basins. *Journal of Geophysical Research*, volume 90, 13 pages, doi.org/10.1029/JB090iB08p06817.
- Bethke, C.M., 1986, Inverse hydrologic analysis of the distribution and origin of Gulf Coast-type geopressured zones. *Journal of Geophysical Research*, volume 91, 10 pages, doi.org/10.1029/JB091iB06p06535.
- Bethke, C.M. and S. Marshak, 1990, Brine migrations across North America—The plate tectonics of groundwater. *Annual Review of Earth and Planetary Sciences*, volume 18, 30 pages, doi.org/10.1146/annurev.ea.18.050190.001443.
- Birch, F.S, 1958, Thermal considerations in deep disposal of radioactive waste. National Academy of Sciences-National Research Council, Pub-588, Washington, DC.

- Blundell, D.J., P.H. Karnkowski, D.H.M. Alderton, S. Oszczepalski, and H. Kucha, 2003, Copper mineralization of the Polish Kupferschiefer: A proposed basement fault-fracture system of fluid flow. *Economic Geology*, volume 98, 10 pages, doi.org/10.2113/gsecongeo.98.7.1487.
- Bouhlef, S., D.L. Leach, C.A. Johnson, E. Marsh, S. Salmi-Laouar, and D.A. Banks, 2016, A salt diapir-related Mississippi Valley-type deposit: The Bou Jaber Pb-Zn-Ba-F deposit, Tunisia: Fluid inclusion and isotope study. *Mineralium Deposita*, volume 51, 31 pages, doi.org/10.1007/s00126-015-0634-8.
- Bradley, J.S. and D.E. Powley, 1994, Pressure compartments in sedimentary basins: a review, in P.J. Ortoleva, ed., *Basin Compartments and Seals*. AAPG Memoir 61, p. 3-26.
- Brown, A.C., 2014, Latent thermal effects from Porcupine Volcanics calderas underlying the White Pine-Presque Isle stratiform copper mineralization, northern Michigan. *Economic Geology*, volume 109, 15 pages, doi.org/10.2113/econgeo.109.7.2035.
- Cathles, L.M., 1977, An analysis of the cooling of intrusives by ground-water convection which includes boiling. *Economic Geology*, volume 72, 22 pages, doi.org/10.2113/gsecongeo.72.5.804.
- Cathles, L.M., 1993, A discussion of flow mechanisms responsible for alteration and mineralization in the Cambrian aquifers of the Ouachita—Arkoma Basin—Ozark System. *American Association of Petroleum Geologists*, volume 36, 13 pages, doi.org/10.1306/St36574C8.
- Cathles, L.M. and A.T. Smith, 1983, Thermal constraints on the formation of Mississippi Valley-type lead-zinc deposits and their implications for episodic basin dewatering and deposit genesis. *Economic Geology*, volume 78, 20 pages, doi.org/10.2113/gsecongeo.78.5.983.
- Cathles, L.M., S. Oszczepalski, and E.C. Jowett, 1993, Mass balance evaluation of the late diagenetic hypothesis for Kupferschiefer Cu mineralization in the Lubin basin of southwestern Poland. *Economic Geology*, volume 88, 8 pages, doi.org/10.2113/gsecongeo.88.4.948.
- Cathles, L.M. and J.J. Adams, 2005, Fluid flow and petroleum and mineral resources in the upper (<20-km) continental crust *in* *Economic Geology*, 100th Anniversary Issue 1905–2005, editors, J.W. Hedenquist, J.F.H. Thompson, R.J. Goldfarb, and J.P. Richards. Society of Economic Geologists, 35 pages, doi.org/10.5382/AV100.05.
- Chi, G., S. Bosman, and C. Card, 2013, Numerical modeling of fluid pressure regime in the Athabasca basin and implications for fluid flow models related to the unconformity-type uranium mineralization. *Journal of Geochemical Exploration*, volume 125, 11 pages, doi.org/10.1016/j.gexplo.2012.10.017.
- Chi, G., Z. Li, H. Chu, K.M. Bethune, D.H. Quirt, P. Ledru, C. Normand, C. Card, S. Bosman, W.J. Davis, and E.G. Potter, 2018, A shallow-burial mineralization model for

- the unconformity-related uranium deposits in the Athabasca Basin. *Economic Geology*, volume 113, 9 pages, doi.org/10.5382/econgeo.2018.4588.
- Combarous, M.A. and S.A. Bories, 1975, Hydrothermal convection in saturated porous media. *Advances in Hydroscience*, volume 10, 76 pages, doi.org/10.1016/B978-0-12-021810-3.50008-4.
- Cox, S.F., 2005, Coupling between deformation, fluid pressures, and fluid flow in ore-producing hydrothermal systems at depth in the crust *in* *Economic Geology 100th Anniversary*, editors, J.W. Hedenquist, J.F.H. Thompson, R.J. Goldfarb, and J.P. Richards. Society of Economic Geologists, 35 pages, doi.org/10.5382/AV100.04.
- Cui, T., J. Yang, and I.M. Samson, 2010, Numerical modeling of hydrothermal fluid flow in the Paleoproterozoic Thelon Basin, Nunavut, Canada. *Journal of Geochemical Exploration*, volume 106, 7 pages, doi.org/10.1016/j.gexplo.2009.12.008.
- Cui, T., J. Yang, and I.M. Samson, 2012, Solute transport across basement/cover interfaces by buoyancy-driven thermohaline convection: Implications for the formation of unconformity-related uranium deposits. *American Journal of Science*, volume 312, 33 pages, doi.org/10.2475/09.2012.02.
- Czamanske, G.K., E. Roedder, and F.C. Burns, 1963, Neutron activation analysis of fluid inclusions for copper, manganese, and zinc. *Science*, volume 140, 3 pages, <https://www.science.org/doi/10.1126/science.140.3565.401>.
- Deming, D., 1992, Catastrophic release of heat and fluid flow in the continental crust. *Geology*, volume 20, 3 pages, [doi.org/10.1130/0091-7613\(1992\)020<0083:CROHAF>2.3.CO;2](https://doi.org/10.1130/0091-7613(1992)020<0083:CROHAF>2.3.CO;2).
- Deming, D., J.A. Nunn, and D.G. Evans, 1990, Thermal effects of compaction-driven groundwater flow from overthrust belts. *Journal of Geophysical Research Solid Earth*, volume 95, 15 pages, doi.org/10.1029/JB095iB05p06669.
- Deming, D. and J.A. Nunn, 1991, Numerical simulations of brine migration by topographically driven recharge. *Journal of Geophysical Research*, volume 96, 15 pages, doi.org/10.1029/90JB02392.
- Domenico, P.A. and V.V. Palciauskas, 1973, Theoretical analysis of forced convective heat transfer in regional ground-water flow. *Geological Society of America Bulletin*, volume 84, issue 12, 12 pages, [doi.org/10.1130/0016-7606\(1973\)84%3C3803:TAOFCH%3E2.0.CO;2](https://doi.org/10.1130/0016-7606(1973)84%3C3803:TAOFCH%3E2.0.CO;2).
- Field, J.D., M.S. Appold, R.M. Coveney Jr., and R.J. Bodnar, 2020, Data for geochemical characteristics of trace occurrences of Mississippi Valley-type mineralization in the US Mid-Continent: Implications for deposit growth. *Journal of Geochemical Exploration*, volume 213, 23 pages, doi.org/10.1016/j.gexplo.2020.106514.
- Freeze, R.A. and J.A. Cherry, 1979, *Groundwater*. The Groundwater Project, Guelph, Ontario, Canada, 604 pages, <http://gw-project.org/books/groundwater/>.
- Fusswinkel, T., T. Wagner, M. Wälle, T. Wenzel, C.A. Heinrich, and G. Markl, 2013, Fluid mixing forms basement-hosted Pb-Zn deposits: Insight from metal and halogen

- geochemistry of individual fluid inclusions. *Geology*, volume 41, 4 pages, doi.org/10.1130/G34092.1.
- Garven, G., 1985, The role of regional fluid flow in the genesis of the Pine Point deposit, Western Canada sedimentary basin. *Economic Geology*, volume 80, 18 pages, doi.org/10.2113/gsecongeo.80.2.307.
- Garven, G., 1989, A hydrogeologic model for the formation of the giant oil sands deposits of the Western Canada sedimentary basin. *American Journal of Science*, volume 289, 62 pages, doi.org/10.2475/ajs.289.2.105.
- Garven, G. and R.A. Freeze, 1984a, Theoretical analysis of the role of groundwater flow in the genesis of stratabound ore deposits; 1, Mathematical and numerical model. *American Journal of Science*, volume 284, 40 pages, doi.org/10.2475/ajs.284.10.1085.
- Garven, G. and R.A. Freeze, 1984b, Theoretical analysis of the role of groundwater flow in the genesis of stratabound ore deposits; 2, Quantitative results. *American Journal of Science*, volume 284, 50 pages, doi.org/10.2475/ajs.284.10.1125.
- Garven, G., S. Ge, M.A. Person, and D.A. Sverjensky, 1993, Genesis of stratabound ore deposits in the Midcontinent basins of North America; 1, The role of regional groundwater flow. *American Journal of Science*, volume 293, 72 pages, doi.org/10.2475/ajs.293.6.497.
- Garven, G. and J.P. Raffensperger, 1997, Hydrogeology and geochemistry of ore genesis in sedimentary basins *in* *Geochemistry of Hydrothermal Ore Deposits*, 3rd issue, editor, H.L. Barnes, Wiley and Sons, 25 pages.
- Garven, G., M.S. Appold, V.I. Toptygina, and T.J. Hazlett, 1999, Hydrogeologic modeling of the genesis of carbonate-hosted lead-zinc ores. *Hydrogeology Journal*, volume 7, 18 pages, doi.org/10.1007/s100400050183.
- Ge, S. and G. Garven, 1989, Tectonically induced transient groundwater flow in foreland basin. *Geophysical Monograph Series*, 14 pages, doi.org/10.1029/GM048p0145.
- Ge, S. and G. Garven, 1992, Hydromechanical modeling of tectonically driven groundwater flow with application to the Arkoma foreland basin. *Journal of Geophysical Research*, volume 97, 25 pages, doi.org/10.1029/92JB00677.
- Ge, S. and G. Garven, 1994, A theoretical model for thrust-induced deep groundwater expulsion with application to the Canadian Rocky Mountains. *Journal of Geophysical Research: Solid Earth*, volume 99, 18 pages, doi.org/10.1029/94JB00687.
- Hanor, J.S., 1994, Origin of saline fluids in sedimentary basins *in* *Geofluids: Origin, Migration and Evolution of Fluids in Sedimentary Basins*, editor, J. Parnell. Geological Society of America Special Publication No. 78, 23 pages.
- Hayba, D.O. and S.E. Ingebritsen, 1997, Multiphase groundwater flow near cooling plutons. *Journal of Geophysical Research*, volume 102, 18 pages, doi.org/10.1029/97JB00552.
- Heijlen, W., D.A. Banks, P. Muchez, B.M. Stensgard, and B.W. Yardley, 2008, The nature of mineralizing fluids of the Kipushi Zn-Cu deposit, Katanga, Democratic Republic of

- Congo: Quantitative fluid inclusion analysis using laser ablation ICP-MS and bulk crush-leach methods. *Economic Geology*, volume 103, 23 pages, doi.org/10.2113/gsecongeo.103.7.1459.
- Heinrich, C.A., A.S. Andrew, and M.D. Knil, 2000, Regional metamorphism and ore formation: Evidence from stable isotopes and other fluid tracers *in* *Metamorphosed and Metamorphogenic Ore Deposits*, editors, P.G. Spry, B. Marshall, and F.M. Vokes. *Reviews in Economic Geology*, volume 11, 20 pages, doi.org/10.5382/Rev.11.05.
- Hitzman, M.W., D. Selley, and S. Bull, 2010, Formation of sedimentary rock-hosted stratiform copper deposits through Earth history. *Economic Geology*, volume 105, 13 pages, doi.org/10.2113/gsecongeo.105.3.627.
- Hitzman, M.W., D. Broughton, D. Selley, J. Woodhead, D. Wood, and S. Bull, 2012, The central African copperbelt: Diverse stratigraphic, structural, and temporal settings in the world's largest sedimentary copper district. *Society of Economic Geologists, Special Publication 16*, 28 pages, doi.org/10.5382/SP.16.19.
- Hochstein, M.P. and P.R.L. Browne, 2000, Surface manifestations of geothermal systems with volcanic heat sources *in* *Encyclopedia of Volcanoes: San Diego*, editors, H. Sigurdsson, B.F. Houghton, S.R. McNutt, H. Rymer, and J. Stix. Academic Press, 20 pages.
- Hubbert, M.K., 1940, The theory of ground-water motion. *The Journal of Geology*, volume 48, number 8, part 1, 160 pages.
- Huizenga, J., J. Gutzmer, D. Banks, and L. Greyling, 2006, The Paleoproterozoic carbonate-hosted Poring Zn-Pb deposit, South Africa. II: Fluid inclusion, fluid chemistry and stable isotope constraints. *Mineralium Deposita*, volume 40, 21 pages, doi.org/10.1007/s00126-005-0015-9.
- Ingebritsen, S.E. and R.H. Mariner, 2010, Hydrothermal heat discharge in the Cascade Range, northwestern United States. *Journal of Volcanology and Geothermal Research*, volume 196, 10 pages doi.org/10.1016/j.jvolgeores.2010.07.023.
- Jaupart C. and J.C. Mareschal, 2011, *Heat Generation and Transport in the Earth*. Cambridge University Press, Cambridge, United Kingdom, 464 pages.
- Johnson, K.M., J.M. Hammarstrom, M.L. Zientek, and C.L. Dicken, 2014, Estimate of undiscovered copper resources of the world, 2013. United States Geological Survey, Fact Sheet 2014-3004, 3 pages, <https://pubs.usgs.gov/fs/2014/3004/>.
- Jowett, E.C., 1986, Genesis of Kupferschiefer Cu-Ag deposits by convective flow of Rotliegendes brines during Triassic rifting. *Economic Geology*, volume 81, 15 pages, doi.org/10.2113/gsecongeo.81.8.1823.
- Kharaka, Y.K. and J.S. Hanor, 2004, Deep fluids in the continents: I. Sedimentary basins *in* *Treatise on Geochemistry*, editors, H.D. Holland, K.K. Turekian, volume 5, pages 42.
- Kirkham, R.V., 1989, Distribution, Settings, and Genesis of Sediment-hosted Stratiform Copper Deposits. Geological Association of Canada, Special Paper 36, 35 pages.

- Komninou, A. and D.A. Sverjensky, 1996, Geochemical modeling of the formation of an unconformity-type uranium deposit. *Economic Geology*, volume 91, 17 pages, doi.org/10.2113/gsecongeo.91.3.590.
- Korges, M., P. Weis, and C. Andersen, 2020, The role of incremental magma chamber growth on ore formation in porphyry copper systems. *Earth and Planetary Science Letters*, volume 552, 13 pages, doi.org/10.1016/j.epsl.2020.116584.
- Kouzmanov, K. and G.S. Pokrovski, 2012, Hydrothermal Controls on Metal Distribution in Porphyry Cu (-Mo-Au) Systems. *Society of Economic Geologists, Special Publication 16*, 45 pages, doi.org/10.5382/SP.16.22.
- Koziy, L., S. Bull, R. Large, and D. Selley, 2009, Salt as a fluid driver, and basement as a metal source, for stratiform sediment-hosted copper deposits. *Geology*, volume 37, 3 pages, doi.org/10.1130/G30380A.1.
- Kyser, T.K., E.E. Hiatt, C. Renac, K. Durocher, G.J. Holk, and K. Deckart, 2000, Diagenetic fluids in paleo- and meso-Proterozoic sedimentary basins and their implications for long protracted fluid histories *in* *Fluids and Basin Evolution*, editor, K. Kyser. Mineralogical Association of Canada, 38 pages.
- Lamy-Chappuis, B., C.A. Heinrich, T. Driesner, and P. Weis, 2020, Mechanisms and patterns of magmatic fluid transport in cooling hydrous intrusions. *Earth and Planetary Science Letters*, volume 535, 11 pages, doi.org/10.1016/j.epsl.2020.116111.
- Lapwood, E., 1948, Convection of a fluid in a porous medium. *Mathematical Proceedings of the Cambridge Philosophical Society*, volume 44, issue 4, 14 pages, doi.org/10.1017/S030500410002452X.
- Large, D.J. and J.S. Small, 2000, Diffusion and reaction-controlled Cu-Pb-Zn ore mineral precipitation in a reducing system: A model applied to the pattern of ore mineral precipitation in the Kupferschiefer and other black shales. *Economic Geology*, volume 95, 9 pages, doi.org/10.2113/gsecongeo.95.3.577.
- Lee, C.T.A. and M. Tang, 2020, How to make porphyry copper deposits. *Earth and Planetary Science Letters*, volume 529, 11 pages, doi.org/10.1016/j.epsl.2019.115868.
- Li, Z., G. Chi, and K.M. Bethune, 2016, The effects of basement faults on thermal convection and implications for the formation of unconformity-related uranium deposits in the Athabasca Basin, Canada. *Geofluids*, volume 16, 23 pages, doi.org/10.1111/gfl.12180.
- Li, Z., G. Chi, K.M. Bethune, K. Eldursi, D. Quirt, P. Ledru, and D. Thomas, 2020, Interplay between thermal convection and compressional fault reactivation in the formation of unconformity-related uranium deposits. *Mineralium Deposita*, volume 56, 15 pages, doi.org/10.1007/s00126-020-01011-6.
- Lowell, J.D., 1974, Regional characteristics of porphyry copper deposits of the southwest. *Economic Geology*, volume 69, 18 pages, doi.org/10.2113/gsecongeo.69.5.601.

- Manga, M., 1998, Advective heat transport by low-temperature discharge in the Oregon Cascades. *Geology*, volume 26, 4 pages, [doi.org/10.1130/0091-7613\(1998\)026<0799:AHTBLT>2.3.CO;2](https://doi.org/10.1130/0091-7613(1998)026<0799:AHTBLT>2.3.CO;2).
- Mathieu, J., E.C. Turner, D.J. Kontak, and M. Tang, 2022, Geochemical evidence for a topographically driven regional mineralization fluid in the Polaris Zn district, Arctic Canada, volume 117, 30 pages, doi:10.5382/econgeo.4959, 30p.
- Misra, K.C., 2000, *Understanding Mineral Deposits*. Dordrecht, Netherlands, Kluwer, 845 pages.
- Muir-Wood, R. and G.C.P. King, 1993, Hydrological signatures of earthquake strain. *Journal of Geophysical Research*, volume 98B, 34 pages.
- Nield, D.A. and C.T. Simmons, 2007, A discussion on the effect of heterogeneity on the onset of convection in a porous medium. *Transport in Porous Media*, volume 68, 9 pages, doi.org/10.1007/s11242-006-9045-8.
- Norton, D. and J.E. Knight, 1977, Transport phenomena in hydrothermal systems: Cooling plutons. *American Journal of Science*, volume 277, 45 pages, doi.org/10.2475/ajs.277.8.937.
- Nunn, J.A. and D. Deming, 1991, Thermal constraints on basin-scale flow systems. *Geophysical Research Letters*, volume 18, 4 pages, doi.org/10.1029/91GL00986.
- Nunn, J.A. and G. Lin, 2002, Insulating effect of coals and organic rich shales: Implications for topography-driven fluid flow, heat transport, and genesis of ore deposits in the Arkoma Basin and Ozark Plateau. *Basin Research*, volume 14, 17 pages, doi.org/10.1046/j.1365-2117.2002.00172.x.
- Ogata, A. and R.B. Banks, 1961, A Solution of the Differential Equation of Longitudinal Dispersion in Porous Media. U.S. Geological Survey Professional Paper 411-A, 13 pages, <https://pubs.usgs.gov/pp/0411a/report.pdf>.
- Pagel, M., B. Poty, and S.M.F. Sheppard, 1980, Contribution to some Saskatchewan uranium deposits mainly from fluid inclusion and isotopic data *in* Uranium in the Pine Creek Geosyncline. *Proceedings of the International Uranium Symposium on the Pine Creek Geosyncline*, editors, J. Ferguson, and A.B. Goleby. International Atomic Energy Agency, 16 pages.
- Parmigiani, A., S. Faroughi, C. Huber, O. Bachmann, and Y. Su, 2016, Bubble accumulation and its role in the evolution of magma reservoirs in the upper crust. *Nature*, volume 532, 4 pages, doi.org/10.1038/nature17401.
- Parmigiani, A., W. Degruyter, S. Leclaire, C. Huber, and O. Bachmann, 2017, The mechanics of shallow magma reservoir outgassing. *Geochemistry, Geophysics, Geosystems*, volume 18, 19 pages, doi.org/10.1002/2017GC006912.
- Pelch, M.A., M.S. Appold, P. Emsbo, and R.J. Bodnar, 2015, Constraints from fluid inclusion compositions on the origin of Mississippi Valley-type mineralization in the Illinois-Kentucky district. *Economic Geology*, volume 110, 22 pages, doi.org/10.2113/econgeo.110.3.787.

- Person, M.A., J.P. Raffensperger, S. Ge, and G. Garven, 1996, Basin-scale hydrogeologic modeling. *Reviews of Geophysics*, volume 34, issue 1, 27 pages.
- Pinckney, D.M., and J. Haffty, 1970, Content of zinc and copper in some fluid inclusions from the Cave-in-Rock District, southern Illinois. *Economic Geology*, volume 67, 19 pages, doi.org/10.2113/gsecongeo.65.4.451.
- Piqué, À., À. Canals, F. Grandia, and D.A. Banks, 2008, Mesozoic fluorite veins in NE Spain record regional base metal-rich brine circulation through basin and basement during extensional events. *Chemical Geology*, volume 257, 14 pages, doi.org/10.1016/j.chemgeo.2008.08.028.
- Raffensperger, J.P., and G. Garven, 1995a, The formation of unconformity-type uranium ore deposits; 1, Coupled groundwater flow and heat transport modeling. *American Journal of Science*, volume 295, 56 pages, doi.org/10.2475/ajs.295.5.581.
- Raffensperger, J.P., and G. Garven, 1995b, The formation of unconformity-type uranium ore deposits; 2, Coupled hydrochemical modeling. *American Journal of Science*, volume 295, 58 pages, doi.org/10.2475/ajs.295.6.639.
- Rezeau, H. and O. Jagoutz, 2020, The importance of H₂O in arc magmas for the formation of porphyry Cu deposits. *Ore Geology Reviews*, volume 126, 14 pages, doi.org/10.1016/j.oregeorev.2020.103744.
- Richard, A., M. Cathelineau, M.C. Boiron, J. Mercadier, D.A. Banks, and M. Cuney, 2016, Metal-rich fluid inclusions provide new insights into unconformity-related U deposits (Athabasca Basin and Basement, Canada). *Mineralium Deposita*, volume 51, 29 pages, doi.org/10.1007/s00126-015-0601-4.
- Seedorff, E., J.H. Dilles, J.M. Proffett, M.T. Einaudi, L. Zurcher, W.J. Stavast, D.A. Johnson, and M.D. Barton, 2005, Porphyry deposits: Characteristics and origin of hypogene features *in* *Economic Geology*, 100th Anniversary Issue 1905–2005, editors, J.W. Hedenquist, J.F.H. Thompson, R.J. Goldfarb, J.P. Richards. Society of Economic Geologists, 51 pages, doi.org/10.5382/AV100.10.
- Sharp Jr., J.M., 1978, Energy and momentum transport model of the Ouachita basin and its possible impact on formation of economic mineral deposits. *Economic Geology*, volume 73, 12 pages, doi.org/10.2113/gsecongeo.73.6.1057.
- Shepherd, T.J. and S.R. Chenery, 1995, Laser ablation ICP-MS elemental analysis of individual fluid inclusions: An evaluation study. *Geochimica et Cosmochimica Acta*, volume 59, 11 pages, [doi.org/10.1016/0016-7037\(95\)00294-A](https://doi.org/10.1016/0016-7037(95)00294-A).
- Sillitoe, R.H., 2010, Porphyry copper systems. *Economic Geology*, volume 105, 39 pages, doi.org/10.2113/gsecongeo.105.1.3.
- Sillitoe, R.H., 2012, Copper provinces. Society of Economic Geologists, Special Publication 16, 19 pages, doi.org/10.5382/SP.16.01.
- Simmons, C.T., T.R. Fenstemaker, and J.M. Sharp Jr., 2001, Variable-density groundwater flow and solute transport in heterogeneous porous media: approaches, resolutions and future challenges. *Journal of Contaminant Hydrology*, volume 52, 31 pages.

- Simmons, C.T., J.M. Sharp Jr., and D.A. Nield, 2008, Modes of free convection in fractured low-permeability media. *Water Resources Research*, volume 44, 31 pages, [doi.org/10.1016/S0169-7722\(01\)00160-7](https://doi.org/10.1016/S0169-7722(01)00160-7).
- Simmons, S.F. and K.L. Brown, 2006, Gold in magmatic hydrothermal solutions and the rapid formation of a giant ore deposit: *Science*, volume 314, 4 pages, doi.org/10.1126/science.1132866.
- Smith-Schmitz, S.E. and M.S. Appold, 2018, Prediction of ore fluid metal concentrations from solid solution concentrations in ore-stage calcite: Application to the Illinois-Kentucky and Central Tennessee Mississippi Valley-type districts. *Geochimica et Cosmochimica Acta*, volume 225, 18 pages, doi.org/10.1016/j.gca.2018.01.022.
- Stoffell, B., M.S. Appold, J.J. Wilkinson, N.A. McClean, and T.E. Jeffries, 2008, Geochemistry and evolution of Mississippi Valley-Type mineralizing brines from the Tri-State and Northern Arkansas districts determined by LA-ICP-MS microanalysis of fluid inclusions. *Economic Geology*, volume 103, 25 pages, doi.org/10.2113/gsecongeo.103.7.1411.
- Stoltzow, M., P. Weis, and M. Korges, 2023, Hydrological controls on metal precipitation and zoning at the porphyry-epithermal transition constrained by numerical modeling. *Nature Scientific Reports*, volume 13, 15 pages, doi.org/10.1038/s41598-023-30572-5.
- Strengel-Martinez, M., S. Speczik, and J. Jankowski, 1993, Epigenetic veins in Kupferschiefer deposits of SW Poland. *Archiwum Mineralogiczne*, volume 49, 2 pages.
- Sverjensky, D.A., 1986, Genesis of Mississippi Valley-type lead-zinc deposits: *Annual Review of Earth and Planetary Sciences*, volume 14, 21 pages, doi.org/10.1146/annurev.ea.14.050186.001141.
- Swenson, J.B., M. Person, J.P. Raffensperger, W.F. Cannon, L.G. Woodruff, and M.E. Berndt, 2004, A hydrogeologic model of stratiform copper mineralization in the Midcontinent Rift system, northern Michigan, USA. *Geofluids*, volume 4, 23 pages, doi.org/10.1111/j.1468-8123.2004.00062.x.
- Tóth, J., 1963, A theoretical analysis of groundwater flow in small drainage basins. *Journal of Geophysical Research*, volume 68, 18 pages, doi.org/10.1029/JZ068i016p04795.
- Weis, P., 2015, The dynamic interplay between saline fluid flow and rock permeability in magmatic-hydrothermal systems. *Geofluids*, volume 15, 22 pages, doi.org/10.1111/gfl.12100.
- Weis, P., T. Driesner, and C.A. Heinrich, 2012, Porphyry-copper ore shells form at stable pressure-temperature fronts within dynamic fluid plumes. *Science*, volume 338, 4 pages, doi.org/10.1126/science.1225009.
- Weis, P., T. Driesner, D. Coumou, and S. Geiger, 2014, Hydrothermal, multi-phase convection of H₂O-NaCl fluids from ambient to magmatic temperatures: A new

- numerical scheme and benchmarks for code comparison. *Geofluids*, volume 14, 25 pages, doi.org/10.1111/gfl.12080.
- Wenz, Z.J., M.S. Appold, K.L. Shelton, and S. Tesfaye, 2012, Geochemistry of Mississippi Valley-type mineralizing fluids of the Ozark Plateau: A regional synthesis. *American Journal of Science*, volume 312, 59 pages, doi.org/10.2475/01.2012.02.
- Wilde, A.R., T.P. Mernagh, M.S. Bloom, and C.F. Hoffmann, 1989, Fluid inclusion evidence on the origin of some Australian unconformity-related uranium deposits. *Economic Geology*, volume 84, 16 pages, doi.org/10.2113/gsecongeo.84.6.1627.
- Wilkinson, J.J., B. Stoffell, C.C. Wilkinson, T.E. Jeffries, and M.S. Appold, 2009, Anomalously metal-rich fluids from hydrothermal ore deposits. *Science*, volume 323, 4 pages, doi.org/10.1126/science.1164436.
- Ypma, P.J. and K. Fuzikawa, 1980, Fluid inclusion and oxygen isotope studies of the Nabarlek and Jabiluka uranium deposits, Northern Territory, Australia *in* Uranium in the Pine Creek Geosyncline. Proceedings of the International Uranium Symposium on the Pine Creek Geosyncline, editors, J. Ferguson, and A.B. Goleby. International Atomic Energy Agency, 26 pages.

6 Exercise Solutions

Part I - Constraints and Implications of Groundwater Temperature on the Formation of Mississippi Valley-type Zn-Pb Deposits

Solution Exercise 1

The expected range is:

$$T_1 = 1.5 \text{ km } (25 \text{ }^\circ\text{C/km}) + 20^\circ \text{ C} = 57.5^\circ \text{ C}$$

$$T_2 = 1.5 \text{ km } (35 \text{ }^\circ\text{C/km}) + 20^\circ \text{ C} = 72.5^\circ \text{ C}$$

[Click to return to where text linked to Exercise 1](#) ↑

[Return to Exercise 1](#) ↑

Solution Exercise 2

The pattern of groundwater flow in the model is characterized by strong recharge in the south, discharge over the crest of the Ozark Dome, and greatly reduced groundwater flow north of the crest of the Ozark Dome. Comparatively little groundwater flow occurs in the basement rock, i.e., below the bold line in the interior of the cross section.

Temperatures are significantly depressed in the recharge zone, where cool water is descending. Temperatures are significantly elevated in the discharge zone over the crest of the Ozark Dome, where the Southeast Missouri MVT ore district is located, and where warmer deep groundwater is ascending. Isotherms parallel streamlines in the lower stratigraphic units along much of the flow path to the Southeast Missouri district, meaning that temperature does not change much along the flow path before the Southeast Missouri district is reached. North of the Southeast Missouri district, the thermal regime is primarily conductive.

[Click to return to where text linked to Exercise 2](#) ↑

[Return to Exercise 2](#) ↑

Solution Exercise 3

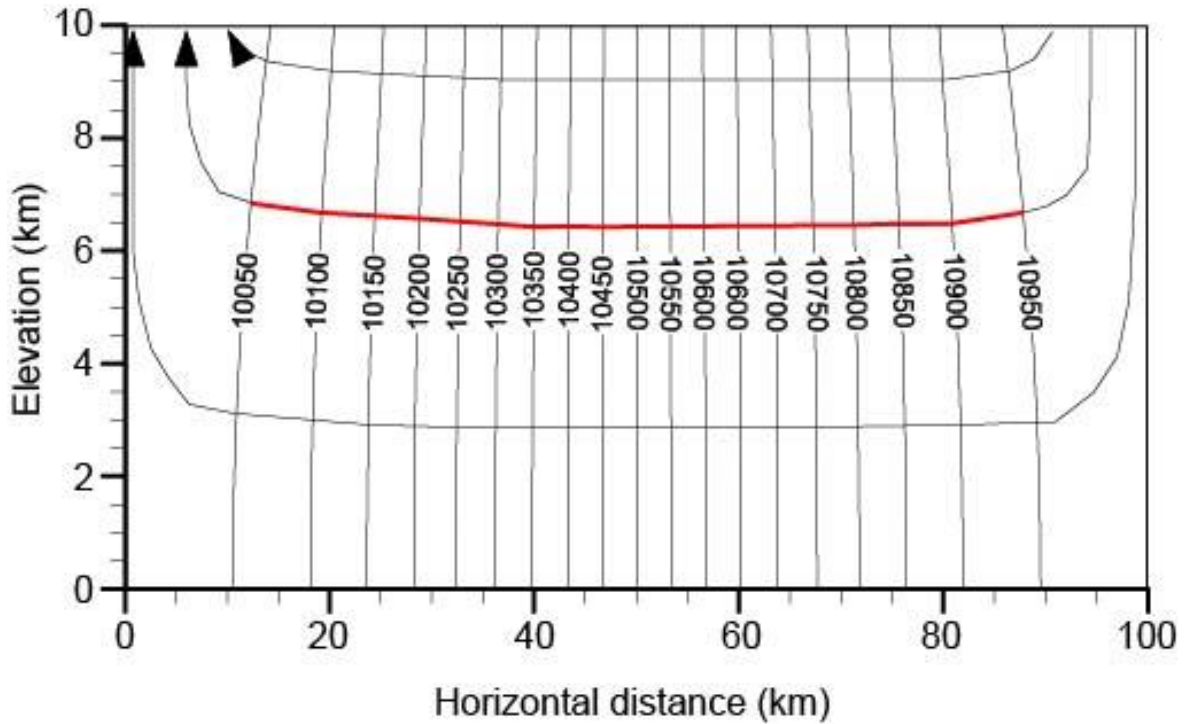
The steady-state hydraulic heads were calculated in meters for each cell in a spreadsheet by defining the value of x and z for the cell along a row at the top and a column at the side respectively and placing the equation of Exercise 3 (shown again below) in each cell with reference to the cell containing the appropriate x and z values, as well as the model parameters (B , L , z_0 , and $A=B+z_0$). The calculated head values are shown below and a spreadsheet presenting the solution is provided in the [zipped file of exercise solutions](#) included as supplemental material on the Groundwater Project web page for this book.

$$h(x, z) = A - \left[\frac{B \cosh\left(\frac{\pi z}{L}\right)}{\cosh\left(\frac{\pi z_0}{L}\right)} \right] \cos\left(\frac{\pi x}{L}\right)$$

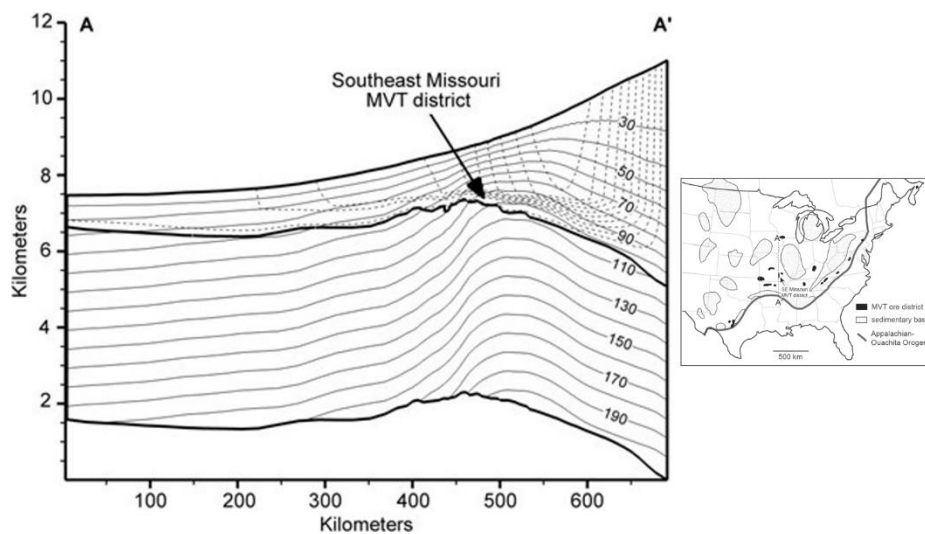
Hydraulic head (m) as a function of z and x from equations of Domenico and Palciauskas (1973).

		Horizontal distance, x (m)										
		0	10,000	20,000	30,000	40,000	50,000	60,000	70,000	80,000	90,000	100,000
Elevation, z (m)	10,000	10,000.00	10,024.45	10,095.40	10,205.91	10,345.19	10,499.60	10,654.05	10,793.44	10,904.13	10,975.31	11,000.00
	9,000	10,004.53	10,028.75	10,099.06	10,208.58	10,346.59	10,499.61	10,652.66	10,790.78	10,900.47	10,971.00	10,995.47
	8,000	10,008.57	10,032.60	10,102.33	10,210.95	10,347.84	10,499.61	10,651.41	10,788.41	10,897.21	10,967.16	10,991.43
	7,000	10,012.12	10,035.98	10,105.21	10,213.04	10,348.94	10,499.61	10,650.32	10,786.33	10,894.34	10,963.78	10,987.88
	6,000	10,015.20	10,038.90	10,107.70	10,214.85	10,349.89	10,499.61	10,649.37	10,784.52	10,891.85	10,960.86	10,984.80
	5,000	10,017.79	10,041.37	10,109.80	10,216.38	10,350.70	10,499.62	10,648.57	10,783.00	10,889.75	10,958.39	10,982.21
	4,000	10,019.91	10,043.39	10,111.51	10,217.63	10,351.35	10,499.62	10,647.92	10,781.75	10,888.04	10,956.38	10,980.09
	3,000	10,021.56	10,044.95	10,112.84	10,218.60	10,351.86	10,499.62	10,647.41	10,780.79	10,886.71	10,954.81	10,978.44
	2,000	10,022.74	10,046.07	10,113.80	10,219.29	10,352.23	10,499.62	10,647.05	10,780.10	10,885.76	10,953.69	10,977.26
	1,000	10,023.44	10,046.74	10,114.37	10,219.70	10,352.45	10,499.62	10,646.83	10,779.68	10,885.19	10,953.02	10,976.56
	0	10,023.68	10,046.96	10,114.56	10,219.84	10,352.52	10,499.62	10,646.76	10,779.55	10,885.00	10,952.80	10,976.32

The head values were used to draw contour lines and flow lines as shown in the following image. Each reader's result may look slightly different depending on the number of cells they use to define x and z .



The flow results predicted by the Domenico and Palciauskas analytical solution broadly resemble those of the image of Exercise 2 which is repeated below for the reader's convenience (the red line segment pertains to the solution for Exercise 5). Recharge is predicted on the right and discharge is predicted on the left side of the basin. The analytical solution corresponds reasonably well to the portion of the numerical model between the crest of the Ozark Dome and A' (i.e., between $x = 500$ km and 600 km).



[Click to return to where text linked to Exercise 3 ↑](#)

[Return to Exercise 3 ↑](#)

Solution Exercise 4

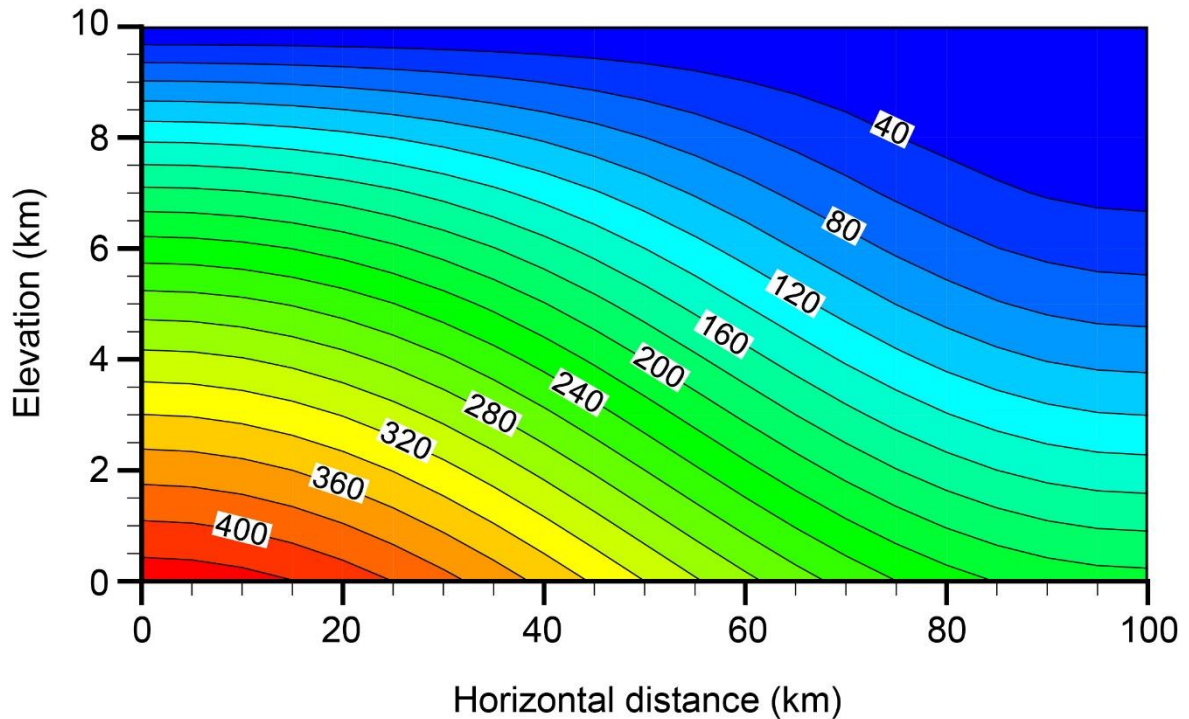
- a) The temperatures were calculated in °C for each cell in a spreadsheet by defining the value of x and z for the cell along a row at the top and a column at the side respectively and placing the equation shown below in each cell with reference to the cell containing the appropriate x and z values, as well as the model parameters ($B, L, z_0, T, T_l, T'_0, K, \text{ and } \kappa$). The calculated temperature values are shown below and a spreadsheet presenting the solution is provided in the [zipped file of exercise solutions](#) included as supplemental material on the Groundwater Project web page for this book.

$$T(x, z) = T_1 + T'_0(z - z_0) - \frac{T'_0KB}{2\kappa} \left(\frac{\cos\left(\frac{\pi x}{L}\right)}{\cosh\left(\frac{\pi z_0}{L}\right)} \right) \left\{ (z_0 - z) \cosh\left(\frac{\pi z}{L}\right) + \frac{L}{\pi} \left[\frac{\sinh\left(\frac{\pi(z - z_0)}{L}\right)}{\cosh\left(\frac{\pi z_0}{L}\right)} \right] \right\}$$

Temperature values (°C) for $K = 5 \times 10^{-8}$ m/s for x, z from equations of Domenico and Palciauskas (1973).

		Horizontal distance, x (m)										
		0	10,000	20,000	30,000	40,000	50,000	60,000	70,000	80,000	90,000	100,000
Elevation, z (m)	10,000	20	20	20	20	20	20	20	20	20	20	20
	9,000	81.2	79.7	75.3	68.4	59.7	50.0	40.4	31.7	24.8	20.3	18.8
	8,000	136.0	133.3	125.4	113.0	97.4	80.0	62.7	47.1	34.7	26.7	24.0
	7,000	185.2	181.6	170.9	154.2	133.3	110.1	86.8	65.8	49.2	38.5	34.8
	6,000	229.5	225.1	212.4	192.7	167.7	140.1	112.4	87.5	67.6	54.9	50.5
	5,000	269.6	264.8	250.6	228.6	200.9	170.1	139.3	111.5	89.5	75.3	70.4
	4,000	306.3	301.1	286.0	262.5	232.9	200.1	167.2	137.6	114.1	98.9	93.7
	3,000	340.3	334.9	319.2	294.9	264.1	230.1	196.0	165.3	140.9	125.2	119.7
	2,000	372.2	366.8	350.8	326.0	294.8	260.1	225.4	194.1	169.3	153.3	147.8
	1,000	402.9	397.4	381.4	356.4	325.0	290.1	255.2	223.7	198.8	182.7	177.1
	0	433.0	427.4	411.4	386.4	355.0	320.1	285.2	253.7	228.7	212.6	207.0

The temperature values were used to draw contour lines as shown in the following image. Each reader's result may look slightly different depending on the level of cells they use to define x and z . The vertical axis is exaggerated by approximately a factor of 5.5.



- b) Cool, descending meteoric recharge at the right side (near $x = 100,000$ m) depresses the isotherms and increases their spacing, leading to lower heat flux. Warmer, ascending deep groundwater at the left side (near $x = 0$) elevates the isotherms and decreases their spacing, leading to higher heat flux.
- c) Measuring graphically from the plot or interpolating from the spreadsheet, the temperature is about 108°C . This is in the range of MVT ore-forming temperatures.
- d) The temperature gradient at $x = 0$ is much larger than the background conductive temperature gradient (about -0.06 versus -0.03 $^{\circ}\text{C}/\text{m}$), whereas the temperature gradient at $x = 100,000$ m is much smaller than the background conductive temperature gradient (about -0.002 versus -0.03 $^{\circ}\text{C}/\text{m}$). MVT deposits might be expected to occur in regions where hydrothermal groundwater discharged in the geologic past.

[Click to return to where text linked to Exercise 4 ↑](#)

[Return to Exercise 4 ↑](#)

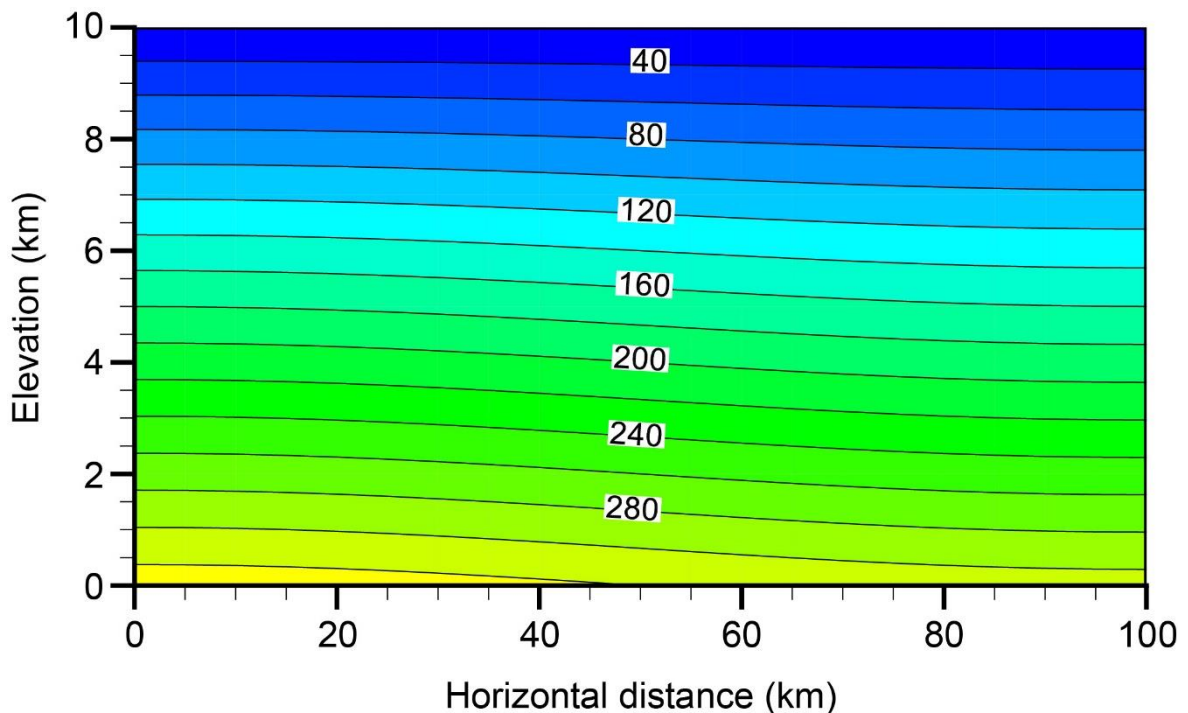
Solution Exercise 5

- a) Temperatures were calculated as described in the solution for Exercise 4 but using the lower hydraulic conductivity. They are shown below and a spreadsheet presenting the solution is provided in the [zipped file of exercise solutions](#) included as supplemental material on the Groundwater Project web page for this book.

Temperature values ($^{\circ}\text{C}$) for $K = 5 \times 10^{-9}$ m/s for x, z from equations of Domenico and Palciauskas (1973)

		Horizontal distance, x (m)										
		0	10,000	20,000	30,000	40,000	50,000	60,000	70,000	80,000	90,000	100,000
Elevation, z (m)	10,000	20.0	20.0	20.0	20.0	20.0	20.0	20.0	20.0	20.0	20.0	20.0
	9,000	53.1	53.0	52.5	51.8	51.0	50.0	49.0	48.2	47.5	47.0	46.9
	8,000	85.6	85.3	84.5	83.3	81.7	80.0	78.3	76.7	75.5	74.7	74.4
	7,000	117.5	117.2	116.1	114.4	112.3	110.0	107.7	105.6	103.9	102.8	102.5
	6,000	149.0	148.5	147.2	145.3	142.8	140.0	137.2	134.7	132.8	131.5	131.0
	5,000	180.0	179.5	178.1	175.9	173.1	170.0	166.9	164.2	161.9	160.5	160.0
	4,000	210.6	210.1	208.6	206.3	203.3	200.0	196.7	193.8	191.4	189.9	189.4
	3,000	241.0	240.5	238.9	236.5	233.4	230.0	226.6	223.5	221.1	219.5	219.0
	2,000	271.2	270.7	269.1	266.6	263.5	260.0	256.5	253.4	250.9	249.3	248.8
	1,000	301.3	300.7	299.1	296.6	293.5	290.0	286.5	283.4	280.9	279.3	278.7
	0	331.3	330.7	329.1	326.6	323.5	320.0	316.5	313.4	310.9	309.3	308.7

The temperature values were used to draw contour lines as shown in the following image. Each reader's result may look slightly different depending on the level of cells they use to define x and z . The vertical axis is exaggerated by approximately a factor of 5.5.



- a) The isotherms are much less deflected at the lower hydraulic conductivity. The temperature pattern more closely resembles a conductive pattern.
- b) No, the temperature is not sufficient for MVT ore formation. The temperature is only about 70° C.
- c) Using Darcy's law and the resulting hydraulic head change along the representative flow path shown in red in the solution to Exercise 3, q is given by the following equation.

$$q = -K \frac{\Delta h}{\Delta x}$$

$$q = -(5 \times 10^{-8} \text{ m/s}) \left(\frac{10,950 - 10,050 \text{ m}}{88,000 - 12,400 \text{ m}} \right)$$

$$q = -6 \times 10^{-10} \text{ m/s}$$

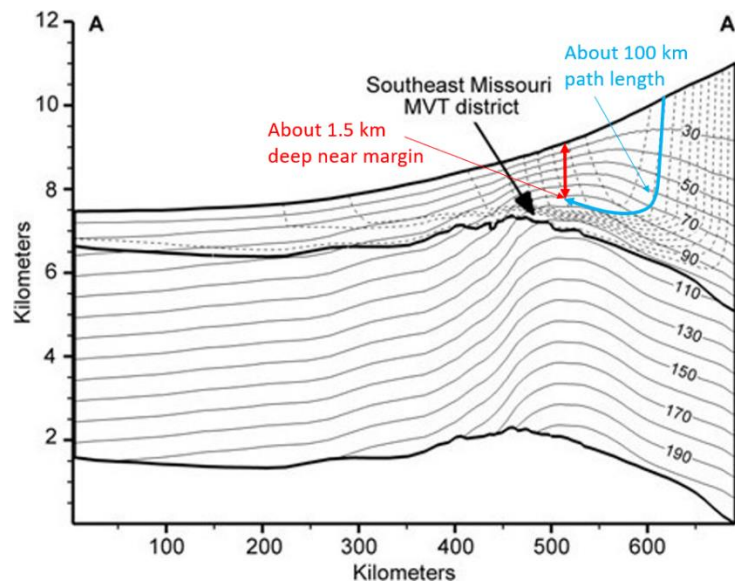
$$q = -1.9 \times 10^{-2} \text{ m/y}$$

[Click to return to where text linked to Exercise 5](#) ↑

[Return to Exercise 5](#) ↑

Solution Exercise 6

a) Measuring graphically from the plots, the flow length is about 100,000 m.



b) t is given by the expression:

$$t = \frac{\text{flow length}}{\text{average linear velocity}}$$

$$t = \frac{d}{v}$$

$$t = \frac{d}{q/n}$$

$$t = \frac{100,000 \text{ m}}{\left(1.9 \times 10^{-2} \frac{\text{m}}{\text{y}}\right) / (0.2)}$$

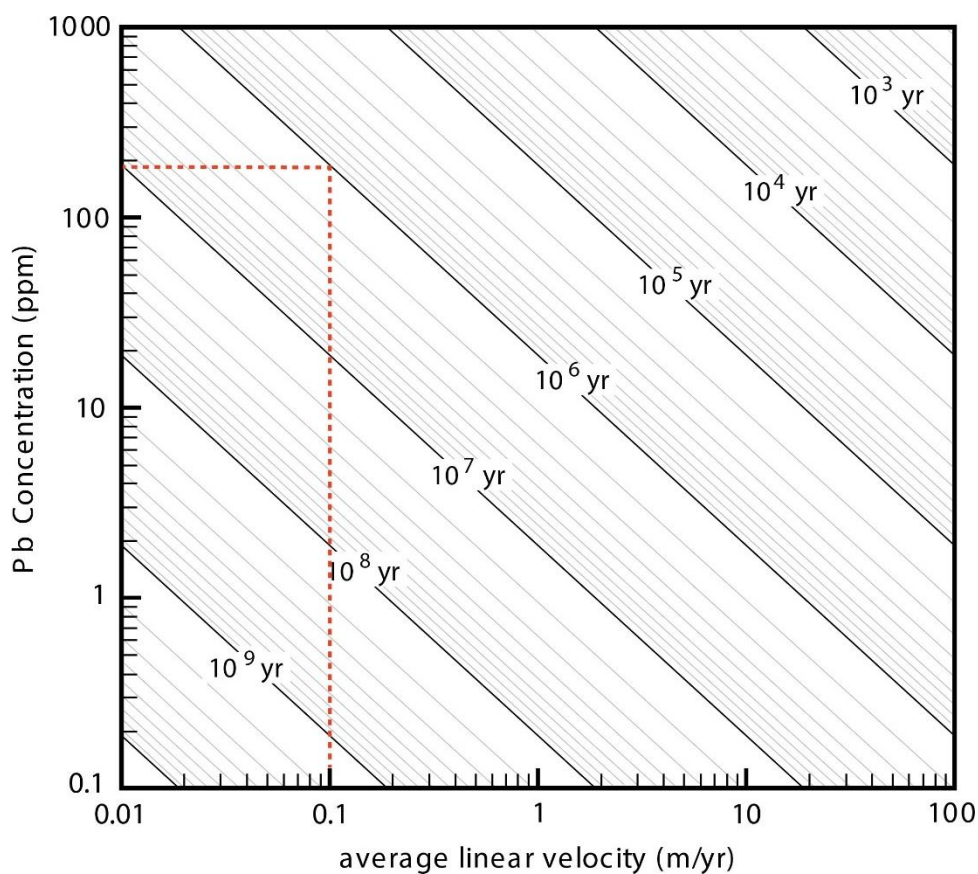
$$t = 1.05 \times 10^6 \text{ y.}$$

[Click to return to where text linked to Exercise 6](#)

[Return to Exercise 6](#)

Solution Exercise 7

The Darcy velocity computed in Exercise 5 was $q = 0.019$ m/y. Thus, the corresponding average linear velocity, which is the horizontal axis variable in the Pb mass balance figure shown below, is $v = q/n = 0.019/0.2 = 0.095$ m/y. The time needed for the fresh water to arrive at the site of MVT deposition in the Southeast Missouri district, which is also the time available for ore formation, is 1.05×10^6 y, which are the contours in the figure below. Plotting these values on the figure below leads to a Pb concentration of slightly less than 200 ppm.



[Click to return to where text linked to Exercise 7](#)

[Return to Exercise 7](#)

Solution Exercise 8

Write the mass action expression for the chemical reaction as shown here.

$$K = \frac{a_{PbS} a_{Cl^-}^4 a_{H^+}^2}{a_{PbCl_4^{2-}} a_{H_2S}}$$

Convert total lead concentration determined in Exercise 7 from ppm to moles per kilogram of solution:

$$\frac{200 \text{ g Pb}}{10^6 \text{ g solution}} \frac{1 \text{ mol Pb}}{207.2 \text{ g Pb}} \frac{1000 \text{ g solution}}{1 \text{ kg solution}} = 9.7 \times 10^{-4} \frac{\text{mol Pb}}{\text{kg solution}}$$

Assume that the concentration of lead and sulfur are equal in order to maximize lead sulfide ore formation from a single fluid.

Thus, total sulfur concentration = 9.7×10^{-4} mol per kg of solution.

Assume that the concentrations of moles of solute per kg of solution are equal to the moles of solute per kg of solvent (water), i.e., molality.

Recall the assumptions and facts indicated in Exercise 8: the galena is composed purely of PbS (i.e., activity is 1), the chloride concentration is 3 mol/kg, dissolved lead and sulfur are present in the same molar concentrations (9.7×10^{-4}), and the equilibrium constant for this reaction at a temperature of 100° C and a pressure of 16 MPa is $K = 7603$. The activity coefficients for the aqueous species are $\gamma_{PbCl_4^{2-}} = 0.110$, $\gamma_{H_2S} = 1.0$, $\gamma_{Cl^-} = 0.873$, and $\gamma_{H^+} = 0.873$.

Assuming that all of the lead is in the form of $PbCl_4^{2-}$ and all of the sulfur is in the form of H_2S , substitute values into the mass action expression show at the beginning of this solution and solve for the activity of H^+ as shown here.

$$K = \frac{(1) [(0.873)(3)]^4 a_{H^+}^2}{[(0.110)(9.7 \times 10^{-4})] [(1)(9.7 \times 10^{-4})]} = 7603$$

$$a_{H^+}^2 = \frac{7603 [(0.110)(9.7 \times 10^{-4})] [(1)(9.7 \times 10^{-4})]}{(1) [(0.873)(3)]^4} = 1.7 \times 10^{-5}$$

$$a_{H^+} = 4.1 \times 10^{-3}$$

$$\text{pH} = -\log(a_{H^+}) = 2.4$$

A pH of 2.4 is low for natural waters unless the water has been impacted by acid mine drainage or by magmatic fluids. Most MVT deposits are thought to have formed from fluids that had a pH between about 4 and 5.5. Thus, it is unlikely that this much sulfur could have been transported with the amount of Pb calculated. This means that an ore precipitation mechanism for the Southeast Missouri district that relies on simultaneous transport of lead and sulfide together in the same fluid is unlikely. More likely precipitation mechanisms are the transport of lead and sulfide in separate fluids in which the

concentration of lead and sulfide could be high in each fluid, or the transport of lead with sulfur in the form of sulfate in a single fluid (which allows high concentrations of both lead and sulfur), where sulfate is reduced to sulfide at the site of ore deposition.

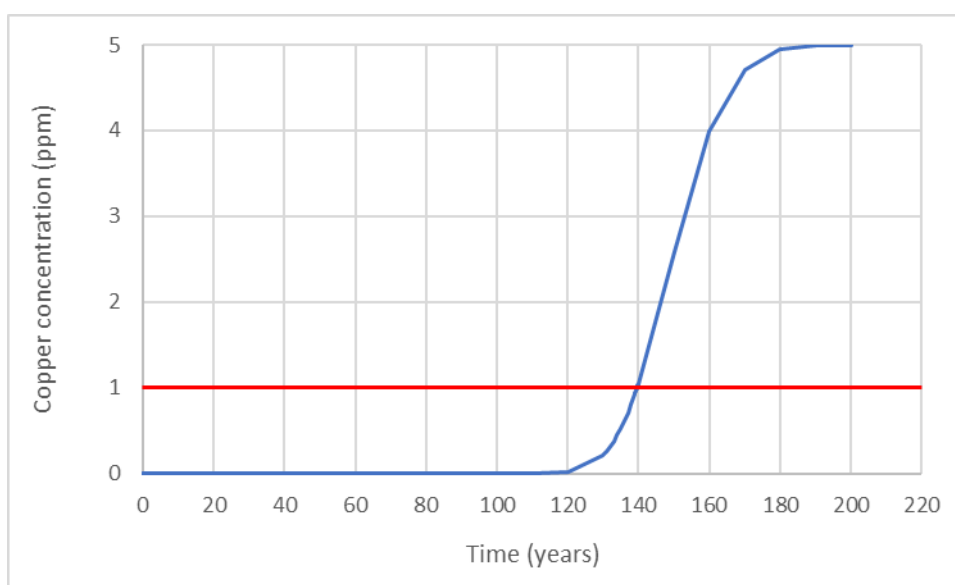
[Click to return to where text linked to Exercise 8↑](#)

[Return to Exercise 8↑](#)

Part II - Solute Transport in a Magmatic Hydrothermal Environment

Solution Exercise 9

Concentrations were calculated as a function of time using the Ogata-Banks (1961) analytical solution to the solute transport equation as described in Exercise 9. The concentrations are presented graphically as well as in the table below. A spreadsheet presenting the solution is provided in the [zipped file of exercise solutions](#) ↑ included as supplemental material on the Groundwater Project web page for this book. By successively refining the time increment on the spreadsheet near the calculated concentration of 1 ppm or reading graphically from the plot, the length of time needed is slightly less than 140 years.



Calculated copper concentration as a function of time using Ogata-Banks solution (red line indicates 1 ppm required for copper precipitation).

Time (years)	Concentration (ppm)
1×10^{-99}	0
80	1.64466×10^{-14}
120	0.01732491
125	0.070014158
130	0.215937865
135	0.527047467
139	0.929610357
139.4	0.977540446
139.5	0.989731074
139.6	1.002004081
139.7	1.01435901
140	1.051910551

150	2.581298702
160	3.986460298
170	4.712403637
180	4.943277565
190	4.99192548
200	4.999137959

[Click to return to where text linked to Exercise 9↑](#)

[Return to Exercise 9↑](#)

Part III - Subsurface Fluid Dynamics

Solution Exercise 10

- a) Assuming a horizontal, homogeneous, isotropic aquifer with $\kappa = 0.01 \text{ cm}^2/\text{s}$, $\nu = 0.01 \text{ cm}^2/\text{s}$, $H = 100 \text{ m}$, $\alpha = 2.5 \times 10^{-4} \text{ }^\circ\text{C}^{-1}$, and $k = 5.9 \times 10^{-7} \text{ cm}^2$, the critical gradient is calculated as shown below.

$$\beta = \frac{4\pi^2 \kappa \nu}{H^2 \alpha g k}$$

$$\beta = \frac{4\pi^2 (10^{-6} \text{ m}^2/\text{s})(10^{-6} \text{ m}^2/\text{s})}{(100 \text{ m})^2 (2.5 \times 10^{-4} \text{ }^\circ\text{C}^{-1})(9.8 \text{ m/s}^2)(5.9 \times 10^{-11} \text{ m}^2)}$$

$$\beta = 0.027 \text{ }^\circ\text{C}/\text{m}$$

- b) If a hot magmatic fluid is injected into a confined aquifer of (a) raising the critical thermal gradient to $6.5 \text{ }^\circ\text{C}/100 \text{ m}$, and the aquifer is homogeneous but anisotropic, with $k_x = 5.90 \times 10^{-7}$ and $k_z = 2.95 \times 10^{-7} \text{ cm}^2$, the maximum thickness of the aquifer, H_{max} , in which no free convection occurs is calculated as follows.

$$k' = \frac{4k_x k_z}{(\sqrt{k_x} + \sqrt{k_z})^2}$$

$$k' = \frac{4(5.90 \times 10^{-7} \text{ cm}^2)(2.95 \times 10^{-7} \text{ cm}^2)}{(\sqrt{5.90 \times 10^{-7} \text{ cm}^2} + \sqrt{2.95 \times 10^{-7} \text{ cm}^2})^2}$$

$$k' = 4.05 \times 10^{-7} \text{ cm}^2 = 4.05 \times 10^{-11} \text{ m}^2$$

$$H_{max} = \sqrt{\frac{4\pi^2 \nu D}{g \alpha \beta k'}}$$

$$H_{max} = \sqrt{\frac{4\pi^2 (10^{-6} \text{ m}^2/\text{s})(10^{-6} \text{ m}^2/\text{s})}{(9.8 \text{ m/s}^2)(2.5 \times 10^{-4} \text{ }^\circ\text{C}^{-1})(0.027 \text{ }^\circ\text{C}/\text{m})(4.05 \times 10^{-11} \text{ m}^2)}} = 121.4 \text{ m}$$

$$H_{max} \sim 120 \text{ m}$$

[Click to return to where text linked to Exercise 10](#)

[Return to Exercise 10](#)

Solution Exercise 11

- a) First recognize that Hubbert's (1940) fluid potential expresses the mechanical energy of a fluid per unit mass:

$$\Phi = gh$$

The change in Hubbert's potential is caused by change in hydraulic head, assuming the gravitational acceleration constant (g). Therefore, the mechanical energy expended to move a unit mass of fluid:

$$\begin{aligned}\Delta\Phi &= g\Delta h \\ \Delta\Phi &= \frac{9.8 \text{ m}}{\text{s}^2} 100 \text{ m} \\ \Delta\Phi &= \frac{980 \text{ m}^2}{\text{s}^2}\end{aligned}$$

Hubbert's fluid potential expressed in SI units is Joules per kilogram (J/kg), where a Joule (J) has units equivalent to ($\text{kg m s}^{-2} \text{ m}$). Thus,

$$\frac{J}{\text{kg}} = \frac{\text{kg} \cdot \text{m} \cdot \text{s}^{-2} \cdot \text{m}}{\text{kg}} = \frac{\text{m}^2}{\text{s}^2}$$

Thus, $\Delta\Phi = 980 \text{ J/kg}$, which is all converted to heat due to the frictional resistance of flow through a permeable porous medium.

- b) Given the following attributes of this flow field:

- average linear (pore fluid seepage) velocity = $v_s = 1 \frac{\text{m}}{\text{d}}$
- $n = 0.15$

calculate the following:

- Darcy velocity (fluid flux) = $q = v_s n = 1 \frac{\text{m}}{\text{d}} 0.15 = 0.15 \frac{\text{m}}{\text{d}} = 54.8 \frac{\text{m}}{\text{y}}$
- Groundwater mass flux = $\rho q = 1000 \frac{\text{kg}}{\text{m}^3} 54.8 \frac{\text{m}}{\text{y}} = 54,800 \frac{\text{kg}}{\text{y m}^2}$
- Convective heat flow = $\rho q \Delta\phi = 54,800 \frac{\text{kg}}{\text{y m}^2} 980 \frac{\text{J}}{\text{kg}} = 5.37 \times 10^7 \frac{\text{J}}{\text{y m}^2}$

This is the heat flow from a $1 \text{ m} \times 1 \text{ m} \times 10 \text{ km}$ section of a confined aquifer. The heat is moving laterally due to groundwater flow in the aquifer. Assuming this heat joins the vertical heat flow at an evenly distributed rate across the entire 10 km length of the basin (L), the land surface heat flow (per unit land surface area and per meter unit thickness of the aquifer) due to forced convection is:

$$\frac{\rho q \Delta\Phi}{L} = \frac{5.37 \times 10^7 \frac{\text{J}}{\text{y m}^2}}{10,000 \text{ m}} = 5370 \frac{\text{J}}{\text{y m}^2}$$

- c) Therefore, the total convective heat flow J_q associated with $H = 100 \text{ m}$ thick aquifer,

$$J_q = 5370 \frac{J}{y m^2} 100 m = 5.37 \times 10^5 \frac{J}{y m^2}$$

where $1 \frac{J}{y} = 3.168876 \times 10^{-5}$ milliWatts (mW), and therefore the convective contributions to heat flow at the surface is:

$$J_q = 17 \frac{mW}{m^2}$$

If the *conductive* heat flux due to natural radioactive decay in the deep crust, $J_c = 70 \frac{mW}{m^2}$, then the fraction F of the total heat flow at the land surface due to groundwater flow across the basin:

$$F = \frac{17}{(17 + 70)} = \frac{17}{87} = 0.195 \sim 20\%$$

[Click to return to where text linked to Exercise 11](#)↑

[Return to Exercise 11](#)↑

7 Notations

A	height of inflection point of the water table (L)
α	coefficient of thermal expansion (Θ^{-1})
B	distance between top of rectangular domain and A (L)
β_T	thermal expansivity of the groundwater (Θ^{-1})
C	solute concentration (ML^{-3})
C_0	initial source concentration (ML^{-3})
ΔT	temperature difference (Θ)
D_L	longitudinal dispersion coefficient (L^2T^{-1})
g	gravitational acceleration (LT^{-2})
h	hydraulic head (L)
H	thickness of aquifer (L)
K	hydraulic conductivity (LT^{-1})
k	intrinsic permeability (L^2)
k'	effective permeability (L^2)
κ	thermal diffusivity (L^2T^{-1})
μ	groundwater viscosity ($ML^{-1}T^{-1}$)
ν	kinematic viscosity (L^2T^{-1})
v	average linear groundwater velocity (LT^{-1})
ρ	water density (ML^{-3})
t	time (T)
T'_o	vertical temperature gradient due solely to conduction (ΘL^{-1})
T_1	temperature on top boundary (Θ)
z_0	height of rectangular problem domain (L)

8 About the Authors



Dr. Martin Appold is a Professor of Geological Sciences at the University of Missouri. Dr. Appold studies the physical and chemical behavior of subsurface fluids using numerical modeling and petrology. His research has focused on hydrothermal mineral deposits, hydrocarbon transport, and CO₂ sequestration. He teaches courses in general groundwater hydrology, groundwater modeling, hydrogeologic processes, and geochemistry. Dr. Appold received the Geological Association of Canada's Julian Boldy Award in Mineral Deposits Research in 2000, is a Fellow of the Society of Economic Geologists, is a former Associate Editor of *Geofluids*, and is a current editor of *Hydrogeology Journal*.



Dr. Grant Garven is a Professor Emeritus of Hydrogeology at Tufts University. He is a groundwater geologist who studies hydrologic, geothermal, geochemical, and hydromechanical processes in the Earth's shallow crust. Ore deposits, hydrothermal vents, petroleum seeps, oil migration, and diagenetic fluids have all been the primary objects of his research. Grant was the founding North American editor of the journal *Geofluids* and served as an associate editor of the *American Journal of Science* during 1990-2022. His awards and honors include a two Senior Fulbright Awards at the University of Tasmania and a U.S. Department of Energy award for Outstanding Contributions in Geoscience Research. He was also the recipient of a U.S. Presidential Young Investigator Award and was honored with the O.E. Meinzer Award from the Geological Society of America. He also been honored with the A.I. Levorsen Memorial Award from the American Association of Petroleum Geologists. Grant has taught both geology and civil engineering courses in groundwater hydrology, groundwater modeling, and subsurface fluid dynamics. He also taught a hands-on hydrogeology field methods course over the past 16 years to engage students in outdoor learning of applied hydrogeology and geotechnical engineering, which has resulted in a unique network of over 50 deep bedrock and overburden monitoring wells across the Tufts University (Medford) campus. The network includes instrumentation of bedrock wells for monitoring levels and water quality, for sports field irrigation, for well hydraulics, for geothermal heating, and for geoscience exploration, including the deepest borehole drilled in the Boston metro area.

Please consider signing up to the GW-Project mailing list to stay informed about new book releases, events and ways to participate in the GW-Project. Signing up to our email list helps us build a global groundwater community. [Sign up](#)[↗].

